# INTEGRATION OF DIFFERENT WAVE FORCING FORMULATIONS WITH NEARSHORE CIRCULATION MODELS

A Thesis

by

ABHISHEK SHARMA

Submitted to the Office of Graduate Studies of
Texas A&M University
in partial fulfillment of the requirements for the degree of

MASTER OF SCIENCE

December 2010

Major Subject: Ocean Engineering

Integration of Different Wave Forcing Formulations with Nearshore Circulation Models

# INTEGRATION OF DIFFERENT WAVE FORCING FORMULATIONS WITH NEARSHORE CIRCULATION MODELS

A Thesis

by

ABHISHEK SHARMA

Submitted to the Office of Graduate Studies of
Texas A&M University
in partial fulfillment of the requirements for the degree of

MASTER OF SCIENCE

Approved by:

| | |
|---|---|
| Co-Chairs of Committee, | Vijay Panchang |
| | Jennifer L. Irish |
| Committee Members, | David Brooks |
| Head of Department, | John Niedzwecki |

December 2010

Major Subject: Ocean Engineering

# ABSTRACT

Integration of Different Wave Forcing Formulations with Nearshore Circulation Models. (December 2010)

Abhishek Sharma, B.S., Institute of Technology, Banaras Hindu University (BHU)

Co-Chairs of Advisory Committee: Dr. Vijay Panchang,
Dr. Jennifer Irish

Wave-induced circulation in general coastal environments is simulated by coupling two widely-used finite-element models, namely, a refraction-diffraction-reflection model based on the elliptic mild-slope equation, and a two-dimensional (depth-averaged) shelf-scale circulation model. Such models yield wave-induced current-fields and set-up/down. This involves exploration of some numerical and practical issues, for example, the selection of appropriate boundary condition and grid resolution, numerical errors owing to higher-order derivatives, etc. Computations of the wave forcing from the elliptic wave model, and the wave-induced quantities from the circulation model, are validated with theoretical and published results. The coupled system is then used to simulate the wave-induced circulation in the domains where structures (e.g. breakwater, jetty, etc.) and bathymetric features (e.g. shoal, etc.) are present.

In practice, usually an approximate form of the wave-induced forcing is used. This has certain limitations in some application, which have been poorly studied so far. Therefore, here we consider two alternative approaches. The performance of these wave

forcing formulations is examined in the regions where the effects of wave reflection, diffraction and focusing are significant. It is observed that the “generalized approach” provides satisfactory results in most situations, provided a grid resolution of L/10 or more is achievable for the wave model domain. The widely-used simplified approach may produce a chaotic pattern of set-up/down and current field in the regions where the wave field is not purely progressive. The third approach ignores the effect of wave diffraction and reflection, and primarily simulates the effect of energy dissipation. Differences up to 25% are observed between the modeled current fields obtained with the generalized and the simplified approach. The results suggest that the generalized approach can be used with little practical difficulty and greater reliability.

# ACKNOWLEDGEMENTS

First and foremost, I am heartily grateful to my advisor, Dr Vijay Panchang, for his invaluable guidance and support from the beginning to the final level of my thesis. I greatly appreciate his patience, his knowledge about the subject and the freedom he provided for me to work in my own way. One simply could not wish for a better advisor.

I owe my deepest gratitude to Dr. Zeki Demirbilek of the US Army Corps of Engineers for his prompt assistance on many occasions during the course of this study. I really enjoyed over-the-phone discussions with him and have learnt a lot of new things in the last one and a half year. Some parts of this study were not possible without his support.

I would also acknowledge my committee co-chair, Dr. Jennifer L. Irish, and committee member, Dr. David Brooks, for their helpful suggestions to improve the thesis. I also appreciate their motivating compliments towards my efforts, and the recommendations they provided for future work.

I am thankful to all my colleagues and friends for their support in the successful completion of this thesis. Being a sports fan, I am thankful to Gaurav for teaching me tennis when I missed playing cricket a lot. Thanks to my roommate, Ashwin, for the delicious South Indian cuisine.

Last, but not the least, words fail to express my appreciation for my family. I feel extraordinarily fortunate to have an unwavering support and love from my parents and

my brother. Without my parents' sacrifices and the hardships in their life, I would have never succeeded in my endeavors.

TABLE OF CONTENTS

Page

Page

# LIST OF FIGURES

FIGURE Page

FIGURE Page

FIGURE Page

# 1. INTRODUCTION, LITERATURE REVIEW AND STUDY OBJECTIVES

## 1.1 Introduction

Wave-induced circulation, resulting from wave transformation, is a typical feature of coastal environments. Strong currents and large variations in the mean sea level (MSL) are commonly observed in unsheltered portions of beaches. In these regions, many coastal management projects are carried out to tackle the prevailing challenges, such as, regulating littoral transport, managing the discharge of wastes and effluents into the sea, shore protection and stabilization, erosion control, etc. Artificial structures like breakwaters, seawalls, groins, jetties, piers, etc., are constructed as a part of these projects. Jetties are mostly designed to improve the transport of sediments and pollutants in a predictable way and to protect and restore coasts. Breakwaters are designed to reduce the wave-heights and the formation of strong rip-currents. Similar to breakwaters, seawalls are solid structures but usually constructed inside the surf-zone to protect coastal land and buildings from wave-overtopping and erosion. While jetties can function like breakwaters and groins, they may also be utilized to alter river flow and to protect inlets and ship channels from tidal erosion and wave action. Despite these advantages, the cost of construction and maintenance of these structures is very high.

---

This thesis follows the style of *Journal of Waterway, Port, Coastal, and Ocean Engineering.*

Therefore, the task for coastal engineers and designers is to design them in an efficient way to minimize the probability of structural failure. Silvester and Hsu (1997) presented a global study of structural damage in coastal areas. In most cases, strong scouring because of currents has been the major reason for structural failure, rather than the structural design. The study of scouring effects in the vicinity of structures (for example, Jyothi et al. (2000), Whitehouse (1998)) often requires the reliability of available information of nearshore depth-averaged velocity field. Hence, the accuracy of available information related to nearshore dynamics, either from field observations and theoretical relations or from available numerical models, is crucial for the successful completion of these projects.

In this study, we examine nearshore circulation in a variety of coastal environments exposed to waves. To explain the mechanism of nearshore circulation, the concept of the radiation stress tensor was first introduced by Longuet-Higgins and Stewart (1964). They defined these stress components as the excessive momentum flux associated with waves, which in fact is analogous to normal and shear stress on the water column underneath the surface**.** The spatial gradients of the radiation stress tensor, also called the wave-induced forcing, are mainly responsible for the wave-induced nearshore circulation. In later years, efforts have been made by researchers (Bettess and Bettess (1982), Dingemans et al. (1987)) to modify the existing formulations for wave-induced forcing.

In practice, several depth-integrated, time-averaged, formulations for radiation stress or wave forcing can be used for coastal engineering applications. Among these

formulations are: (1) a simplified expression for the radiation stress (Longuet-Higgins and Stewart (1964)) valid for a forward propagating wave over a flat bottom; (2) a generalized expression for the radiation stress (Bettess and Bettess (1982)) applicable to an arbitrary linear wave field and (3) a direct expression for wave-forcing proposed by Dingemans et al. (1987), hereafter referred to as "Dingemans' approach", which is basically the rotational part of generalized wave-forcing. The first objective of this study is to investigate the performance of these forcing formulations under different conditions.

As regards the three methods, the computation of wave-forcing, in general, is performed using the modeled quantities obtained from a wave model. In recent years, extensive research efforts have been invested in developing wave models which incorporate one of these formulations for wave-forcing. These wave models can be categorized into two distinctive classes: the phase resolving models (e.g. REF/DIF (Kirby and Dalrymple (1994)), PHAROS (Kostense et al.(1988)), CGWAVE (Demirbilek and Panchang (1998)), RCPWAVE (Ebersole (1985)), etc) that are based on mass-balance equation and the phase averaged/decoupled models (SWAN (Booij et al. (1999)), STWAVE (Smith et al. (2001)) , etc) that are based on energy-balance equation. In most wave models (for example, STWAVE, REF-DIF1 and SWAN), the simplified expression for wave-forcing is used. In fact, this appears to be widely used in the literature (see later discussion). It is important to note that the implementation of the simplified expression in a wave model requires prior knowledge of the wave propagation angle at grid points. Hence, the simplified expression may not be appropriate in the

presence of structures because the wave-field no longer remains progressive, due to the reflection and diffraction. Furthermore, for domains where substantial irregularities occur in the bathymetry, wave rays may cross forming a focusing zone (caustic). For example, in the case of wave propagation over a large submerged shoal, caustics can occur behind the shoal (Bondzie and Panchang (1993)). The wave propagation angle in such situations is not defined. Despite these limitations, several published studies in the field of wave-induced circulation (e.g. Liu and Mei (1976); Choi et al. (2009), Pham (2009)), have used the simplified expression for wave-forcing. For a case of wave propagating over a submerged shoal, Choi et al. (2009) obtained the wave-induced current field using the simplified expression of wave-forcing, evaluated with the wave models of both categories discussed above. They mentioned that the use of a single representative angle (from the complex potential of REF-DIF1) to calculate the radiation stress (instead of using the correct approach of decomposing the waves into directional components and estimating individual contributions, results in an unrealistic circulation pattern. However, using the output from the SWAN model, in which each grid point has a wave direction for a particular spectral bin, the modeled currents were reasonable, despite some inconsistencies in modeled wave-heights resulting from ignoring phase interference between multi-directional components. Other than this passing examination by Choi et al. (2009), the effect of using the simplified formulation in such situations has not been rigorously addressed in the past.

In the context of wave reflection, several published studies explain the role of wave reflection in altering the nearshore processes. In the presence of structures,

phenomena like wave-diffraction and reflection may lead to a complex wave and circulation patterns. In many studies of wave-induced circulation and scouring in the presence of breakwaters and seawalls, it has been stated that the formation of equilibrium scour/deposition profile on the offshore side of the structure is mainly due to the formation of partial or full standing waves. Silvester and Hsu (1997) concluded that the deposition occurs underneath the antinodes of wave profile whereas scouring occurs under the nodes. Sumer and Fredsoe (2000) noticed the similar pattern for the scour/deposition profile. They also mentioned that for the case of oblique wave incidence, the alongshore currents together with the wave action may increase the scour depth in comparison to the normal incidence case. Herbich (1991) studied the scouring effects for the waves breaking near the seawall and suggested that the combination of breaking and reflection may increase the severity of erosion problem near the structures. In a similar study of wave-interaction with the seawalls in nearshore areas, the experimental and theoretical results of Jones (1975) showed that the corresponding longshore current has a maximum value at the toe of the seawall which leads to maximum net erosion near the toe line. The use of simplified expression for wave-forcing in these situations may lead to design flaws as a consequence of using erroneous modeled quantities. To overcome this problem, Ruggiero and McDougal (2001) and Rakha and Kamphuis (1997) used a modified expression for the wave radiation stress in their analytical models to predict wave set-up and longshore currents on the beaches with seawalls. Although the modified expression accounts for the reflected component of the waves, their models are strictly one-dimensional and can only be applied to an

infinite beach sheltered by a seawall parallel to the beach. modified expression of wave radiation stress which accounts for the reflected component of the waves, their models are strictly one-dimensional and can only be applied to an infinite beach sheltered by a seawall parallel to the beach.

As an alternative, one could suggest using the generalized expression of Bettess and Bettess (1982) for the cases where wave reflection or back-scattering is considerable. The generalized expression is a function of the complex velocity potential; unlike the simplified expression, a prior knowledge of wave propagation angle is not required; and it is applicable in all cases. Although the generalized formulation was proposed many years ago, studies of its implementation in the coastal engineering field are limited. Watanabe and Maruyama (1986) have used it to calculate the radiation stress components for the case of a detached breakwater but they did not discuss the wave-induced circulation driven by this forcing. Newell et al. (2005) utilized velocity potentials obtained from an elliptical mild-slope equation based model to calculate generalized wave-forcing and the corresponding current field for the case of a detached breakwater. However, their emphasis was more on the development of a finite-element circulation model and they did not discuss advantages of choosing the generalized form over other two approaches. In most of their applications, either the effect of reflection on the induced circulation was not substantial or the results were not presented in the areas of strong reflection, for example, on the offshore side of the detached breakwater. Also, there was no discussion about many numerical (see below) and practical issues that involve the coupling of models of this kind.

In general, the implementation of the generalized form in a wave prediction model requires the calculation of higher-order derivatives. Dingemans et al. (1987) hypothesized that this can be a source of numerical errors. They recommended ignoring the irrotational part in the generalized form that, based on their hypothesis, is unable to drive depth–averaged currents. This may eliminate undesirable and unpredictable numerical errors. Again, the applicability and the limitations of their proposed modification for complex domains have not been addressed in published studies. We consider some additional cases to better understand the performance of Dingemans' approach. However, this formulation is unsuited to the simple case of a standing wave and has been explored by Dingemans et al. (1987) only for a simple coastal geometry of a cosine-squared protuberance of coastline on a sloping beach. Therefore, a thorough investigation of their approach is carried out in this thesis for more complex domains. In addition, for these domains the performance of the generalized wave forcing expression is also examined to address the effect of numerical errors.

To ascertain the accuracy of wave-forcing from various formulations, a robust wave model which can handle wave reflection, refraction, diffraction and the energy dissipation due to breaking is a prerequisite. It is well known that the phase-resolving wave models are better suited to domains with complex bathymetric and geometric features, where the effects of wave diffraction and reflection can be important. Therefore, a phase resolving model based on the elliptic mild-slope equation is used in this study. Unlike mild-slope wave models based on parabolic approximation the elliptic equation is more general and has no intrinsic limitations domain shape, angle of wave

incidence or the degree and direction of wave reflection and scattering of waves. Wave breaking effects in two-dimensional mild-slope elliptic wave model can be included as discussed by Zhao et al. (2001).

As discussed in the preceding paragraphs, various expressions for wave-forcing are available and the elliptic mild-slope wave model is used to compute the wave-forcing However, the actual quantities of interest for coastal engineering applications are mainly the set-up/set-down and the current field driven by wave-induced forcing. To study the effects of different formulations on these quantities of engineering interest, an appropriate two-dimensional circulation model that must be coupled with the wave model. Here we use the finite-element model ADCIRC since it has been used for coastal engineering applications related to nearshore circulation (see for example, Blain and Cobb (2003)). A series of tests is performed to check the performance of the ADCIRC model with analytical and published results.

In summary, in this study, we wish to address the following questions:

(1) Can the engineer use the existing models, which are mostly based on the simplified expression for wave-forcing, for a general coastal engineering application? If no, under what circumstances is it reasonable to use these models?

(2) Does the use of generalized expression produce unacceptable numerical errors? If no, can it be used for general coastal applications?

(3) What are the advantages and disadvantages of Dingemans' approach? Does it perform better than other two forcing formulations?

(4) What are the issues associated with the coupling of two widely-used finite-element models: a wave model of resolution L/10 (L=wavelength), say and a shelf-scale circulation model? How do various aspects of the circulation model (e.g. boundary conditions, grid resolution etc.) affect the solution?

The outline of this thesis is as follows: Section 2 describes the governing equation and some salient features of the elliptic mild-slope wave model. A brief discussion of various boundary conditions relevant to this study is also included. In Section 3, we provide a detailed description and the expressions for different wave-induced forcing formulations. The implementation of these formulations in the wave model is discussed and then verified using some analytical and published results. The governing equations along with the relevant features of the circulation model are described in Section 4. Some validation cases pertaining to this study are also included. Section 5 provides the results of wave-induced setup/down and current field for domains with general coastal features. For each case, the physical mechanism of circulation is explained and the comparison of results from different wave forcing formulations is presented. Concluding remarks and recommendations for future research are given in Section 6.

# 2. WAVE PREDICTION MODEL

Reliable information about wave climate in coastal areas is crucial to coastal engineering applications, such as, near-shore circulation and morphological changes, shore-protection and design and maintenance of navigation channels, ports and harbors and other coastal structures, etc. When observational studies at sites are not sufficient and the available data from buoys and satellite measurements are inadequate, engineers and designers often simulate the wave climate using wave prediction models.

Most wave prediction models can be categorized into two distinct classes: phase resolving models that are based on the mass-balance equation and phase-averaged models that are based on the energy-balance equation. The phase-resolving wave models are better suited to domains with complex bathymetric and geometric features, where the effects of wave diffraction and reflection can be important. On the other hand, the phase-averaged models are mostly used to study wave growth and transformation over large domains where wave diffraction and reflection are less important.

In this thesis, we simulate wave-induced circulation in a general coastal environment, which may contain numerous complexities, for example, completely arbitrary geometric shape and bathymetric features, natural and artificial structures like islands, jetties, breakwaters, etc. These complexities may induce wave reflection, diffraction, refraction and dissipation due to friction, breaking, etc. These phenomena can contribute to wave transformation in coastal areas and consequently alter the nearshore circulation. An appropriate wave model to accommodate these complexities

for the spectrum of practical wave conditions is therefore a primary requirement. Hence for this study we use a phase-resolving, finite-element model which solves the elliptic form of mild-slope equation (see later discussion). Although the governing equation and several related models (CGWAVE, PHAROS, EMS) have been developed in the last two decades, some important features relevant to this study are discussed in the following sections.

## 2.1 Elliptic mild slope wave models

### *2.1.1 The governing equation*

The standard form of the two-dimensional elliptic mild-slope wave equation is given as follows:

$$\nabla(CC_g\nabla\phi) + (CC_g k^2)\phi = 0 \tag{2.1}$$

where $C(x,y)$ is the phase velocity; $C_g(x,y)$ is the group velocity and $k(x,y)$ is the wavenumber evaluated using the dispersion relation of the form:

$$\sigma^2 = gk\tanh(kd) \tag{2.2}$$

Eq. (2.1) is a two-dimensional, vertically-integrated form of the time-harmonic complex Laplace equation:

$$\nabla^2\Phi(x,y,z) = 0 \tag{2.3}$$

where the velocity potential, $\Phi$, can be expressed for periodic waves in the form:

$$\Phi(x,y,z) = \mathrm{Re}\left(\phi(x,y)\frac{\cosh(k(h+z))}{\cosh(kh)}\exp(-i\omega t)\right) \tag{2.4}$$

where $i = \sqrt{-1}$, Re stands for the real part of and $\phi$ is the complex velocity potential:

$$\phi(x, y) = \phi_1(x, y) + i\phi_2(x, y) = A\exp(is) \tag{2.5}$$

where $\phi_1$ and $\phi_2$ are real and imaginary parts of complex velocity potential and A(x,y) and s(x,y) are the amplitude and phase of the complex potential which result from the solution of Eq. (2.1). The wave height (H), sea surface elevation ($\eta$) and wave propagation angle ($\theta$) at a grid location can be obtained from complex potential $\phi(x, y)$ as follows:

$$H = \frac{2\sigma}{g}\sqrt{\phi_1^{\,2} + \phi_2^{\,2}} \tag{2.6}$$

$$\eta(t) = (\eta_1 + i\eta_2)\exp(-i\omega t) = -\frac{1}{g}\frac{\partial \phi}{\partial t} \tag{2.7}$$

$$\theta = \arctan\left(\frac{\partial s/\partial y}{\partial s/\partial x}\right) \tag{2.8}$$

The expression for $\theta$ given by Eq. (2.8) is strictly valid for a progressive wave field only. At locations where wave reflection, diffraction and focusing (crossing of wave rays) occurs; the use of Eq. (2.8) may produce spurious results. In fact, in such situations the wave direction (propagation angle) is not defined, even though it has been used in several studies (e.g. Liu and Mei (1976), Choi et al. (2009)).

Eq. (2.1) is valid for mildly sloping (such that $|\nabla h| / kh << 1$) beaches (Berkhoff 1976). Although this condition is usually met in most coastal engineering applications, the extended form of Eq. (2.1) with steep slope modifications is described later. More

important, the solution of $\Phi$ from Eq. (2.4) does not inherit the assumption of constant water depth in the domain.

### *2.1.2 Other relevant mechanisms*

#### *2.1.2.1 Depth-induced wave breaking*

As mentioned earlier, in this thesis, for the most part we are concerned with the modeling of waves and wave-induced circulation in a coastal environment. Wave transformation inside the surf-zone and the nearshore circulation pattern are largely influenced by the manner in which wave energy dissipates inside the surf-zone. Therefore, for this study we need a proper wave-breaking model for use with a two-dimensional elliptic mild-slope equation model. A number of breaking models to account for the energy-dissipation inside surf-zone are found in the literature.

Many researchers ( Booij (1981); de Girolamo et al. (1988)) have proposed a parameterized dissipation term to include wave breaking effects in the mild-slope equation (Eq. (2.1)):

$$\nabla(CC_g\nabla\Phi) + (CC_g k^2 + iC_g\sigma W)\Phi = 0 \qquad (2.10)$$

where $W$ represents a dissipation factor.

Zhao et al. (2001) developed a technique to incorporate wave breaking effects in a two-dimensional mild-slope equation and explored the behavior of solution when breaking is included. They examined five different parameterizations for $W$ and concluded that the formulations of Battjes and Jansen (1978) and Dally et al. (1985) produce the most reliable results with mild-slope models. For the current study, we are

using the breaking model of Dally et al. (1985) because of its capability to handle wave reflection in a reliable manner (de Girolamo (1988)).

According to Dally et al. (1985), when waves propagate towards a shoreline on a sloping beach, if the wave height (H) to depth (h) ratio decreases below a certain threshold value (H/h $\cong$ 0.35-0.40), the waves reach a stable condition and stop breaking. At this point, waves attain a stable energy flux $(C_g E)_S$ which can be defined as the energy flux at H/h = 0.35-0.40. Based on this theory, they proposed an energy propagation model of the form:

$$\frac{\partial}{\partial x}(C_g E) = -\frac{K}{h}\left[C_g E - (C_g E)_S\right] = -D \qquad , \quad H_S = \Gamma h \tag{2.11}$$

where $D = WE$ *and* $E$ = wave energy per unit square area; $K$ and $\Gamma$ are the parameters known as the stable wave factor and wave decay factor.

For situations where bottom slope varies over a large range, Dally et al. (1985) recommended to use the values $K$ =0.15 and $\Gamma$= 0.40. Further, for shallow water $W$ in Eq. (2.10) can be expressed in a simplified form as:

$$W = \frac{K}{h}\left[1 - \frac{\Gamma^2 d^2}{H^2}\right] \tag{2.12}$$

Therefore, to apply the model of Dally et al. (1985) for a given domain, the following information is required: (1) the wave height and still water depth at a known near-shore location, (2) the wave height to water depth ratio at the point of incipient breaking, and (3) the bottom profile.

#### *2.1.2.2 Steep slope effects*

To overcome the "mild-slope" requirement discussed above, Chamberlain and Porter (1995) and Chandrasekera and Cheung (1997) developed extensions of Eq. (2.1) to include steep slope effects. The extended form may be described by the following equation:

$$\nabla(CC_g\nabla\Phi)+(CC_gk^2+iC_g\sigma W+f_1(\Delta h)^2+f_2(\Delta^2 h))\Phi=0 \qquad (2.13)$$

where $f_1$ and $f_2$ are the functions of local depth.

For this study, we solve Eq. (2.13) to obtain wave field at all grid locations.

### *2.1.3 Boundary conditions*

A typical coastal domain, on which the elliptic equation (Eq. (2.13)) is solved, is shown in Fig. 2.1. This model domain may include closed and open boundaries. Along these boundaries, appropriate boundary conditions must be specified. A description of a closed and an open boundary together with associated boundary conditions is provided here.

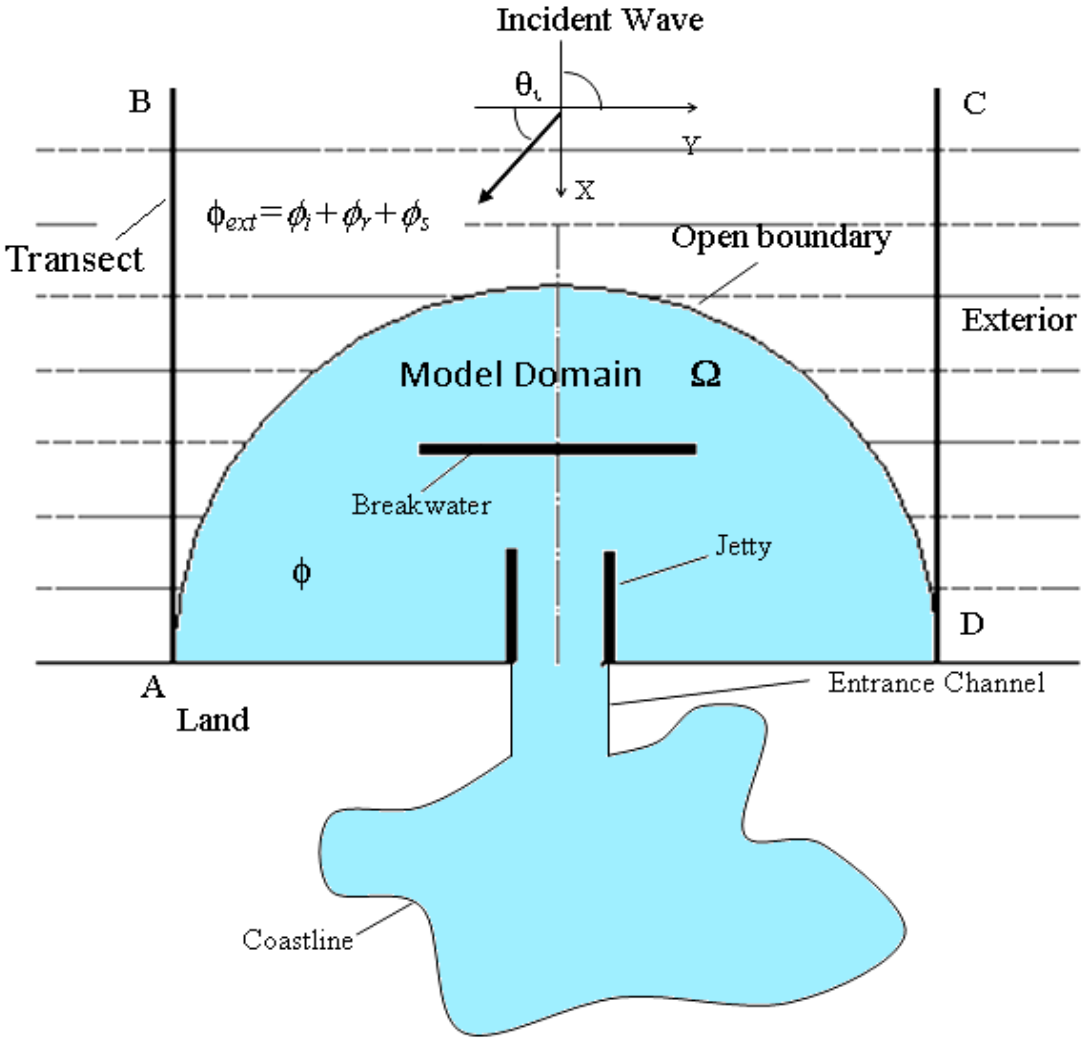


Fig. 2. 1. Definition sketch of a typical wave model domain

### *2.1.3.1 Closed boundary condition*

The elliptic mild-slope equation is applied to the domains which are enclosed by closed boundaries represented by arbitrary shaped coastlines or surface-penetrating structures like breakwaters, jetties, pier legs, seawalls, etc. The following boundary condition (e.g. Berkhoff, 1976) has been used in this study:

$$\frac{\partial \phi}{\partial n} = ik\frac{1-K_r}{1+K_r}\phi \tag{2.14}$$

where n is the normal directed outward to the boundary and $K_r$ is the reflection coefficient which varies between 0 and 1.

### *2.1.3.2 Open boundary condition*

As depicted in Fig. 2.1, the open-boundary is an artificial semi-circular boundary separating the area being modeled from the exterior region. In the area outside the open boundary, total potential is comprised of three wave components:

$$\phi = \phi_i + \phi_r + \phi_s \tag{2.15}$$

where $\phi_i$ = incident wave potential used to force the model at open boundary, $\phi_r$ = a reflected wave that would exist in the absence of the harbor and $\phi_s$ = a backscattered wave created by the harbor that leaves the domain from the open boundary and must satisfy Sommerfield boundary condition.

A summary of the procedure developed by Zhao et al. (2001) to formulate a boundary condition along the semicircle is given here. The exterior region is represented by two one-dimensional transects (see Fig. 2.1) denoted by AB and CD (with depth variation in the cross-shore direction only). The incident wave is specified at the offshore end. The following one-dimensional version of the governing equation is used to solve for the combination of $\phi_i$ and $\phi_r$ (denoted by $\phi_0$) along the transects:

$$\frac{d}{dx}(CC_g\frac{d\phi_0}{dx}) + CC_g k(k\cos^2\theta + iW) = 0 \tag{2.16}$$

This equation is solved using a finite difference scheme and the result $\phi_o$ is then laterally mapped on to the semicircle. For the scattered wave, the radiation condition can be written in approximate form as follows:

$$\frac{\partial \phi_s}{\partial n} = (ik - \frac{1}{2r})\phi_s \tag{2.17}$$

For certain specific cases, an alternative form of $\phi_s$ is given by the Bessel-Fourier series (for details, see Panchang et al. (2000)).

Substituting $\phi_s = \phi - \phi_0$ into equation Eq. (2.17) gives the appropriate radiation equation for the scattered wave and completes the treatment of the open boundary condition:

$$\frac{\partial \phi}{\partial n} = \frac{\partial \phi_0}{\partial n} + (ik - \frac{1}{2r})(\phi - \phi_0) \tag{2.18}$$

### *2.1.4 Solution procedure*

Typically, Eq. (2.1) can be solved by discretizing the model domain using finite-element or finite-difference method. After discretization, the governing equation (Eq. (2.1)) along with appropriate boundary conditions may be expressed in matrix form as

$$[A][\phi] = [B] \tag{2.19}$$

where $[\phi]$ is the vector of all unknown potentials. Depending upon the domain size and the desired resolution of L/10, a typical harbor domain can have a large number of nodes, leading to a very large matrix ([A]). Several methods (e.g. Li (1994); Panchang et

al. (1991)), mostly based on some variation of the conjugate gradient (CG) method, have been derived in recent years to obtain a solution of Eq. (2.19).

In this thesis, we use the solution procedure suggested by Panchang et al. (1991) to solve the governing equation using the finite-element method.

### *2.1.5 Nonlinear iteration*

Since the dissipation factor $W$ in Eq. (2.13) is a function of the wave height (according to Eq. 2.12) and is unknown, Eq. (2.13) is solved by iterations. Each set of the solution for a specified $W$ is obtained with several thousand iterations. For the first iteration, linear (without breaking) solution is obtained with $W$ equal to 0. Thereafter, Eq. (2.13) is solved again by updating $W$ every nonlinear round using the resulting wave heights. The process is repeated until the solutions converge.

In summary, for a general domain, the elliptic wave model provides the solution of primary quantities of a wave model, such as wave height or velocity potential, propagation angle, etc. These quantities are then used to evaluate the secondary quantities, such as wave-induced forcing, etc. In Section 3, we provide a brief discussion about the wave-induced forcing and its computation from elliptic wave models.

# 3. WAVE-INDUCED FORCING

Oceanic circulation is driven by the forces acting upon the water mass, such as wind stress, the Coriolis force, wave radiation stress, the gradients of salinity, temperature and tidal forcing, etc. However, in the nearshore regions, where phenomena like wave shoaling, wave breaking, friction, etc. occurs, the wave-induced forcing generally predominates. As a consequence, fluctuations in the Mean Sea Level (MSL) are observed in the nearshore regions. A rise in the MSL above the Still Water Level (SWL) in the region shoreward to the breaker line is called wave set-up; a decline in the MSL is referred to as wave set-down. These changes in the sea level may sometimes lead to complex circulation patterns in nearshore areas. For the better understanding of these nearshore phenomena, in this section we discuss their mathematical and physical relationship with wave-induced forcing. In addition, we discuss various wave-forcing formulations, associated approximations, and their implementation in elliptic mild-slope wave models discussed earlier in Section 2.

## 3.1 Introduction to wave-induced forcing

After the introductory reports by Munk (1949) on the field studies of wave-induced set-up/down and Putnam (1949) who suggested that the magnitude of longshore currents along beaches is somehow related to the momentum flux associated with the waves, Longuet-Higgins and Stewart (1964) introduced the concept of radiation stress, also called excess momentum flux associated with waves. They also explained the

relevance of this forcing in the study of various coastal processes, for example, wave-induced set-up/down, cross-shore and longshore currents, infragravity waves, transport of sediments and pollutants, etc.

The transport of momentum associated with the waves is analogous to normal and shear stresses acting on a water column underneath the sea surface. The horizontal variation in these stress components (due to the variation in wave field) generates forces on a water column (see Fig. 3.1) and creates set-up/down of the MSL. In oceanic waters, since there is negligible spatial variation in the momentum flux or the stress components, change in the MSL is not considerable. Most of the energy acquired by the waves in the open ocean is dissipated when the waves encounter a narrow surf-zone near the coast and start breaking. As a result, a significant variation in momentum flux inside the surf-zone generates forces on the water mass. Other factors, which are responsible for wave transformation and wave-induced forcing, may include wave shoaling, reflection, diffraction, wave-wave and wave-current interaction, etc. Mathematically, the expression for wave induced forcing is given by:

$$F_i = -\frac{1}{\rho}\frac{\partial S_{ij}}{\partial x_j} \tag{3.1}$$

where in general, $S_{ij}$ = radiation stress tensor defined as the excess momentum flux directed in $i^{th}$ direction across plane $j$ = constant, and $F_i$ = wave-induced forcing in $i^{th}$ direction due to the horizontal variation in $S_{ij}$.

In simple words, the concept of wave-induced forcing is analogous to the forces acting on a water column due to the pressure variation. For example, if there is an

increase in pressure along the positive x-direction, a force in the opposite direction acts on the water column. Similarly, if the momentum flux decreases along x-direction (e.g. due to breaking inside the surf-zone), a force is induced in the positive x-direction as shown in Fig 3.1.

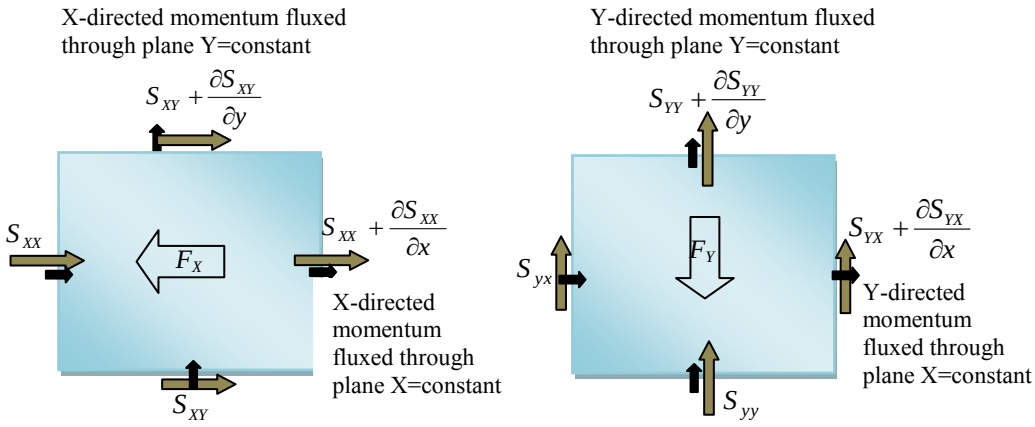


Fig. 3.1. Wave-induced forcing, definition sketch

## 3.2 Balance equation for depth-averaged mean currents

A momentum balance equation for the depth-averaged, wave-averaged nearshore currents was derived by Longuet-Higgins and Stewart (1964). This equation relates nearshore circulation to the active nearshore mechanisms, such as, the wave-induced forcing, bottom and surface stresses, turbulence effects, etc. To better understand the discussion in later sections, we summarize the detailed derivation procedure (Svendsen (2006)) in the following steps:

*Step 1*: Consider the equations for momentum conservation in x, y and z directions respectively for the free surface flow without bottom and surface stresses and turbulence:

$$\frac{\partial u}{\partial t}+\frac{\partial (u^2)}{\partial x}+\frac{\partial (uv)}{\partial y}+\frac{\partial (uw)}{\partial z}=-\frac{1}{\rho}\frac{\partial P}{\partial x} \tag{3.2a}$$

$$\frac{\partial v}{\partial t}+\frac{\partial (uv)}{\partial x}+\frac{\partial (v^2)}{\partial y}+\frac{\partial (vw)}{\partial z}=-\frac{1}{\rho}\frac{\partial P}{\partial y} \tag{3.2b}$$

$$\frac{\partial w}{\partial t}+\frac{\partial (uw)}{\partial x}+\frac{\partial (vw)}{\partial y}+\frac{\partial (w^2)}{\partial z}=-\frac{1}{\rho}\frac{\partial P}{\partial z}-g \tag{3.2c}$$

*Step 2*: Using the Leibniz rule, the bottom boundary condition and the kinematic free surface boundary condition from the linear wave theory, the vertically-integrated form of the x-direction momentum equation (Eq. (3.2a)) is given by:

$$\frac{\partial}{\partial t}\int_{-h}^{\eta} u dz+\frac{\partial}{\partial x}\int_{-h}^{\eta} u^2 dz+\frac{\partial}{\partial y}\int_{-h}^{\eta} uv dz=-\frac{1}{\rho}\frac{\partial}{\partial x}\int_{-h}^{\eta} p dz+\frac{p_{-h}}{\rho}\frac{\partial h}{\partial x} \tag{3.3}$$

where $\eta=\overline{\eta}+\eta_w$ is the total free surface displacement; $\eta_w$ = free surface elevation due to a wave-field (such that $\overline{\eta}_w=0$) and $\overline{\eta}=\left\{\frac{1}{T}\int_0^T \eta(x,y,t)dt\right\}$ is the mean deviation in the MSL from the SWL.

*Step 3:* Similarly, the vertically-integrated form of the z-direction momentum equation (Eq. (3.2c)) is:

$$\frac{\partial}{\partial t}\int_{-h}^{\eta} w dz + \frac{\partial}{\partial x}\int_{-h}^{\eta} uw dz + \frac{\partial}{\partial y}\int_{-h}^{\eta} vw dz - \int_{z}^{\eta} w^2 dz = -\frac{1}{\rho}\int_{z}^{\eta}\frac{\partial P}{\partial z} dz - \int_{z}^{\eta} g dz \tag{3.4}$$

Therefore, the equation for vertical variation in pressure (*P)* from Eq. (3.4) is given as:

$$P = \rho g(\eta - z) - \rho w^2 + \frac{\partial}{\partial t}\int_{z}^{\eta} w dz + \left\{\frac{\partial}{\partial x}\int_{z}^{\eta} uw dz + \frac{\partial}{\partial y}\int_{z}^{\eta} vw dz\right\} \tag{3.5}$$

Using the periodicity of harmonic waves, the following expression for mean bottom reaction force, $\overline{P}_{-h}$, can be obtained by substituting *z* = -*h* in Eq. (3.5):

$$\overline{P}_{-h} = \overline{\rho g(h+\eta)} + \underbrace{\left\{\frac{\partial}{\partial x}\overline{\int_{z}^{\eta} uw dz} + \frac{\partial}{\partial y}\overline{\int_{z}^{\eta} vw dz}\right\}}_{at\ z=-h} \approx \rho g(h+\overline{\eta}) \tag{3.6}$$

*Step 4*: The time-averaging of the depth-averaged x-direction momentum equation (Eq. (3.3)), substitution of $\overline{P}_{-h}$ and a subsequent rearrangement of the terms gives:

$$\overline{\frac{\partial}{\partial t}\int_{-h}^{\eta} u dz} + \frac{\partial}{\partial x}\overline{\int_{-h}^{\eta} u^2 dz} + \overline{\frac{\partial}{\partial y}\int_{-h}^{\eta} uv dz} = -\frac{1}{\rho}\frac{\partial}{\partial x}\overline{\int_{-h}^{\eta} P dz} + g(h+\overline{\eta})\frac{\partial h}{\partial x} \tag{3.7}$$

Using Eq. (3.5), the vertically-integrated, time-averaged form of pressure *P* is given by:

$$\overline{\int_{-h}^{\eta} P dz} = \frac{1}{2}\rho g(h+\overline{\eta})^2 - \rho\overline{\int_{-h}^{\eta} w^2 dz} + \frac{1}{2}\rho g\overline{\eta}^2 + \rho\frac{\partial}{\partial x}\int_{-h-h}^{\eta}\int^{\eta}\overline{uw} dz\, dz + \rho\frac{\partial}{\partial y}\int_{-h-h}^{\eta}\int^{\eta}\overline{vw} dz\, dz \tag{3.8}$$

Eq. (3.7) and Eq. (3.8) can be combined to obtain the following balance equation for the depth-averaged, time-averaged currents:

$$-\rho g(h+\overline{\eta})\frac{\partial\overline{\eta}}{\partial x} = \frac{\partial}{\partial x}\left[\int_{-h}^{\eta}\overline{\rho(u^2 - w^2)} dz + \left\{\rho\frac{\partial}{\partial x}\int_{-h-h}^{\eta}\int^{\eta}\overline{uw} dz\, dz + \rho\frac{\partial}{\partial y}\int_{-h-h}^{\eta}\int^{\eta}\overline{vw} dz\, dz\right\} + \frac{1}{2}\rho g\overline{\eta}^2\right]$$

$$+\frac{\partial}{\partial y}\left[\int_{-h}^{\eta}\overline{uv}dz\right]=\frac{\partial S_{xx}}{\partial x}+\frac{\partial S_{xy}}{\partial y} \tag{3.9}$$

where $S_{xx}$ and $S_{xy}$ are the components of wave radiation stress. A similar balance equation in the y-direction, which contains other two stress components ( $S_{yx}$ and $S_{yy}$ ), can also be derived. Based on these balance equations, the stress components in the most generalized form can be expressed as:

$$S_{XX}=\int_{-h}^{\eta}\overline{\rho(u^2-w^2)}dz+\left\{\rho\frac{\partial}{\partial x}\int_{-h}^{\eta}\int_{-h}^{\eta}\overline{uw}dz+\rho\frac{\partial}{\partial y}\int_{-h}^{\eta}\int_{-h}^{\eta}\overline{vw}dz\right\}+\frac{1}{2}\rho g\overline{\eta}^2 \tag{3.10a}$$

$$S_{XY}=S_{YX}=\int_{-h}^{\eta}\overline{\rho uv}dz \tag{3.10b}$$

$$S_{YY}=\int_{-h}^{\eta}\overline{\rho(v^2-w^2)}dz+\left\{\rho\frac{\partial}{\partial x}\int_{-h}^{\eta}\int_{-h}^{\eta}\overline{uw}dz+\rho\frac{\partial}{\partial y}\int_{-h}^{\eta}\int_{-h}^{\eta}\overline{vw}dz\right\}+\frac{1}{2}\rho g\overline{\eta}^2 \tag{3.10c}$$

The wave-induced forcing is described in terms of the gradients of the wave radiation stress components (viz. RHS of Eq. 3.9):

$$F_1=-\frac{1}{\rho}\left(\frac{\partial S_{xx}}{\partial x}+\frac{\partial S_{xy}}{\partial y}\right);\quad F_2=-\frac{1}{\rho}\left(\frac{\partial S_{yx}}{\partial x}+\frac{\partial S_{yy}}{\partial y}\right) \tag{3.11}$$

The balance equation explains that the spatial gradients of $\overline{\eta}$ (wave set-up/down) are balanced by the wave-induced forcing (the gradients of wave radiation stress). In other words, the spatial gradients of momentum flux or radiation stress components respond to the change in the MSL. In the following section, we consider various formulations for wave-induced forcing available in the literature.

## 3.3 Various formulations for the wave-induced forcing

As mentioned earlier in Section 1, several depth-integrated, time-averaged, formulations for radiation stress or wave-forcing are used for coastal engineering applications. Among these formulations are: (1) a simplified expression for the radiation stress (Longuet-Higgins and Stewart (1964)); (2) a generalized expression for the radiation stress (Bettess and Bettess (1982)) and (3) a direct expression for wave-forcing (Dingemans et al. (1987)), hereafter referred to as "Dingemans' approach". A detailed explanation of these forcing formulations, associated approximations and limitations, and their implementation in the elliptic wave model is described below.

### *3.3.1 The simplified wave forcing*

The simplified form of wave-induced forcing is mostly used in the wave prediction models and published studies (see discussion later). This form of the wave-forcing is calculated using the following components of wave radiation stress:

$$S_{xx} = \frac{1}{8}\rho g H^2 \left\{ \left( 2n - \frac{1}{2} \right) - n\sin^2\theta \right\} \tag{3.11a}$$

$$S_{yy} = \frac{1}{8}\rho g H^2 \left\{ \left( n - \frac{1}{2} \right) + n\sin^2\theta \right\} \tag{3.11b}$$

$$S_{xy} = S_{yx} = \frac{1}{8}\rho g H^2 \sin\theta\cos\theta \tag{3.11c}$$

These expressions can be obtained from Eqs. (3.10a-3.10c) by using the following velocity potential function which represents the wave field corresponding to a linear wave propagating over a flat bottom:

$$\Phi = \frac{Hg}{2\sigma}\frac{\cosh k(h+z)}{\cosh kh}\sin(kx\cos\theta + ky\sin\theta - \sigma t) \qquad (3.12)$$

Hereafter in this thesis, we refer to this approach of wave-forcing calculation as 'the simplified approach'. The underlying assumptions associated with this approach are:

(1) Wave field is strictly linear and progressive; i.e. phenomena like wave reflection, diffraction, wave ray crossing, etc. are absent.

(2) Waves are propagating in a region of uniform water depth.

These assumptions are a result of Eq. (3.12). Despite these assumptions, the simplified wave forcing is widely used in the literature even for the domains where a complex wave field may exist due to wave reflection, diffraction and wave ray crossing (see for example, Liu and Mei (1976); Choi et al. (2009), Pham (2009), Jyothi (2002)). Also, many numerical wave models (REF-DIF, SWAN, RCPWAVE, etc.) which are currently used for complex coastal engineering applications, use the simplified approach.

The computation of simplified wave forcing in a wave model requires the knowledge of wave height (H) and wave direction $(\theta)$ at all grid locations. In fact, the wave direction is not even defined in the regions of wave reflection, diffraction and wave focusing. In such cases, a more accurate way to obtain wave-induce forcing will be to decompose the wave-field into multi-directional components and evaluate individual contribution for all the components using Eq. (3.11a-3.11c). However, the decomposition of wave-field into multi-directional components is not straightforward. Therefore, a single representative angle (from complex velocity potential) is generally used to obtain the simplified wave forcing, although it may not be appropriate in

situations where wave-field is not purely progressive. In this study, we also follow a similar approach to assess the simplified wave-forcing.

### *3.3.2 The generalized wave forcing*

The expressions for the radiation stress components given by Eqs. (3.10a-3.10c) are valid for an arbitrary wave field (irrespective of the wave theory) and can be used to compute the generalized wave forcing (using Eq. (3.1)). The generalized wave forcing is evaluated in a wave model using the wave properties, such as, water surface elevation, water particle velocities, etc. Bettess and Bettess (1982) presented a comprehensive derivation procedure to obtain the expressions for the radiation stress components in mild-slope equation based wave models which give the solution of complex velocity potential ($\phi$) in the form:

$$\phi(x,y) = \phi_1(x,y) + i\phi_2(x,y) \tag{3.13}$$

where $\phi_1$ and $\phi_2$ are the real and the imaginary parts of $\phi$ respectively.

The complex horizontal water particle velocities ($u$ and $v$, in the x and y direction respectively) is computed using:

$$u(x,y) = \frac{\partial \phi}{\partial x} = \left( \frac{\partial \phi_1}{\partial x} + i\frac{\partial \phi_2}{\partial x} \right) = u_1(x,y) + iu_2(x,y) \tag{3.14}$$

$$v(x,y) = \frac{\partial \phi}{\partial y} = \left( \frac{\partial \phi_1}{\partial y} + i\frac{\partial \phi_2}{\partial y} \right) = v_1(x,y) + iv_2(x,y) \tag{3.15}$$

where $u_1, u_2$ are the real and the imaginary part of $u$ respectively and $v_1, v_2$ are the real and the imaginary part of $v$ respectively.

. The following expressions for the radiation stress components, which are consistent with the velocity potential solution of the elliptic wave model used here:

$$S_{xx} = \frac{\rho}{8}\left(\frac{\sinh 2kh + 2kh}{k\cosh^2 kh}\right)\left(u_1^2 + u_2^2\right) + \rho\left(\frac{2kh}{k\cosh^2 kh}\right)k^2\left(\phi_1^2 + \phi_2^2\right) + \frac{\rho}{8}\left(\frac{\cosh 2kh - \dfrac{\sinh 2kh}{2kh}}{k\cosh^2 kh}\right)\left(u_1^2 + u_2^2 + v_1^2 + v_2^2 - k^2\left(\phi_1^2 + \phi_2^2\right)\right) \tag{3.16a}$$

$$S_{yy} = \frac{\rho}{8}\left(\frac{\sinh 2kh + 2kh}{k\cosh^2 kh}\right)\left(v_1^2 + v_2^2\right) + \rho\left(\frac{2kh}{k\cosh^2 kh}\right)k^2\left(\phi_1^2 + \phi_2^2\right) + \frac{\rho}{8}\left(\frac{\cosh 2kh - \dfrac{\sinh 2kh}{2kh}}{k\cosh^2 kh}\right)\left(u_1^2 + u_2^2 + v_1^2 + v_2^2 - k^2\left(\phi_1^2 + \phi_2^2\right)\right) \tag{3.16b}$$

$$S_{xy} = S_{yx} = \frac{\rho}{8}\left(\frac{\sinh 2kh + 2kh}{k\cosh^2 kh}\right)\left(u_1 v_1 + u_2 v_2\right) + \rho\left(\frac{2kh}{k\cosh^2 kh}\right)k^2\left(\phi_1^2 + \phi_2^2\right) \tag{3.16c}$$

The above expressions for the stress components can be computed using the linear quantities $\phi$, $u$ and $v$ from the wave model do not require a prior knowledge of wave propagation angle ($\theta$). Therefore, the use of incorrect wave propagation angle or the decomposition of wave-field into the multi-directional components (as discussed in previous section) can be entirely avoided.

Here we also try to explain the physical differences between the generalized wave forcing and the simplified wave forcing. In general, for a forward propagating wave, the term inside the curly brackets (hereafter "T2") on the RHS of Eq. (3.10a) and Eq. (3.10c) vanishes. However, the term T2 may contribute to the total wave forcing if

the wave-field is not purely progressive, for example, in the case of a standing wave discussed later. It is apparent from the steps of the derivation procedure of the balance equation (Eq. (3.9)) that the term T2 enters in the balance equation trough the term inside the curly brackets in the expression for pressure ($P$). In addition, the term inside the curly bracket in the expression for $P$ physically means that some weight of the water column is transferred to the neighboring columns through the water motion. Intuitively, it can be suggested that in the case of forward propagating waves, this is not possible over a long wave period and each water column carries its own weight. Therefore, in the wave-averaged sense, the term T2 is negligible for progressive waves. However, at times when the wave field is not purely progressive, an individual water column may help carrying the weight of neighboring water columns (for example, for a standing wave).

Although there are no simplifying approximations associated with the generalized wave forcing, it involves the computation of the higher order derivatives which may lead to unpredictable numerical errors (Dingemans et al. (1987)). Therefore, it is necessary to: (1) investigate the performance of this forcing for general coastal applications (see Section 5), and (2) consider the approach suggested by Dingemans et al. (1987) which avoids the computation of higher-order derivatives. In the following section, we discuss in detail the formulations suggested by Dingemans et al. (1987).

### *3.3.3 Wave forcing formulation of Dingemans et al. (1987)*

As noted by Dingemans et al. (1987), the use of the generalized wave forcing involves the computation of the higher-order derivatives of velocity potential. They posit

that these higher-order derivative terms, even when evaluated with higher-order splines, lead to numerical problems. Therefore, they proposed an alternative formulation which involves bypassing the calculation of $S_{ij}$ and directly proceeding to the wave-forcing function. To do so, they decomposed the generalized wave forcing into two distinct parts: the rotational part and the irrotational part, given as (in tensor notation):

$$-\frac{4g}{\rho}F^{i}_{rotational}=i\omega W\left(\phi^{*}\frac{\partial\phi}{\partial x_i}-\phi\frac{\partial\phi^{*}}{\partial x_i}\right)+\left(k^{2}\phi\phi^{*}-\frac{\partial\phi}{\partial x_j}\frac{\partial\phi^{*}}{\partial x_j}\right)\frac{\partial}{\partial x_i}\left(CC_g-gh\right)$$

$$+\frac{1}{2}(CC_g-gh)\left[\frac{\partial}{\partial x_j}\left(\phi\phi^{*}\right)\right]\frac{1}{CC_g}\left[\frac{\partial}{\partial x_j}\left(CC_g\right)\right]\frac{1}{h}\frac{\partial h}{\partial x_i}$$

(3.17a)

$$-\frac{4g}{\rho}F^{i}_{irrotational}=h\frac{\partial}{\partial x_i}\left[\frac{\omega^{2}}{h}\left(\frac{2C_g}{C}-1\right)\phi\phi^{*}\right]+\frac{h}{2}\frac{\partial}{\partial x_i}\left[\frac{gh-CC_g}{h}\frac{\partial^{2}}{\partial x_m\partial x_m}\left(\phi\phi^{*}\right)\right]$$

$$-h\frac{\partial}{\partial x_i}\left[\frac{CC_g}{h}\left(k^{2}\phi\phi^{*}-\frac{\partial\phi}{\partial x_j}\frac{\partial\phi^{*}}{\partial x_j}\right)\right] \qquad (3.17b)$$

where $\phi^{*}$ is the complex conjugate of $\phi$ and $W$ is the ratio of dissipated energy (D) to total wave energy (E), and $F_{rotational}+F_{irrotational}=F$ (described in Eq. (3.9)).

Dingemans et al. (1987) suggested that only the rotational part, which is closely related to the wave energy dissipation, is capable of driving the depth-averaged currents. According to their hypothesis, the irrotational part which includes higher order derivatives has insignificant contribution to the depth-averaged currents. Therefore, they suggested avoiding the irrorotational part while computing the wave-induced forcing.

Although the implementation of their hypothesis in a wave model may reduce the numerical errors, its ability to handle the effects of wave reflection in a general coastal domain has never been addressed. Dingemans et al. (1987) themselves considered a simple two-dimensional case of a sloping beach with cosine-squared protuberance of the coastline to investigate the advantages of their formulation over the generalized wave-forcing. The effects of wave reflection and diffraction do not play a significant role for this domain.

In this study, we also examine as Dingemans' approach. Similar to the generalized wave forcing, the expression for $F_{rotational}$ in Eq. (3.17a) can be evaluated using the complex velocity potential and a prior knowledge of wave propagation angle is not required. We make an effort to investigate the performance of Dingemans' approach in Section 5 by studying the nearshore processes for more complex domains.

Furthermore, we introduce another form of the wave-induced forcing which was introduced by Dingemans et al. (1987) by invoking the geometric optics approximation in rotational part. The expression for this forcing (also called dissipation force, $F_{i_i}^{diss}$), which is not considered for detailed investigation in this study, is given as:

$$F_{i_i}^{diss} = \frac{D}{\omega} k_i \tag{3.18}$$

Lowe et al. (2009) used the expression given in Eq. (3.18) to study wave-induced circulation over the reefs and Lesser et al. (2004) implemented it in a three-dimensional flow model. A care should be taken while using Eq. (3.18) for general coastal applications as the geometric optics approximation is valid under the conditions:

$$\frac{\nabla h}{kh}.\frac{\nabla a}{ka} << 1 \qquad ; \quad \frac{\nabla^2 a}{a} << k^2 \tag{3.19}$$

It is also well-known that that the geometric optics approximation fails to produce reliable wave propagation near areas of high wave convergence (caustics) or divergence.

Having provided a detailed description of all major forcing formulations, we now proceed to implement three forcing formulations (the simplified wave forcing, the generalized wave forcing and Dingemans' approach) in the wave model.

## 3.4 Validation of the code for generalized radiation stress formulation and wave forcing computation

To validate the wave-forcing formulations and to check the accuracy of modeled wave-forcing, we consider the following numerical examples for which either analytical solution or published results are available. Four test cases, of increasing complexity, are described below. While the first two cases are elementary, they help to define expected errors, which in turn is of use in evaluating results for more complex cases. The other two cases are used also to obtain a better understanding of the three wave-induced forcing formulations.

### *3.4.1 Progressive waves over a flat bottom*

Based on the linear theory for water waves, the surface elevation for a normally incident, forward-propagating wave (in the *x*-direction) over a flat bottom is given as:

$$\eta = a\sin(kx - \omega t) \tag{3.20}$$

However, as discussed in Section 2, the solution of free surface elevation from the wave model is in the form:

$$\eta = (\eta_1 + i\eta_2)\exp^{-\omega t} = \eta_1\cos(\omega t) + \eta_2\sin(\omega t) \tag{3.21}$$

Comparison of Eq. (3.20) with Eq. (3.21), and the use of the dynamic free surface boundary condition give:

$$\phi_1 = -\frac{ga}{\omega}\cos kx \quad ; \quad \phi_2 = \frac{ga}{\omega}\sin kx \tag{3.22}$$

The substitution of $\phi_1$ and $\phi_2$ (Eq. (3.22)) into the generalized formulation (Eqs. (3.10a-3.10c)) gives the simplified expressions (Eqs. (3.11a-3.11c)).

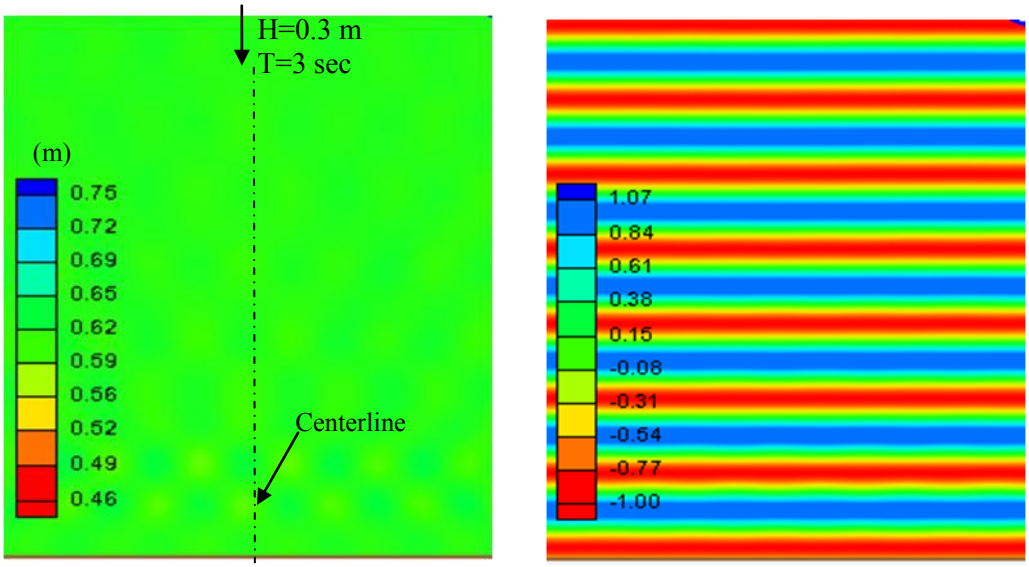


Fig. 3. 2. Progressive wave, modeled wave height (left) and wave phase (right)

To check the accuracy of modeled results, we consider an incident wave condition of normally incident, monochromatic, travelling wave of wave height, $H_0$ =

0.3 m and wave period, T = 3 s. The modeled domain has a uniform water depth of 3 m at all grid locations. Fig. 3.2 depicts the modeled wave height (H) and wave phase for this case. The wave height at most locations is approximately constant ( $\approx$ 0.6 m) with a deviation of 2-3% due to numerical errors. The wave phase diagram shows the characteristics of a purely progressive wave field. Fig. 3.3 shows the comparison between theoretical and modeled stress components ($S_{xx}$ and $S_{yy}$) along the centerline (see Fig. 3.2). Although the modeled results are in good agreement with the theoretical results, differences are of the order of 4-5 %.

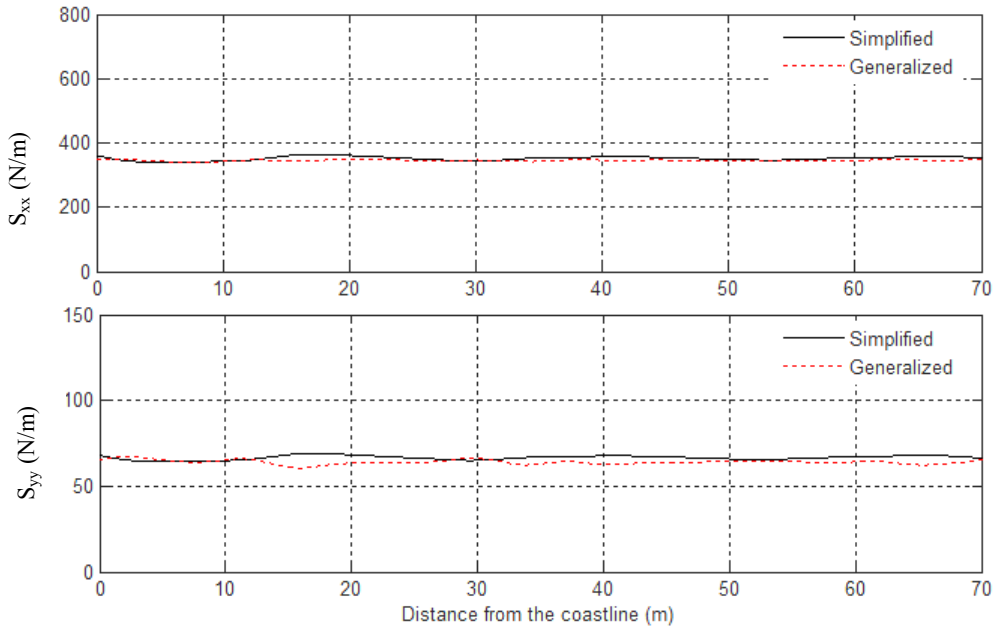


Fig. 3. 3. Radiation stress comparison along the centerline. *Sxx* (top) and *Syy* (bottom)

### *3.4.2 Standing wave in a water tank of uniform depth*

Consider the case of a standing wave formation in a flat-bottom tank due to the superposition of an incident (in the x-direction) and perfectly reflected wave travelling in the opposite direction. Based on the linear theory for water waves, the surface elevation in this case can be expressed as:

$$\eta = a\sin(kx-\omega t) + a\sin(kx+\omega t) = (2a\sin kx)(\cos \omega t) \tag{3.23}$$

Comparison of Eq. (3.23) with Eq. (3.21) and the use of the dynamic free surface boundary condition give:

$$\phi_1 = 0 \qquad ; \qquad \phi_1 = -\frac{2ga}{\omega}\sin kx \tag{3.24}$$

These expressions for $\phi_1$ and $\phi_2$ (Eq. (3.24)) when substituted into the generalized form of radiation stress components (Eqs. (16a-16c)), yields the following expressions for stress components:

$$S_{xx} = \frac{1}{2}\rho g a^2\left[1+\frac{4kh}{\sinh 2kh} - (2kh\coth 2kh)(\cos 2kx)\right] \tag{3.25a}$$

$$S_{yy} = \frac{1}{2}\rho g a^2\left[\frac{4kh}{\sinh 2kh}\sin^2 2kx - \cos 2kx + (2kh\coth 2kh)(\cos 2kx)\right] \tag{3.25b}$$

$$S_{xy} = 0 \tag{3.25c}$$

The above expressions for the stress components are the standard results for a standing wave case. It implies that the derived expressions for the generalized stress components (Eq. (16a-16c)) are correct and able to handle wave reflection. To check the accuracy of modeled results, we consider the case of a standing wave, with the incident wave

condition of wave amplitude, a = 1.0 m and wave period, T = 3 s in a water tank with uniform depth of 3 m. The modeled wave height (H) and wave phase for this case are shown in Fig. 3.4. The wave height, as expected, varies between 0 m and 4 m at most locations and wave phase diagram shows the characteristics of a standing wave (perfect reflection).

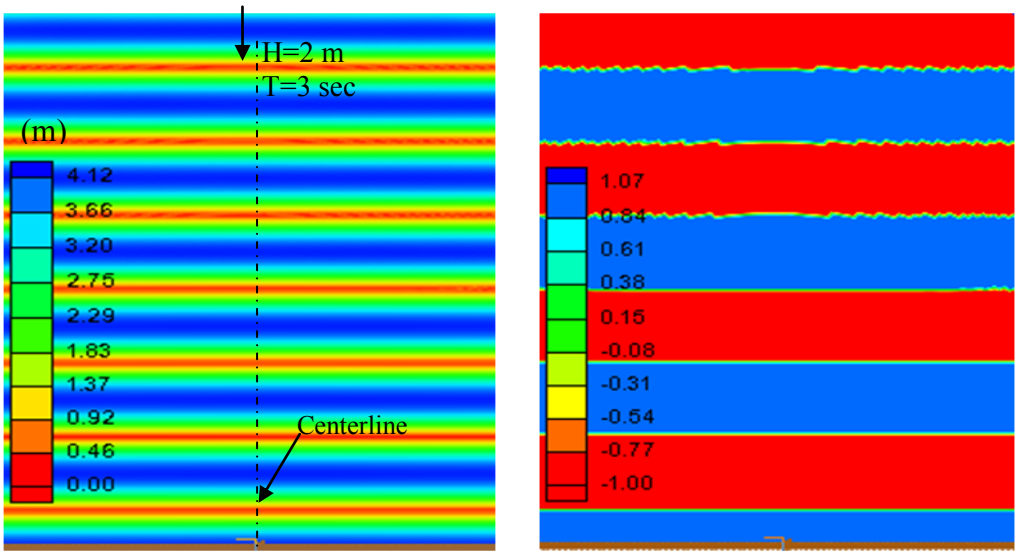


Fig. 3.4. Standing wave, modeled wave height (left) and wave phase (right)

The contour plots of modeled stress components are shown in Fig. 3.5. Fig. 3.6 shows a comparison plot of theoretical and modeled stress components ($S_{xx}$ and $S_{yy}$) along the centerline. Very good agreement is found between the modeled and the theoretical results. In part, this is due to the choice of accurate open boundary condition (i.e. Bessel Fourier).

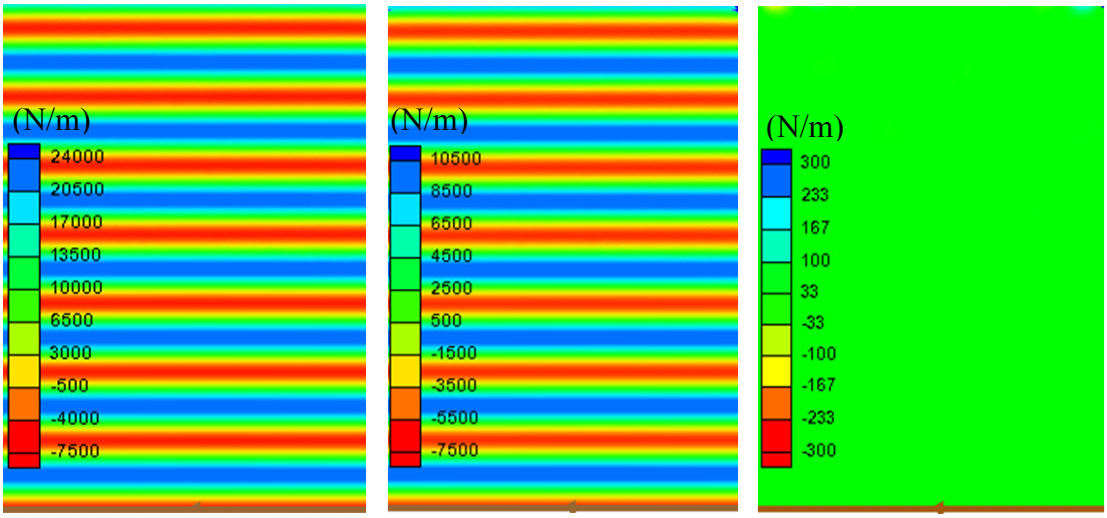


Fig. 3.5. Modeled radiation stress components; $S_{xx}$ (left), $S_{yy}$ (center) and $S_{xy}$ (right)

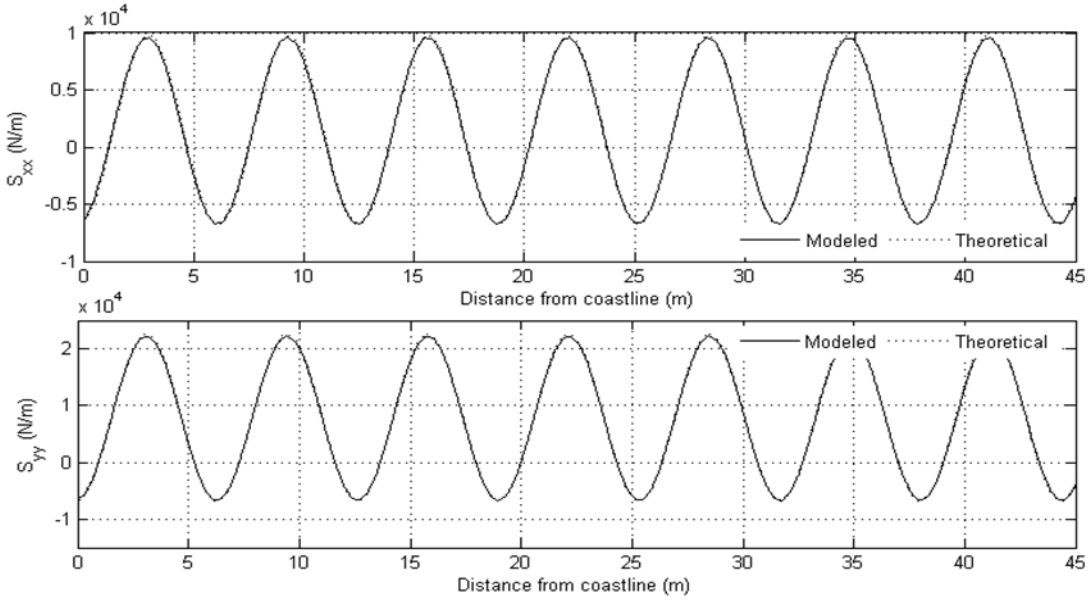


Fig. 3.6. Radiation stress comparison, modeled and theoretical results for $S_{xx}$ (top) and $S_{yy}$ (bottom)

It is important to note here that if the expressions for $\phi_1$ and $\phi_2$ when used to calculate wave forcing with Dingemans' formulations (Eqs. 17a-17b), the rotational part

vanishes and the irrotational part gives an expression which is exactly similar to the wave forcing (the spatial gradients of stress components) for a standing wave case. It implies that the Dingemans' approach ignores the effect of wave reflection. However, a more detailed examination of this approach is carried out in Section 5.

### *3.4.3 Detached breakwater on a sloping beach*

After testing the model's performance for the simple cases of a progressive wave and a standing wave, we now consider the case of a detached breakwater (Watanabe and Maruyama (1986)) on a sloping beach. In the presence of a breakwater, phenomena like wave diffraction and reflection may attribute to a complex wave field. Although analytical solutions for radiation stress components are not available for this case, the calculations of Watanabe and Maruyama (1986) using the generalized formulation, are used to validate the model results. The detached breakwater is situated on a plane beach with uniform slope of 1 in 50. The breakwater was assigned a reflection coefficient of 1.0 to almost perfectly reflect the normally incident waves. The length and thickness of the breakwater are 2.4 m and 0.06 m respectively.

The modeled wave height and wave phase for the input condition of $H_0$ = 2 cm and T = 1.2 s are depicted in Fig. 3.7. The wave height plot shows the presence of a partial standing wave field on the offshore side of the breakwater and the breaking waves near the coastline. The breaking criterion of Dally et al. (1985) is used to account for the energy dissipation inside the surf-zone. It is clear from the phase diagram that the wave field is not purely progressive in the region offshore to the breakwater.

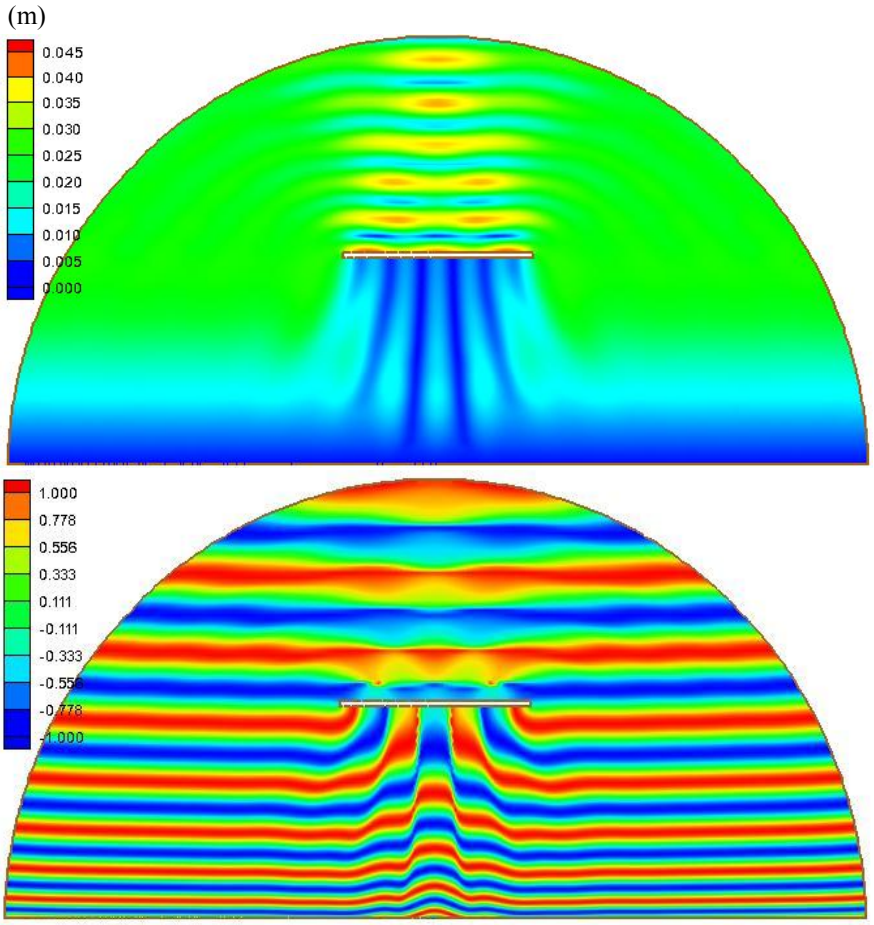


Fig. 3.7. Detached breakwater on sloping beach. Modeled wave height (top) and wave phase (bottom)

The contour plots of radiation stress components from the wave model and the published modeled results of Watanabe and Maruyama (1986) are shown in Fig. 3.8. In both the cases, the calculations are performed using the generalized expressions (Eqs. (16a-16c)).The modeled results are in good agreement with the published results (with some differences in $S_{xy}$ results), since the major contributors in the wave-induced forcing are $S_{xx}$ and $S_{yy}$, we can ignore these differences.

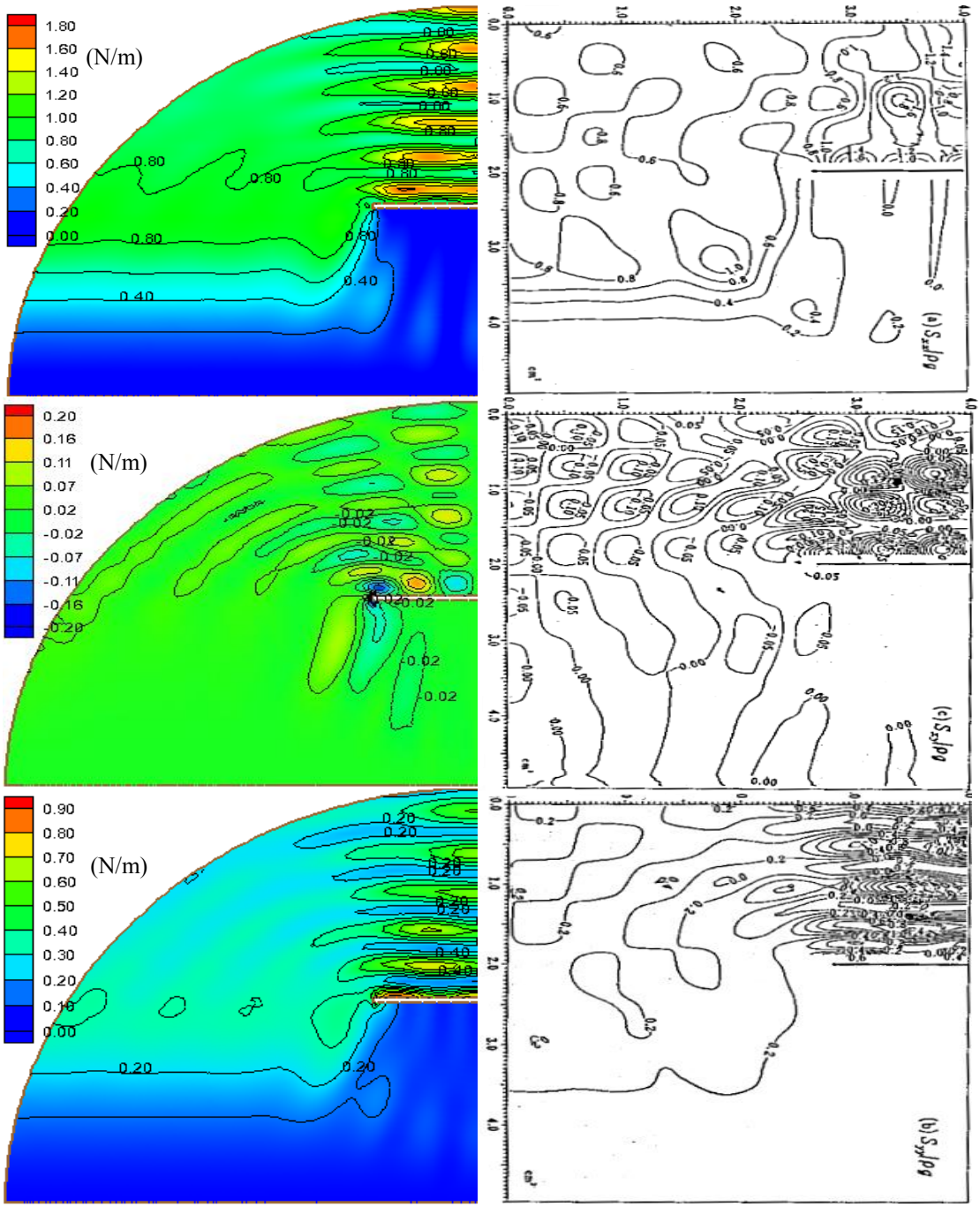


Fig. 3.8 Wave radiation stress comparison, modeled (left column) and published results (right column) of Watanabe and Maruyama (1986); $S_{xx}$ (top), $S_{xy}$ (center), $S_{yy}$ (bottom). Note: geometric scales are different

### *3.4.4 Sloping beach with cosine-squared protuberance of coastline*

In the previous examples, we only focused on the modeled results of wave forcing obtained with the generalized and the simplified approach. As discussed in Section 3.3.3, Dingemans et al. (1987) proposed an alternative approach to calculate wave-induced forcing which avoids the calculation of higher order derivatives. To ascertain the accuracy of the wave forcing computation using Dingemans' approach in the elliptic wave model and to better understand the differences between Dingemans' approach and the generalized approach, we consider a two-dimensional problem of a sloping beach with a cosine-squared protuberance of coastline (Fig. 3.9 – top).

For the input wave condition of a normally-incident, monochromatic wave with incident wave height, $H_0 = 1.0$ m and wave-period, T = 8 s at the offshore boundary, The modeled wave field and wave propagation angle at all grid locations is shown in Fig. 3.9. Wave breaking effects are incorporated using the breaking criterion of Dally et al. (1982). The agreement between the modeled results of wave height and the published results by Dingemans et al. (1987) is satisfactory (not shown here).

Although Dingemans et al. (1987) did not present the variation of wave-induced forcing components over entire domain; a plot of wave-directed component ($F_1$) of wave-forcing along the centerline (see Fig. 3.10) and the vector and streamline plots of nearshore current field were presented. They obtained the wave-driven current field by forcing a finite-difference circulation model with the wave forcing calculated using the generalized formulation and the dissipation force formulation (Eq. 3.18).

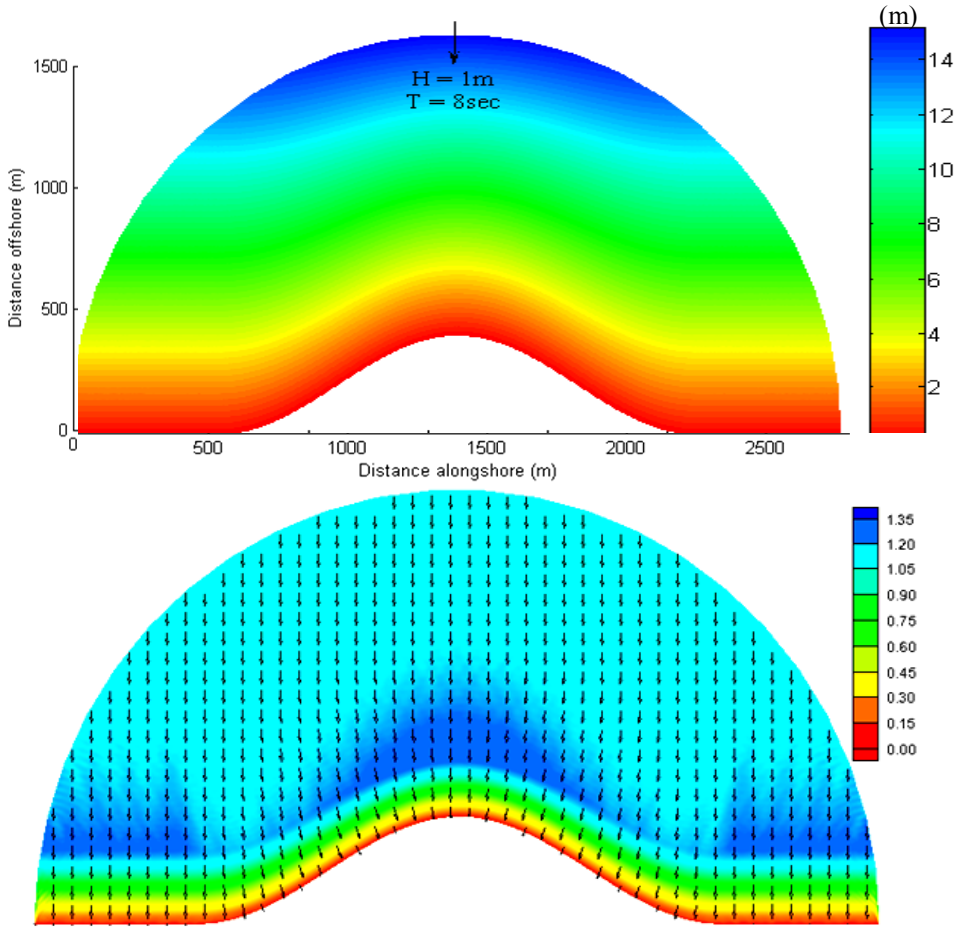


Fig. 3.9. Cosine-squared protuberance of coastline on sloping beach, model bathymetry (top). Modeled wave height (bottom); arrows represent wave direction

The circulation model used by Dingemans et al. (1987) solves the following equations (in tensor notation):

$$\frac{\partial u_i}{\partial t} + u_j \frac{\partial u_i}{\partial x_j} = -\frac{1}{\rho}\frac{\partial P}{\partial x_i} - \frac{\tau_{bi}}{\rho h} + \frac{F_i}{\rho h} \tag{3.26a}$$

$$\frac{\partial \langle \eta \rangle}{\partial t} + u_j \frac{\partial (h u_j)}{\partial x_j} = 0 \tag{3.26b}$$

where $u$ is the horizontal current velocity, $P$ is the pressure, $F$ is the wave forcing and $\tau_b$ is the bottom stress.

In this case, we expect the simplified approach to produce results approximately similar to the generalized approach because the wave field is largely progressive at all grid locations. We therefore consider only the generalized approach and Dingemans' approach. The components $F_1$ and $F_2$ of wave induced forcing from the elliptic wave model are shown in Fig. 3.10 for both the approaches. For model validation, the published results (Dingemans et al. (1987)) of the wave-directed component ( $F_1^{ding}$ ) of wave forcing along the centerline (see Fig. 3.10) are also included in Fig. 3.10. It can be observed that the modeled (contour plots ((a)-(b)) in Fig. 3.10) and published results (Fig. 3.10 (bottom)) for the two approaches show a similar variation in $F_1$ along the centerline. (Notice that the sign of $F_1$ is opposite in the modeled and the published results as the direction of x-axis is reversed). However, due to the unavailability of reliable data and the uncertainty in the model parameters used by Dingemans et al. (1987), we do not expect a perfect match in the magnitudes of the wave-induced forcing. It is important to mention here that the choice of the breaking criterion can significantly influence the magnitudes of wave forcing and consequently the wave induced currents.

In addition, as discussed earlier the generalized form differs from Dingemans' approach as the latter ignores the irrotational part of the total forcing. It can be seen in Figs. 3.10(a-b) that Dingemans' approach ignores the wave forcing outside the surf-zone which is responsible for the wave-induced set-down. The wave-induced set-down may

sometimes alter the flow field as a result of spatial variation in the MSL. Outside the

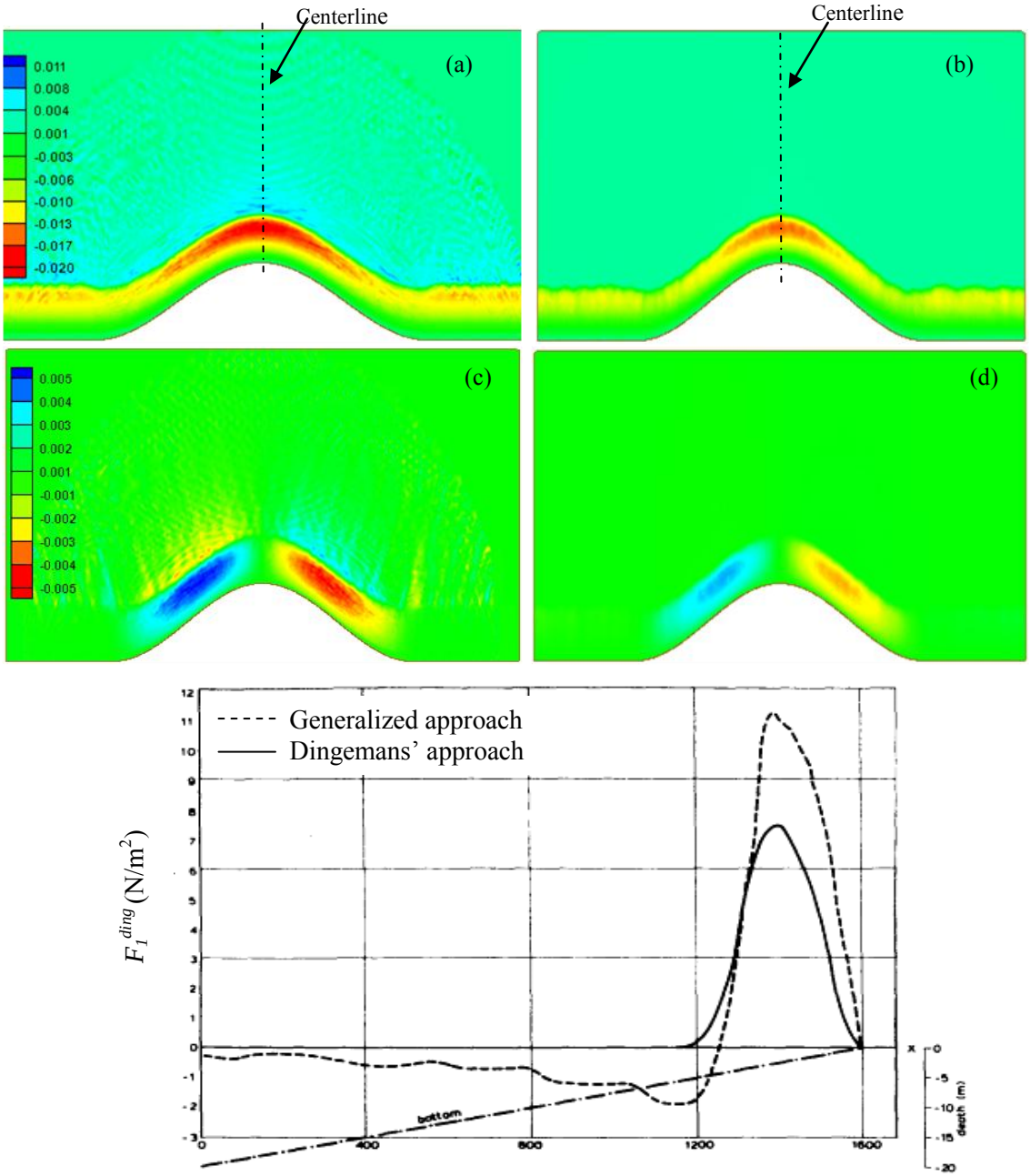


Fig. 3.10. Comparison of wave-induced forcing; (a) and (b) show $F_1$ with the generalized and Dingemans' approach respectively. (c) and (d) show $F_2$ with the generalized and Dingemans' approach respectively. Published results (bottom) of Dingemans et al (1987) along the centerline (note: $F_1^{ding} = -\rho F_1$)

surf-zone, some differences between the modeled results for component $F_2$ obtained with the two approaches can be seen. These differences are most likely due to the diffraction related effects which are ignored by Dingemans' approach.

We also compare the modeled results of wave-driven current field with the published results by Dingemans' et al. (1987). To derive the wave-induced current field driven by the modeled wave forcing, we solve the set of Eqs. (3.26a-3.26b) using a finite-difference model developed in this study. The wave-induced forcing obtained from the elliptic wave model is interpolated on a grid with rectangular elements. The model uses the central-difference scheme, and the CFL criterion for the numerical stability. A no-flow boundary condition is considered at all the boundaries. The results for the current field from this model for both the formulations of wave forcing are shown in Fig. 3.11. It can be observed that Dingemans' approach (both in modeled and published results) produces smoother current field in comparison to the generalized approach. Dingemans' approach produces approximately negligible flow in the region outside the surf-zone. On the other hand, the influence of diffraction effects and numerical errors on the current field corresponding to the generalized approach are not too significant. Some of the noise in the offshore region may be due to the reflected flow from the boundary because a no-flow boundary condition is used at all the boundaries.

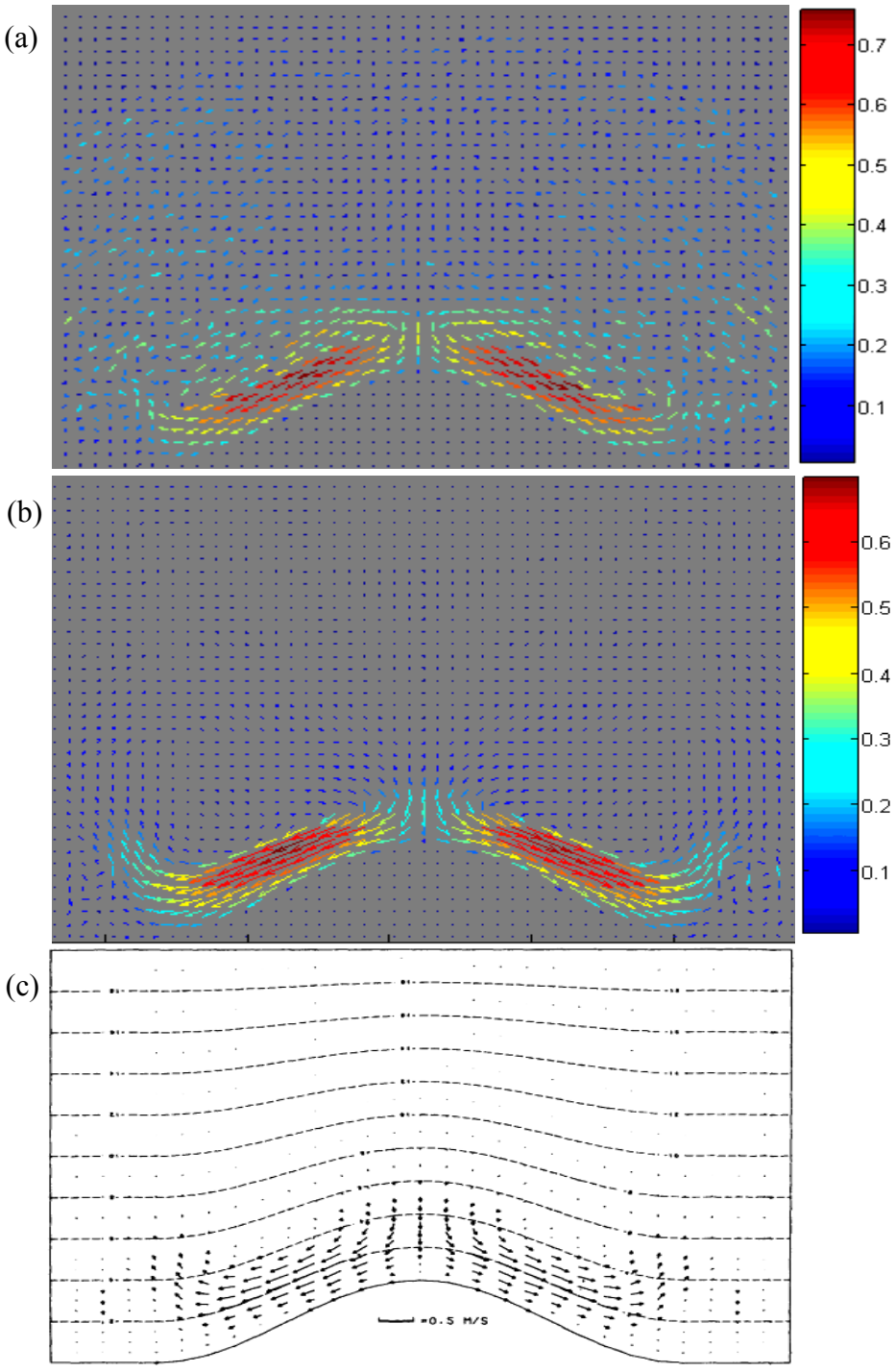


Fig. 3.11. Modeled wave-induced current field; (a) with the generalized wave-forcing, (b) with Dingemans' approach and (c) Modeled current field by Dingemans et al. (1987) with dissipation forces

## 3.5 Numerical issues

### *3.5.1 Effect of term T2*

In Section 3.3.2, we discussed the physical meaning of term T2 in the generalized expressions (Eqs. (3.10a-3.10c)) for stress components. It is also mentioned that the term T2 vanishes for a purely progressive wave field. However, the higher-order derivatives associated with term T2 in the wave-forcing computation may produce numerical errors, so it may be worth considering the effect of ignoring this term for practical applications. To visualize the effect of retaining T2 in the generalized expressions, the variation of wave forcing component $F_1$ (for the validation case 3.4.1), with and without term T2, are shown in Fig. 3.12. It is clear from the contour plots that the results of wave forcing for a progressive wave improve if the term T2 is ignored (especially at the boundary). However, the generalized expressions without term T2 are similar to the simplified expressions and cannot handle the effects of reflection and diffraction. Therefore, to preserve the generality of the expressions, we decided to retain the term T2 in model computations.

### *3.5.2 Boundary errors*

The computation of wave forcing using the generalized expression may produce erroneous results at the offshore boundary. This behavior can be observed in the contour plots of Fig. 3.12. These effects are mainly due to the computation of derivatives at the finite-elements near the boundary and are more pronounced if the term T2 is retained in

Eqs. (3.10a-3.10c) (see Fig. 3.12 (right)). Fortunately, these numerical errors are local and do not affect the wave forcing solution inside the domain. In fact, these boundary errors can easily be treated or their effect on modeled circulation field can be minimized by considering a relatively large domain for the wave forcing computation in the wave model, so that the erroneous wave forcing at the boundary points is not interpolated on to the circulation model domain.

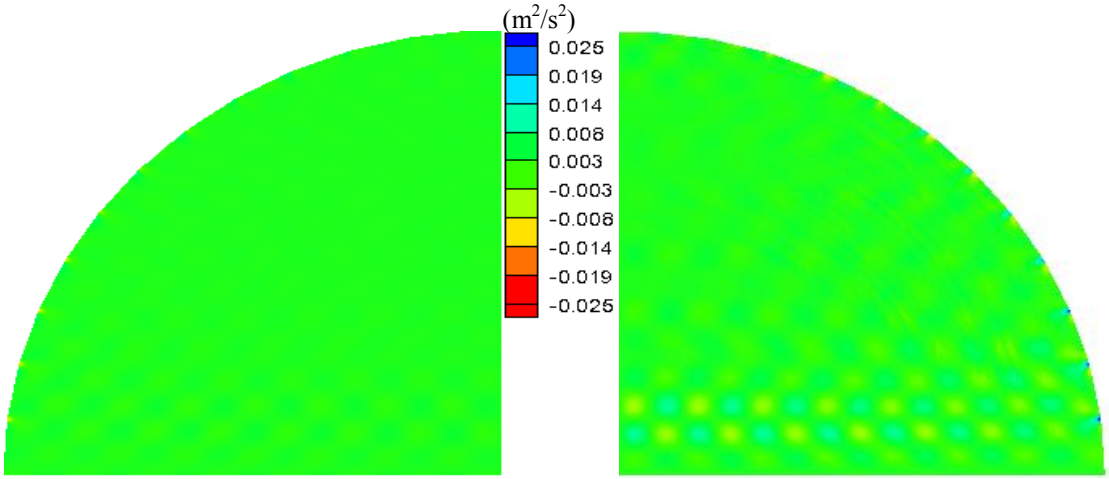


Fig. 3.12 Effect of term T2 on model wave forcing computation; $F_1$ without term T2 (left) and with term T2 (right)

## 3.6 Summary

The elementary test cases showed that the code was very accurate in the computation of wave-induced forcing with all three forcing formulations. The results shown in the standing wave case and the detached breakwater case explain the variation of stress components in the presence of reflection. The results presented in the last case helped us to understand the differences between the generalized approach and Dingemans' approach.

# 4. CIRCULATION MODEL

In Section 3, we discussed the concept of wave-induced forcing and various wave forcing formulations available in the literature. The computation of wave forcing terms from the elliptic wave model was validated with some simple cases. We now proceed to the calculation of wave-induced currents and set-up/down. The focus of this section is a coupled modeling system and the validation for these quantities.

To derive the wave-induced current field in example 3.4.4, a simple finite-difference model was considered. However, the circulation model used earlier has its own limitations and is not powerful enough to be considered for complex coastal environment. Therefore, instead of investing effort in the further development of this model, we use the ADCIRC (ADvanced Circulation) model (Luettich et al. 1992) which is widely used for general coastal applications.

## 4.1 The ADCIRC-2DDI model

ADCIRC is capable of solving the time dependent, free-surface motion equations in two (ADCIRC-2DDI) and three dimensions (ADCIRC-3D). In this study, we use ADCIRC-2DDI which solves the two-dimensional depth-integrated continuity and nonlinear momentum equations to obtain elevation and velocity field respectively. ADCIRC-2DDI is a finite-element model which allows one to use highly flexible unstructured grids and contains an efficient implementation of the boundary conditions. Typical coastal applications for which ADCIRC has widely been used include: (a)

modeling of tides and wind driven currents for harbor design (Luettich et al. 1999), (b) studying coastal flooding and storm surge due to hurricanes (Irish et al. 2008), (c) modeling the transport of sediments, pollutants, larva, etc. to study shoreline erosion and coastal morphology (Edge and Pandoe 2003) and (d) designing nearshore structures.

One of the objectives of this study is to simulate wave-induced nearshore circulation in a complex coastal environment by coupling a finite-element wave model with ADCIRC-2DDI. An effort at coupling models was made by Cobb and Blain (2003b) to simulate the rip currents through a channel between submerged sandbars by forcing ADCIRC-2DDI with the wave forcing obtained using REF-DIF1. In the following sections, we provide a brief discussion about ADCIRC's governing equations, boundary condition and other features which are relevant to this study.

### *4.1.1 The governing equation and relevant mechanisms*

In ADCIRC-2DDI, sea surface elevations and currents are modeled using a set of two-dimensional, nonlinear, depth-averaged mass and momentum balance equations. These equations, which are derived by vertically integrating the three-dimensional mass and momentum balance equations subject to hydrostatic assumption and Boussinesq approximation, are expressed in the vector form:

$$\frac{\partial \eta}{\partial t} + \nabla_{xy} \cdot (h\nu) = 0 \tag{4.1a}$$

$$\frac{\partial u}{\partial t} + \nu \cdot \nabla_{xy}(\nu) = -\frac{1}{\rho}\nabla_{xy}(g\eta) + \frac{M_{xy}}{h} + \frac{F_{xy}}{h} - \frac{\tau_{bxy}}{\rho h} \tag{4.1b}$$

where x, y are the Cartesian coordinate directions, t is time, $v$ is the vector of depth-averaged current velocity, $\eta$ is the free surface elevation, $h = h_0 + \eta$ is the total water depth, $h$ is the still water depth and $\rho$ is the sea water density, $F_{xy}$ is the vector of wave-induced forcing described in Section 3; its components in x and y directions are input in ADCIRC in the form:

$$F_x = -\frac{1}{\rho}\left(\frac{\partial S_{xx}}{\partial x} + \frac{\partial S_{xy}}{\partial x}\right) \tag{4.2a}$$

$$F_y = -\frac{1}{\rho}\left(\frac{\partial S_{yx}}{\partial x} + \frac{\partial S_{yy}}{\partial y}\right) \tag{4.2a}$$

where $S_{xx}, S_{xy}, S_{yx}, S_{yy}$ are the components of wave radiation stress tensor described earlier in Section 3. The second term on the RHS of Eq. (4.1b) incorporates the lateral mixing effects due to horizontal diffusion, where $M_{xy}$ is expressed as:

$$M_{xy} = E_h\left(\nabla^2{}_{xy}(hv)\right) \tag{4.3}$$

where $E_h$ is the eddy viscosity coefficient for horizontal momentum diffusion. The bottom stress terms ($\tau_{bxy}$) in Eq. (4.1b) are calculated using a nonlinear quadratic friction law given by:

$$\tau_{bxy} = \rho C_f\left(U^2 + V^2\right)\cdot v \tag{4.4}$$

where $C_f$ is the bottom friction coefficient, U and V are the components of depth-averaged velocity vector ($v$) in the x and y-direction respectively.

### *4.1.2 Coupling with the elliptic wave model*

ADCIRC is mainly a shelf-scale model and its applications in the field of wave-induced nearshore circulation are limited. Some earlier works by Blain and Cobb (2003) used ADCIRC-2DDI to simulate longshore currents on a plane beach and rip currents on the barred beaches. In both cases, the wave-forcing is obtained from a phase-resolving wave model REF-DIF1.

In this study, we examine a "one-way" coupling of the ADCIRC model with the elliptic wave model. For both models, the same mesh-generation technique (e.g. such as that in Surface Modeling System (SMS) describe by Zundel et al. (1998)) to discretize the model domain into finite elements can be used. This technique uses a size function which governs the size of an element based on the depth at a grid location. There are many advantages associated with the coupling of two finite-element models. In many cases the same computational grid can be used for both the models which may avoid data loss due to interpolation. The mesh generation technique also allows refining the mesh at locations where large variations in wave-induced forcing are observed. For example, in regions of wave reflection, steep gradients of radiation stress may lead to unstable model simulations; a refined mesh can be used to avoid such situations.

In most numerical examples considered in this study, we simulate depth-averaged, steady-state current field and set-up/down. The ADCIRC model is forced with the wave-induced forcing until the solution of current field reaches a steady-state. In the next section, we consider some validation cases to ensure that the coupling of ADCIRC

with the elliptic wave model provides satisfactory results. These simple test cases also help in understanding the nearshore circulation over complex domains.

## 4.2 Validation of the coupled system

Here we consider some simple test-cases to verify the model results from the coupled system. The reason for the selection of these cases is to answer the following questions:

(1) Can ADCIRC produce satisfactory results of wave-induced set-up/down and current field when forced with the wave forcing computed with the elliptic wave model?

(2) The capability of the elliptic wave model to handle the wave reflection is studied in Section 3. However, the studies, where the effect of wave reflection on the wave-induced circulation is considered, are limited. Can depth-averaged models like ADCIRC handle the effect of wave reflection in the wave forcing? Sometimes the effect of wave reflection exists near boundaries (for example, standing wave case discussed later and offshore breakwater case in Section 5), Can these effects be handled with the boundary condition available in ADCIRC?

(3) Is the selection of an appropriate boundary condition crucial for the accuracy of modeled results?

### *4.2.1 Wave-induced setup/down on a plane beach*

On a plane beach, depth contours are straight and parallel to the coastline and the bottom slope is same at all locations. Therefore, in a steady-state sense ( $\overline{\partial/\partial t} = 0$ ), for normally incident waves, the momentum balance equation in the x-direction reduces to:

$$-\rho g(h+\overline{\eta})\frac{\partial \overline{\eta}}{\partial x} = \frac{\partial S_{xx}}{\partial x} + \tau_{xb} \tag{4.5}$$

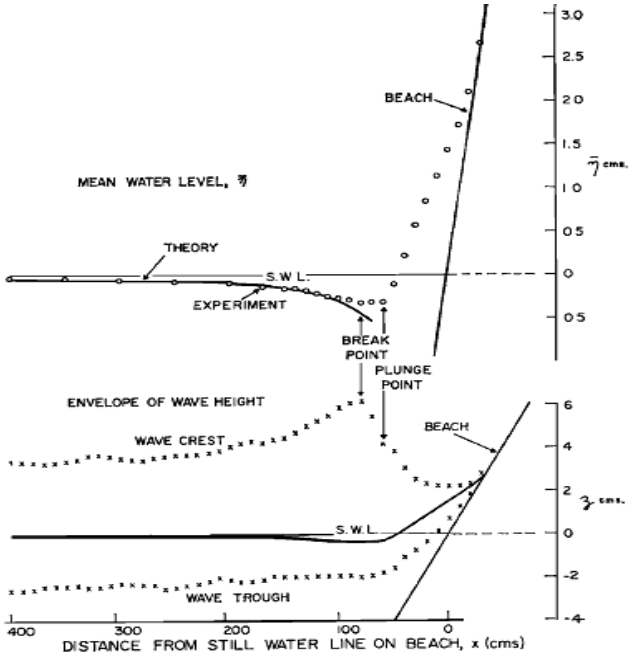


Fig. 4.1. Profile of the mean water level. Experimental results of Bowen et al. (1967)

For validation of the coupled models, we consider one of the experimental cases (Experiment 51/6) listed in Bowen et al. (1967). For a normally-incident wave train of wave period T=1.14 s and deep water height $H_0$=6.45 cm, the experimental results for wave run-up (Bowen et al. (1967)) are shown in Fig. 4.1. The steady-state solution of the modeled set-up/down obtained with the coupled ADCIRC and the elliptic wave model is

shown in Fig. 4.2 (top). In the ADCIRC simulation, the no-flow boundary condition is used at all the boundaries. The normally-incident wave train in this case cannot drive the depth-averaged currents (also observed in the ADCIRC results which are not shown here). The modeled results are in good agreement with the experimental results.

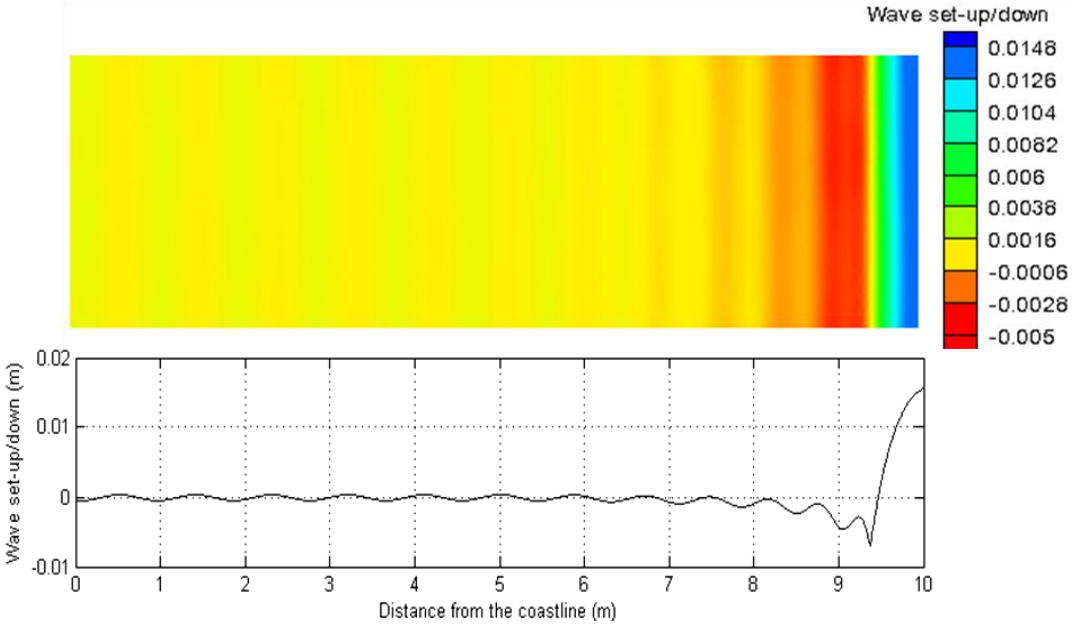


Fig. 4.2. Profile of the modeled mean water level. ADCIRC results (top) and 1-D solution (bottom)

For additional verification, Eq. (4.5) is solved along a 1-D section by using the fourth-order Runge-Kutta scheme; the wave radiation stress ($S_{xx}$) along the 1-D section is calculated with a 1-D version (Eq. 2.16) of the mild-slope equation. The stress components are computed with the 1-D version of the generalized wave forcing. The variation of wave-induced set-up/down shown in Fig. 4.2 (bottom) matches well with the ADCIRC results along any 1-D section perpendicular to the coastline. Also, the set-up values at the location of zero still-water depth ($\approx 1.4$ cm) from the experimental results

of Bowen et al. (1967) is comparable to both the modeled results shown in Fig. 4.2, implying that ADCIRC may be used to model wave-induced set-up/down.

### *4.2.2 Longshore currents on a plane beach*

When a wave propagating on a uniformly sloping beach reaches the breaker line at an appreciable angle, the resulting cross-shore variation of the alongshore radiation stress component creates an alongshore thrust which generates currents in the alongshore direction. With the simplifications for plane beaches addressed in last section, alongshore balance for depth-averaged mean currents can be expressed as:

$$-\frac{\partial S_{xy}}{\partial x} - \tau_{yb} + M_{xy} = 0 \tag{4.6}$$

Eq. (4.6) shows that the bottom stress and lateral mixing effect balances the alongshire thrust in alongshore direction. Longuet-Higgins (1964) studied the effects of lateral mixing on the profile of alongshore currents. However, we do not want to go into the details of this issue; the sensitivity of longshore current to lateral mixing and bottom friction was studied by Blain and Cobb (2003a) using ADCIRC.

Based on Eq. (4.6), many empirical relations were established using the available field data. One of these relations which can be conveniently evaluated on the basis of wave parameters at the breaker zone was given by Komar (1979):

$$\bar{v}_l = 1.17\sqrt{gH_{br}}\sin\alpha_b\cos\alpha_b \tag{4.7}$$

where $H_{br}$, $\alpha_b$, $h_b$ are respectively the wave-height, wave angle and water depth at the breaker line, and $\bar{v}_l$ is the maximum current velocity inside the surf-zone.

For a wave train (input condition: H=1 m, T=10 s and θ=45$^o$) travelling on a plane beach with uniform slope of 1 in 100, the solution of wave field from the wave model gives: $H_{br}$=1.20 m, $\alpha_b$=14.3$^o$ and $h_b$=1.61 m. For these values, Eq. (4.7) predicts a maximum longshore current velocity of 0.95 m/s inside the surf-zone. The cross-shore profile of the longshore current from the ADCIRC model (with $C_f$ = 0.01 and $E_h$=1.0 m$^2$/s) is shown in Fig. 4.3; the profile of the longshore current is comparable to the modeled results (with ADCIRC and REF-DIF1) of Blain and Cobb (2003a) and the maximum current velocity matches well with the analytical solution (Eq. 4.7).

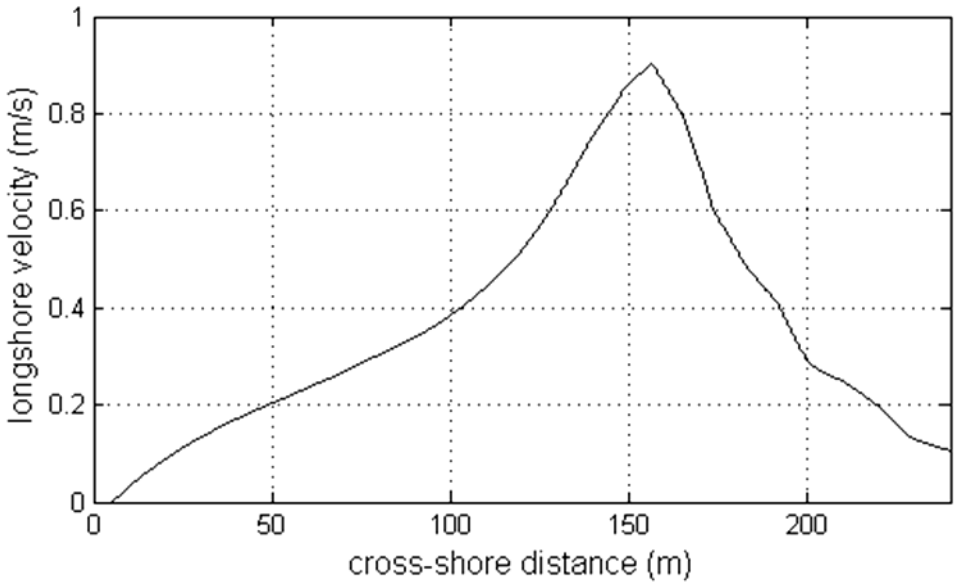


Fig. 4.3 Cross-shore profile of modeled longshore current velocity

### *4.2.3 Wave setup/down for a standing wave*

In the previous cases, there are no geometric features or boundaries which can induce significant wave-reflection inside the domain. Therefore, we consider the case of

a standing wave simulated using the elliptic wave model by assuming the coastline to be a perfectly reflective boundary. For the case of a standing wave on a flat bottom with no variations in the alongshore directions ( $\partial/\partial y = 0$ ), analytical solution (Bettess and Bettess (1982)) for wave-induced set-up/down is given by:

$$\overline{\eta} = a^2 k \coth(2kh)\cos(2ky) \tag{4.8}$$

where a is the amplitude of incident wave, $k$ is the wave number, h is the still water depth.

Here we consider the case of a normally incident wave (on a flat bottom with water depth, h = 5 m) with amplitude, a= 0.5 m and wave period, T = 3 sec, which, on superposition with the reflected component (from the coastline) creates a standing wave. Fig.4.4. shows the modeled wave set-up/down from the ADCIRC model and a comparison plot between ADCIRC results and analytical results. The results are in very good agreement with the analytical solution (Eq. (4.8)).

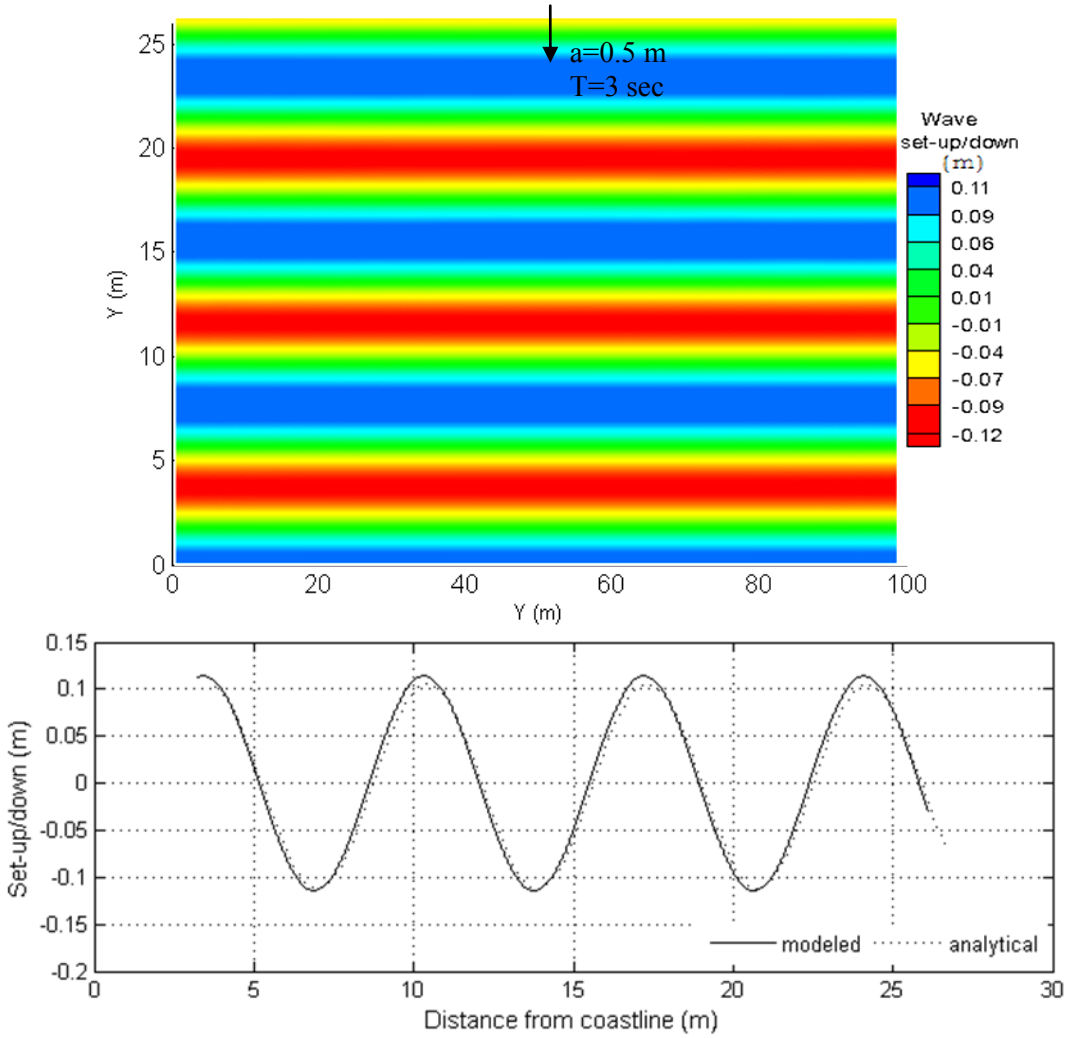


Fig. 4.4. Standing wave case, modeled wave set-up/down (top) and comparison plot (bottom)

### *4.2.4 Cosine-squared protuberance of the coastline*

We have considered the case of a cosine-squared protuberance of coastline in Section 3.3.4 to verify the wave forcing computation from the elliptic wave model. We also discussed the results of wave-induced current field obtained with a finite-difference model. In this section, to check the performance of the coupled system, we use ADCIRC

to derive wave-induced currents and set-up/down for the same domain and same wave forcing.

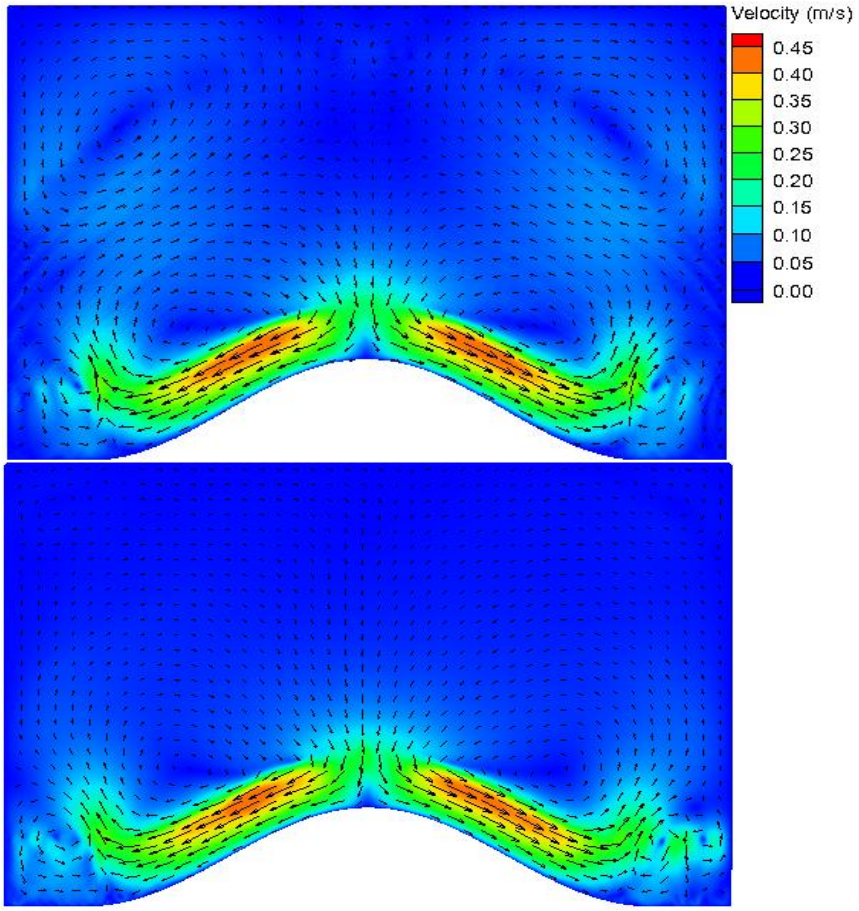


Fig. 4.5. Modeled current field from ADCIRC; the generalized approach (top) and Dingemans' approach (bottom)

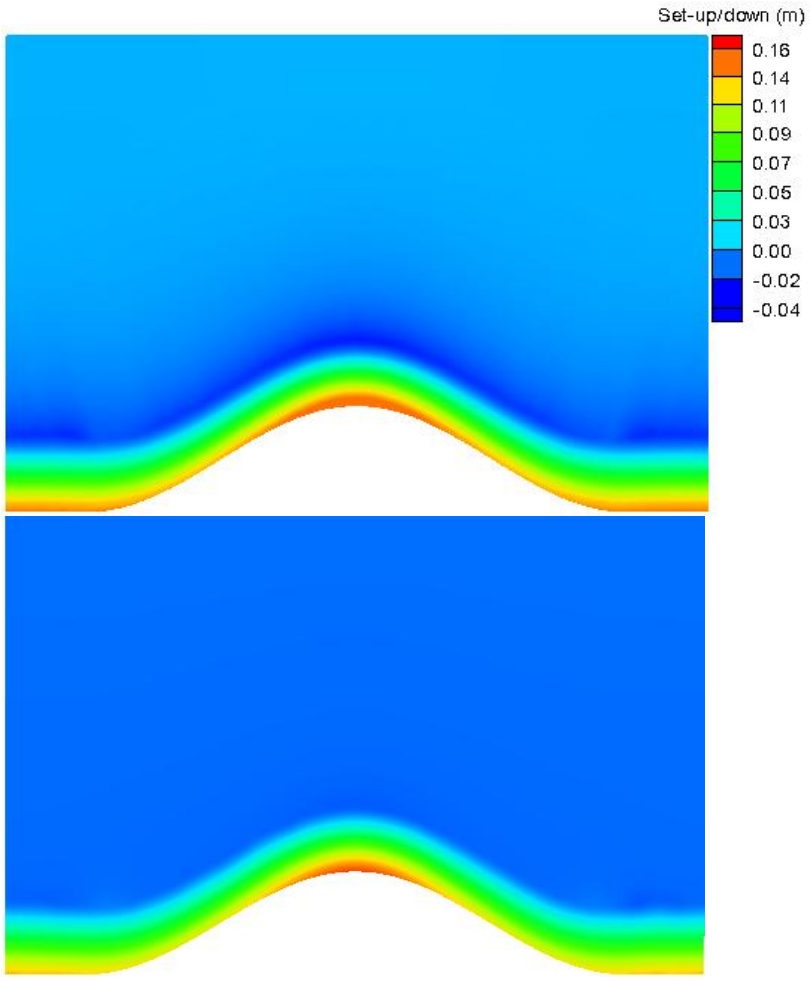


Fig. 4.6. Modeled wave set-up/down from ADCIRC; the generalized approach (top) and Dingemans' approach (bottom)

The contour and vector plots of current field from the ADCIRC model with two different formulations (the generalized and Dingemans' approach) of the wave-induced forcing are shown in Fig. 4.5. The results of wave-induced set-up/down are shown in Fig. 4.6. In ADCIRC, a no-flow boundary condition is applied at all the boundaries to be consistent with the boundary conditions used by Dingemans et al. (1987). Since the information regarding the computation of bottom stresses is not available, a value of

0.02 is assigned to the friction coefficient ($C_f$). The modeled current field in Fig. 4.5 is fairly consistent with the streamline plots of Dingemans et al. (1987).

In addition, in comparison to the current field results (for the same case) obtained in Section 3, the results shown in Fig. 4.5 are smoother. A high resolution (L/15) grid is used in the wave model to obtain the wave forcing, implying that the numerical errors due to higher-order derivatives in the generalized approach can be minimized with high grid resolution.

### *4.2.5 Rip current case*

A rip current system is one of the common cell circulation systems that exist in the nearshore regions. It consists of an offshore-directed, strong jet of water that originates near the coastline and broadens outside the breaker-line. The strong velocity field associated with a rip-current system is responsible for nearshore sediment and pollutant transport. In most coastal areas, bathymetric variations, wave-wave or wave-current interaction, presence of structures, etc. are responsible for the rip-currents. Here we consider the case of a steady-state rip current in a channel through submerged sandbars studied by Cobb and Blain (2003b). Fig. 4.7 shows the bottom topography of a sloping beach with a rip-channel through the sandbars. The barred beach has a slope of 0.009 and extends 1500 m and 700 m in the alongshore and the offshore direction respectively. The rip channel is 255 m wide with the centre located at X = 742.5 m.

Wave-induced forcing is computed using the elliptic wave model for a normally incident wave of wave height, H=1 m and wave period, T=10 sec. The modeled wave

field shown in Fig. 4.8 is in agreement with the modeled results (with ADCIRC and REF-DIF1) of Cobb and Blain (2003b). The primary breaking over the sandbars and the secondary breaking near the shore can be seen in the modeled results (see Fig. 4.8). As a result of spatial variations in the wave field, the wave-induced forcing generates a complex flow pattern inside the domain.

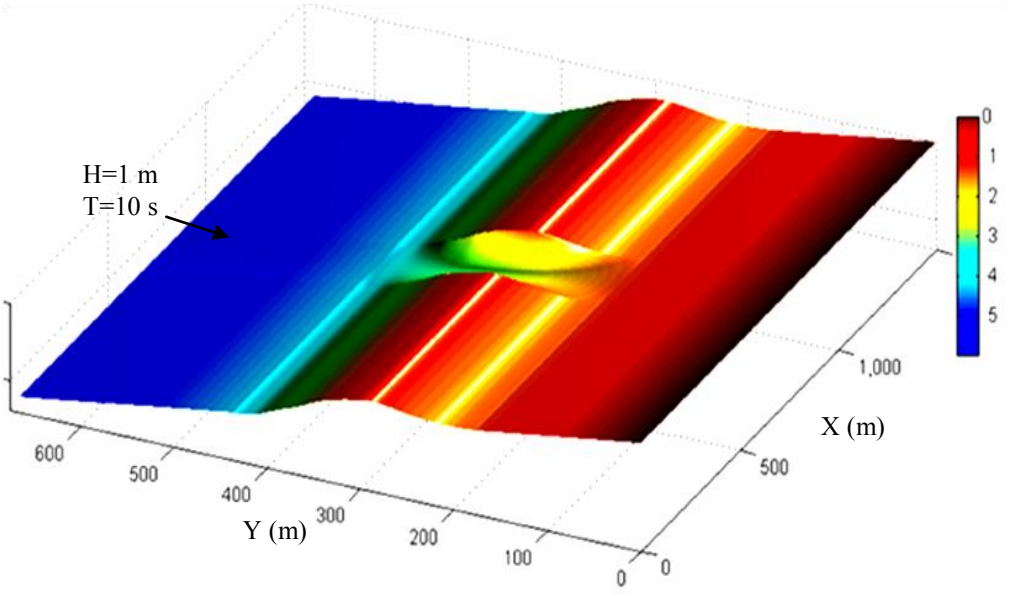


Fig 4.7. Rip channel through submerged sandbars, model bathymetry

The ADCIRC model is forced with the generalized wave forcing and the steady-state results of current field are shown in Fig. 4.9. To allow the rip-head to leave the domain, the normal wave radiation condition is used at the offshore boundary. The coupled system of models is able to simulate the important features of rip current system, such as, rip-head, feeder currents, formation of vortices, etc. These features along with the magnitude of current velocity are in good agreement with the published results by Cobb and Blain (2003b) obtained by the coupling of REF-DIF1 and ADCIRC.

Details of the physics of wave-induced circulation are not included in this thesis. A reference can be made to Cobb and Blain (2003b) for more details.

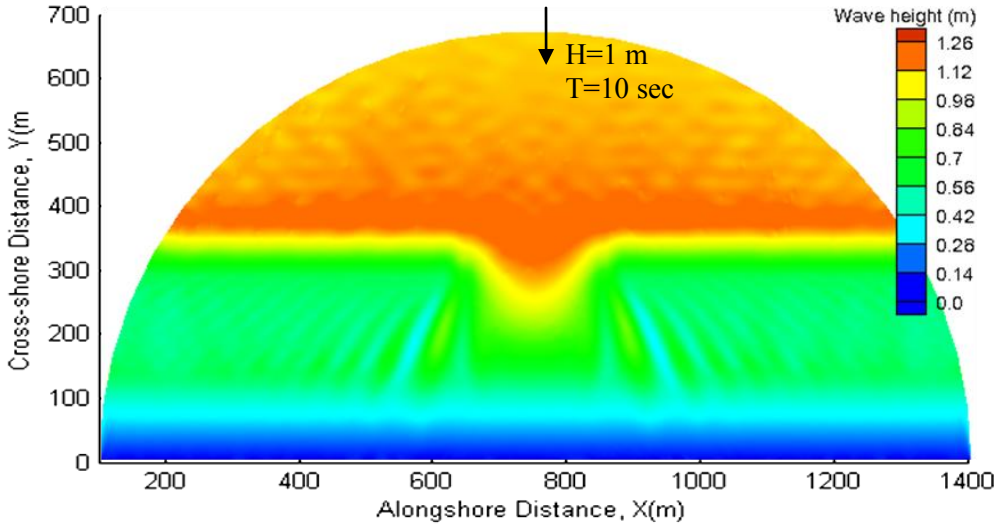


Fig 4.8. Modeled wave height

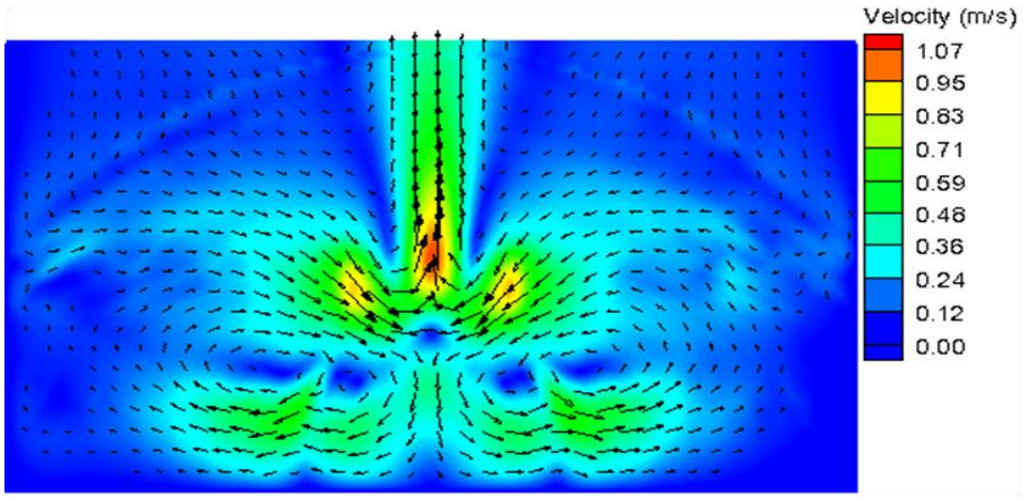


Fig 4.9. Modeled rip-current velocity field from ADCIRC

## 4.3 Selection of boundary condition

In Section 4.2, we verified ADCIRC's performance to handle the wave reflection and to simulate wave set-up/down and current field. The selection of boundary condition is crucial at times. The 'no-flow boundary condition' at all the boundaries in ADCIRC domain is preferred (if possible) to obtain the reliable results of wave-induced set-up/down and currents. For example, the 'no-flow boundary condition' is used for the cases in Sections 4.2.1, 4.2.3 and 4.2.4. However, for the case of rip current and longshore current in Sections 4.2.2 and 4.2.5 respectively, since the flow (rip-head and longshore current) is directed towards the boundary, a 'normal wave radiation' condition in ADCIRC is used to allow the flow to leave the domain. However, in such cases, some flow can enter or leave the domain at the boundary points and affect the solution of wave set-up down. Another alternative approach is to consider a larger domain with 'no-flow boundary condition', so that, the boundary effects on the flow field can be kept away from the modeled region of interest. For example, for the same domain of rip-current case (Section 4.2.5), we considered the 'no-flow boundary condition' also at the offshore boundary, the reflected flow from this boundary (due to the rip-head)) will affect the solution at other locations. However, if we increase the domain size by shifting the offshore boundary to a farther offshore location, we can obtain almost the similar results as shown in Fig. 4.9.

In most cases considered in this thesis, we have selected the computational domain in a way that the boundary related effects can be minimized.

## 4.4 Summary

To summarize, in the preceding examples, we tried to capture several possible features of wave-induced circulation in coastal environments. For example, two common features viz, the longshore current and the cell-circulation system, are simulated in Section 4.2.2 and Section 4.2.5 respectively. The effect of wave reflection is simulated for the standing wave case in Section 4.2.3. In addition, the results showed that the generalized approach produced results that matched analytical cases. The choice of circulation model and the generalized forcing yielded results similar to Dingemans' approach. This would suggest that the approach of neglecting the irrotational part in the wave forcing is valid, at least for this test. The similarity also shows that, in contrast to the expectations of Dingemans et al. (1987), the result of current field obtained with the generalized approach was not corrupted by numerical errors (However, we did find that for low grid resolution, the solution did contain some noise (not shown)).

This rigorous validation of the coupled system allows us to consider the complex domains where the combined effect of wave reflection, diffraction and breaking may create complex circulation patterns.

# 5. RESULTS AND DISCUSSION

Satisfactory validation in Section 4 of the ADCIRC model with the analytical and published results (where wave forcing for the ADCIRC model was obtained using the elliptic wave model) now allows us to use the one-way coupled (no wave-current interaction) system for the study of more complex coastal environments. Therefore, in this section, we consider the domains with general coastal features, such as breakwaters, jetties, shoals, etc. The presence of these structures induce phenomena like wave reflection, diffraction, focusing, shoaling, etc. which can produce a complex wave field and consequently a complex nearshore circulation pattern. In such cases, the widely used method (the simplified approach) of radiation stress calculation may not be appropriate to use; on the other hand the generalized approach may produce erroneous numerical errors, and the performance of Dingemans' approach has never been studied in these scenarios. Therefore, in this Section, we wish to address the following questions:

(1) How is the physical mechanism of the nearshore wave-induced circulation affected by the presence of coastal features?

(2) Does the coupled system of the elliptic wave model and ADCIRC produce satisfactory results for complex coastal domains?

(3) How does the selection of wave-induced forcing formulation affect the modeled wave-induced currents and set-up/down?

We consider the following numerical examples: (1) Detached breakwater (Liu and Mei (1976)); (2) Shore-perpendicular breakwater (Liu and Mei (1976)); (3) CERC shoal (Vincent and Briggs (1989)) and (4) Two adjacent submerged shoals. For all these cases, we use the coupled system of the elliptic wave model and the ADCIRC model (discussed in Section 4) to obtain the wave field, current field and set-up/down. A discussion regarding the nature of wave-field and wave-induced circulation, the performance of various formulations of wave-forcing and the published results available in the literature is included. The first two cases involve significant reflection and diffraction, while the last two cases involve the wave focusing effects. In such situations, the wave-induced circulation has been poorly addressed in the past.

## 5.1 Detached breakwater

### *5.1.1 Introduction*

In this section, we consider the case of a thin detached offshore breakwater (Liu and Mei (1976)) located on a plane beach with uniform slope of 1 in 50. The offshore breakwater is located at a distance 350 m from the shoreline and extends 700 m in the direction parallel to the shoreline. The breakwater is designed to perfectly reflect the waves. The model domain shown in Fig. 5.1 is comparable to a real-life situation where a coast is sheltered by a breakwater. The modeled results of wave-induced circulation, their comparison with the modeled results of Liu and Mei (1976) and the performance of various wave forcing formulations are discussed in the following section.

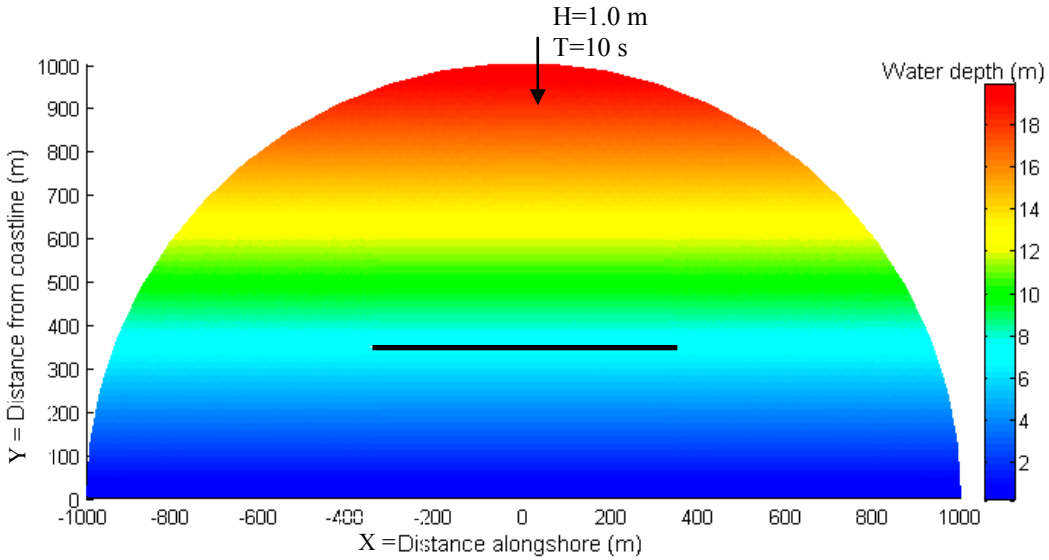


Fig. 5.1. Detached breakwater on sloping beach, model bathymetry

### *5.1.2 Numerical results and discussion*

We consider an input wave condition of a monochromatic, normally-incident wave of wave period T=10 s and wave height 1.0 m. The wave field is simulated using the elliptic wave model. The contour plots of modeled wave height and wave phase are shown in Fig. 5.2. As expected, on the shoreward side of the breakwater, a shadow region is formed where wave heights are negligible at most locations. Phenomena, such as wave reflection in the region offshore of the breakwater and wave diffraction shoreward of the breakwater can be observed in these plots. These phenomena alter the progressive nature of the wave field.

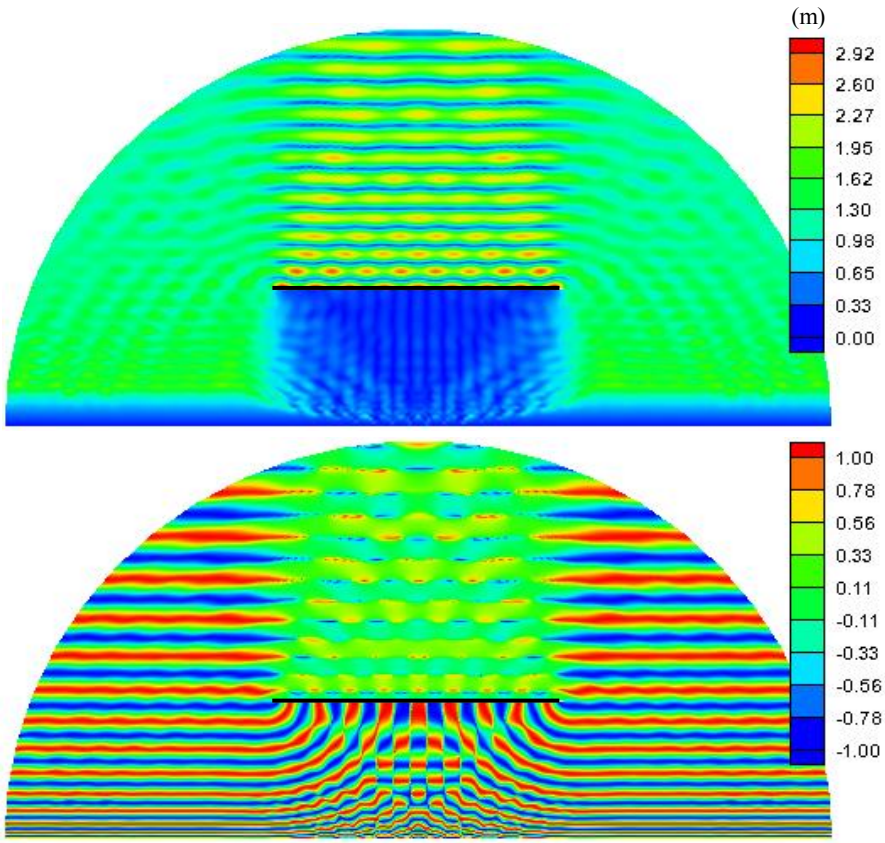


Fig. 5.2. Modeled wave height (top) and wave phase (bottom)

Inside the surf-zone, the energy dissipation due to breaking is simulated using the breaking criterion of Dally et al. (1987). Due to wave breaking inside the surf-zone away from the shadow region, the cross-shore variation in the wave height (or momentum flux) generates the cross-shore directed component of the wave forcing. This wave induced forcing, as discussed in Section 3, is in static balance with the gradients of wave-induced set-up/down. Fig. 5.3 (top) represents the modeled wave set-up/down as a result of the wave forcing at all grid locations. The modeled results of wave set-up/down are obtained by forcing the ADCIRC model with the wave forcing calculated

using the generalized formulation. The results are shown only for the left half of the domain as the problem is symmetric about the line X=0. Away from the surf-zone, the set-up/down of the MSL is also observed in the region offshore to the breakwater where the wave field varies significantly due to wave reflection.

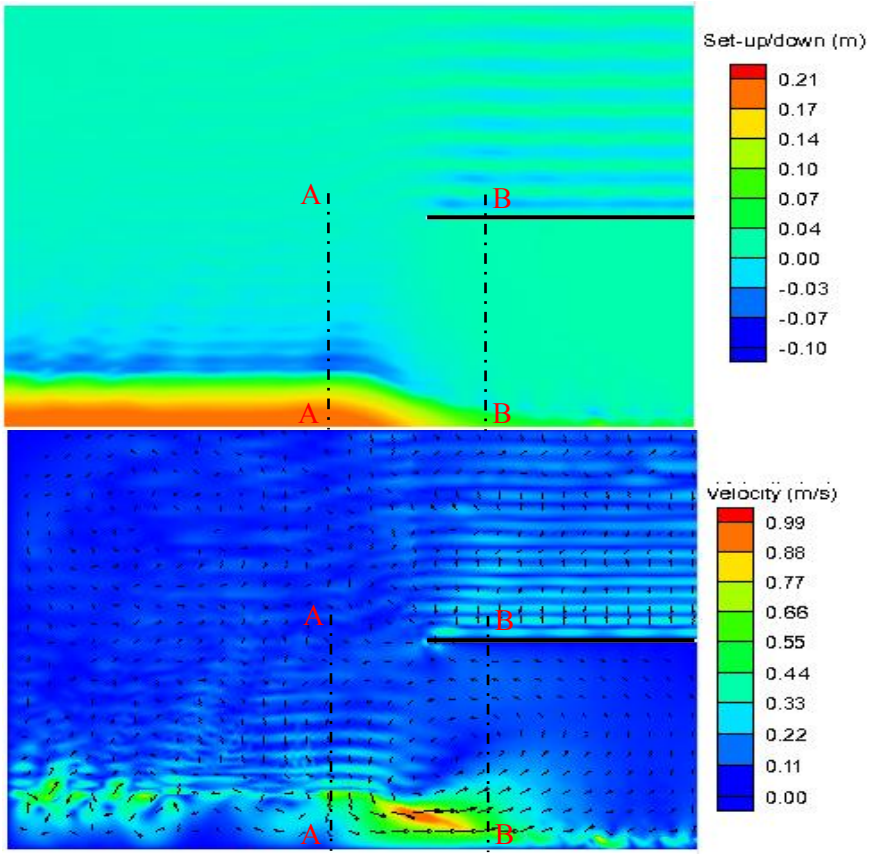


Fig. 5.3. Modeled wave set-up/down (top) and current field (bottom) for X<0

The spatial variation in the set-up/down (for instance between section AA and BB in Fig. 5.3 (top)) creates the hydrostatic gradients of pressure which, in fact, are responsible for the generation of wave-induced currents (see velocity vectors between section AA and BB in Fig. 5.3 (bottom)). The modeled current field is depicted in Fig. 5.3(bottom). The most important feature of the current field is the formation of two cell

circulation systems inside the shadow region mainly due to the alongshore pressure gradients inside the surf-zone. The counter-rotating cells converge at the center of the shadow region to form a weak offshore-directed rip current. This circulation system inside the shadow regions is sometimes responsible for the formation of a tombolo which may link the offshore breakwater to the coastline in the long run.

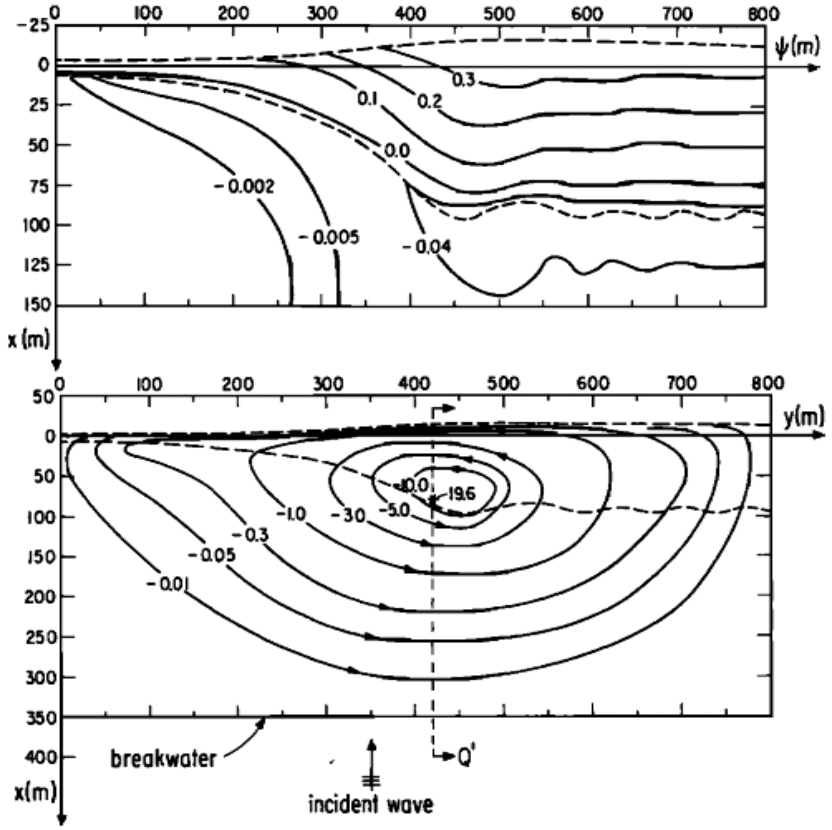


Fig. 5.4. Published results of Liu and Mei (1976); wave set-up/down (top) and current field (bottom)

For comparison, the published modeled results (Liu and Mei (1976)) of wave set-up/down and the streamline plots of current field are shown in Fig. 5.4. The qualitative aspects of model results, such as, the position of breaker line, the formation of counter-

rotating cells and the spatial variation in set-up/down, etc. in the region shoreward to the breakwater are fairly consistent with the results shown in Fig. 5.4.

The results of modeled quantities for the region offshore of the breakwater were not published by Liu and Mei et al. (1976). Also, quantitative comparison may not be valid because of various approximations used by Liu and Mei (1976) and because of the differences in the models (e.g. breaking formulation, etc).

We now compare the results obtained with different wave forcing formulations discussed earlier in Section 3. The results of wave-induced set-up/ down and the current field are shown in Fig. 5.5 and Fig. 5.6 respectively for the three forcing formulations. As mentioned earlier, the simplified formulation is inappropriate in the regions where wave field is influenced by reflection and diffraction. This can now be observed from the modeled results of currents and set-up/down obtained with the simplified formulation. For instance, in the region offshore to the breakwater, the simplified approach produces chaotic pattern (Fig. 5.6(top)) with velocities as high as 1.2 m/s as opposed to maximum of 0.4 m/s from the generalized approach. The results obtained by Liu and Mei (1976) are also based on the simplified formulation. However, their results (Fig. 5.4) are smoother than the modeled results shown in Fig. 5.5 (top) and Fig. 5.6 (top). This may be attributed to the type of wave model (analytical solution proposed by Liu and Mei (1976) is an approximate theory for wave diffraction and assumes small modulations in the wave field) used and the size of their computational domain (the region offshore to the breakwater is not included in Liu and Mei (1976)) considered in the study.

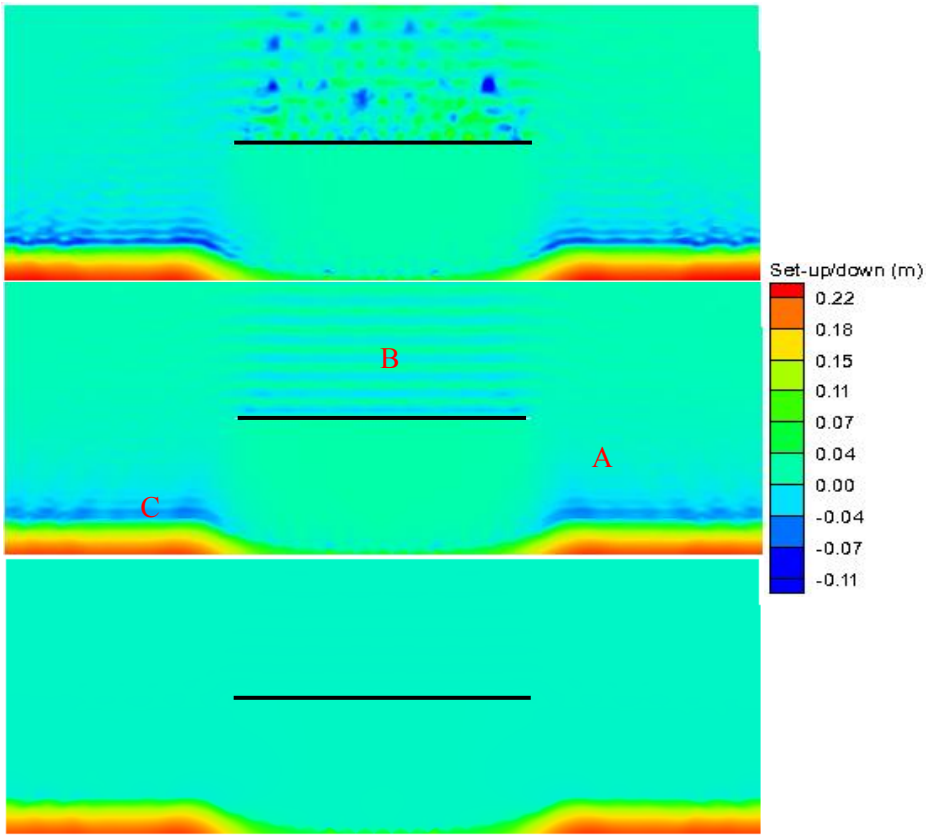


Fig. 5.5. Modeled wave-induced set-up/down; the simplified approach (top), the generalized approach (center) and Dingemans' approach (bottom)

The results for currents and set-up/down obtained with the generalized approach and Dingemans' approach are also presented in Fig. 5.5 and Fig. 5.6 for entire domain. Three areas (A, B, and C in Fig. 5.5) of distinct differences are apparent. As discussed in Section 3, Dingemans' approach ignores diffraction related effects (area A). More important, it is now clear that Dingemans' approach also ignores the contribution of wave reflection (area B) in the circulation pattern. In the region offshore to the breakwater (area B) and just outside the surf-zone (area C), Dingemans approach produces no current field and set-up/down (Fig. 5.5 (bottom) and Fig. 5.6 (bottom)). On

the other hand, the generalized approach produces the effect of wave diffraction and wave reflection is seen on the modeled results (Fig. 5.5 (center) and Fig. 5.6 (center)). This would suggest that Dingemans' approach provides set-up/down primarily due to dissipation, and not due to other mechanisms.

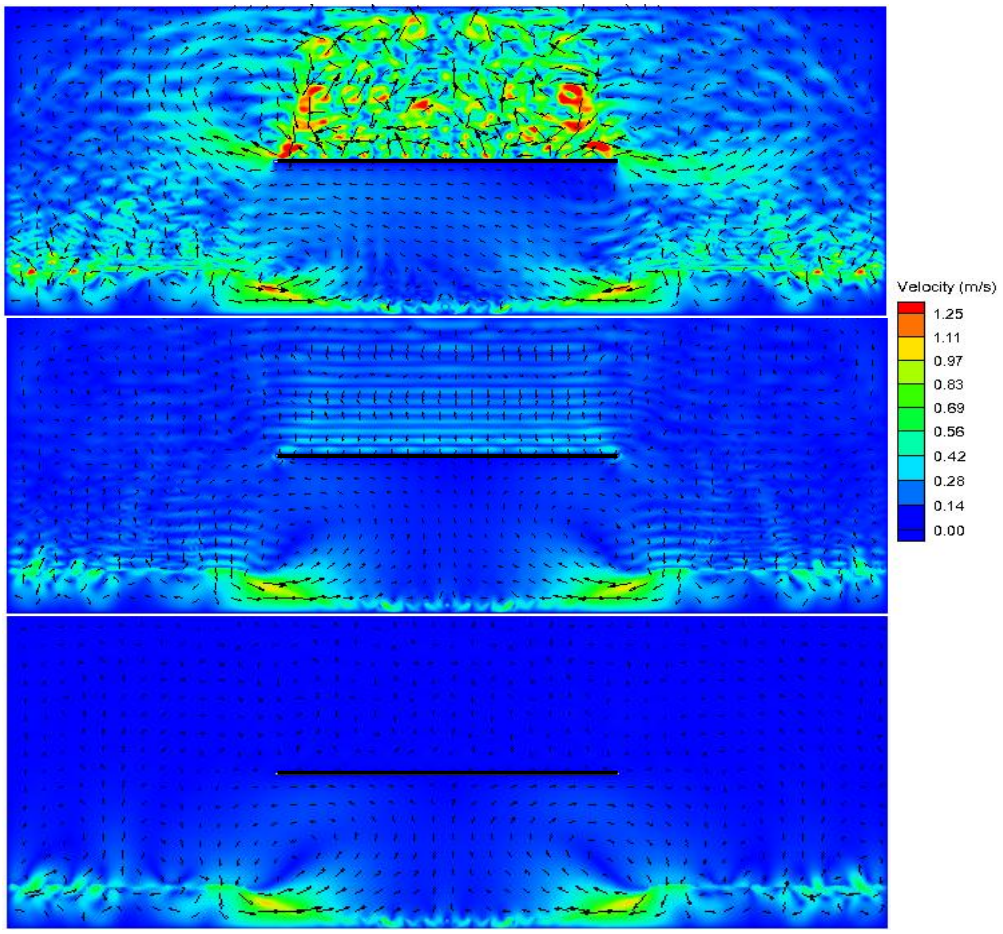


Fig. 5.6. Modeled current field; the simplified approach (top), the generalized approach (center) and Dingemans' approach (bottom)

## 5.2 Shore-perpendicular breakwater

### *5.2.1 Introduction*

In Section 5.1, we studied the wave-induced circulation around an offshore breakwater where the effect of wave-reflection on the modeled quantities was not considerable inside the surf-zone. Here, we consider the case of a thin shore-connected breakwater (jetty) (Liu and Mei (1976)) resting on a beach with uniform slope of 1 in 10 for X<100 m, and uniform water depth of 10 m for X>100 m. The jetty, which has a length of 400 m, is perpendicular to the shoreline and is designed to perfectly reflect the waves on the upwave side of the jetty. The model domain shown in Fig. 5.7 is comparable to a real-life situation where a jetty is connected to the beach. The modeled results of wave-induced circulation, their comparison with the published results of Liu and Mei (1976) and the performance of various wave forcing formulations is discussed in the following section:

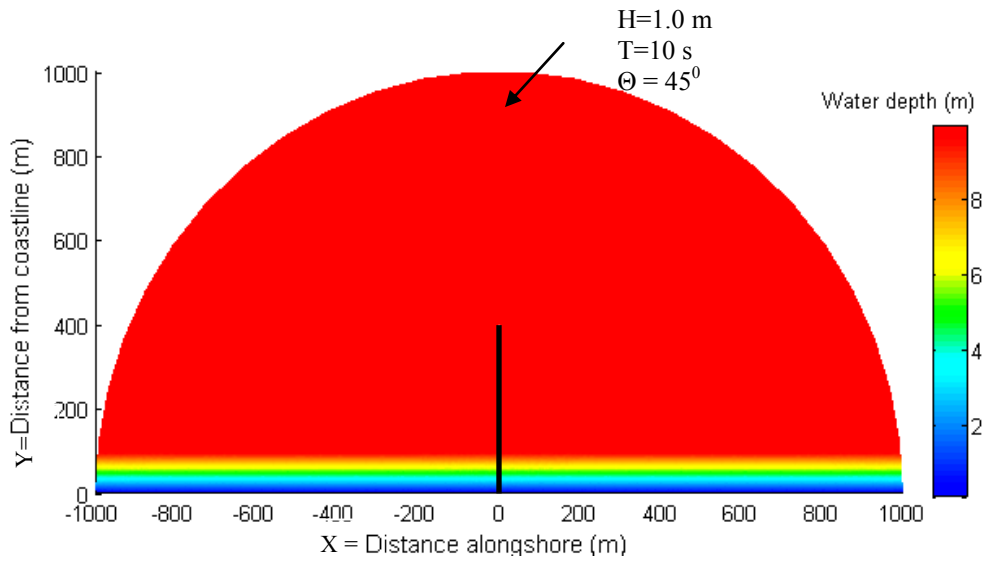


Fig. 5.7. Shore-perpendicular breakwater connected to beach, model bathymetry

### *5.2.2 Numerical results and discussion*

We consider an input condition of a monochromatic wave train of period T=10 s and wave height 1.0 m incident obliquely at an angle of $45^0$. The contour plots of modeled wave height and wave phase obtained with the elliptic wave model are shown in Fig. 5.8. Similar to the offshore breakwater case, a shadow zone with almost no wave activity is formed on the downwave side (X< 0) of the breakwater. On the upwave side (X> 0), the formation of nodes and anti-nodes due to the superposition of incoming and reflected wave components is apparent in Fig 5.8 (top).

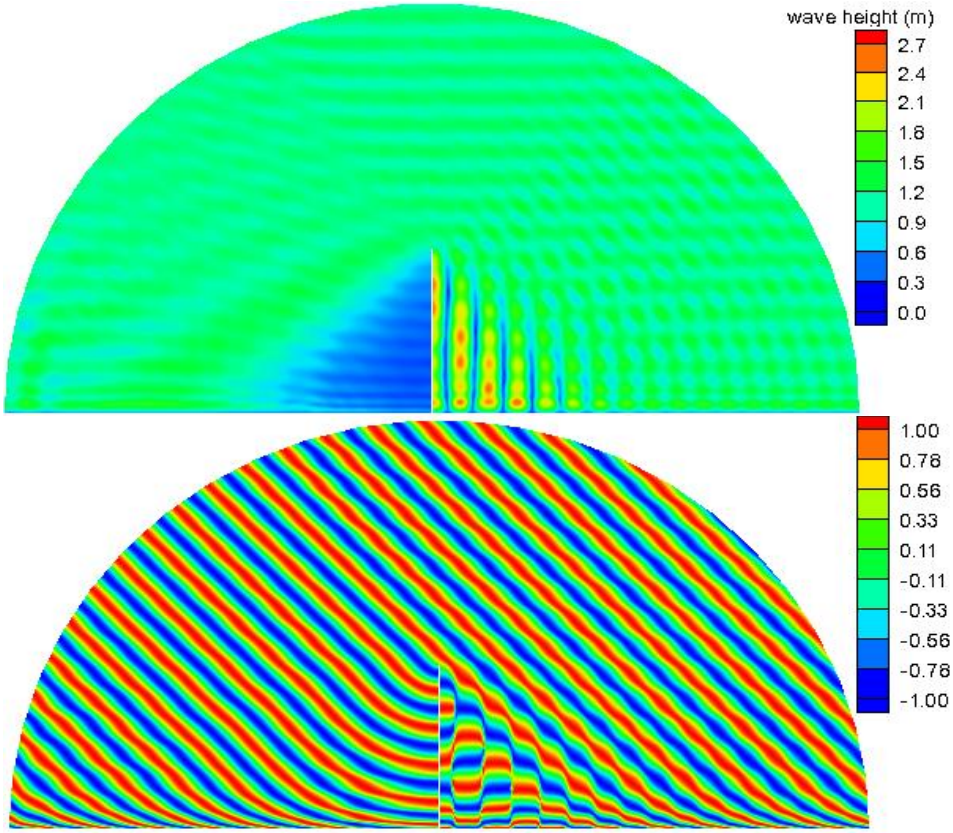


Fig. 5.8. Modeled wave height (top) and wave phase diagram (bottom)

The energy dissipation due to wave breaking inside the surf-zone is modeled using the breaking model of Dally et al. (1987). On the upwave side, because of the wave reflection, the energy dissipation due to breaking is more pronounced at the anti-nodes with larger wave heights. However, at nodal points, wave heights are sufficiently small to be stable without breaking. This alongshore variation in the wave field due to wave reflection and wave breaking affects the mechanism of nearshore circulation inside the surf-zone on the upwave side.

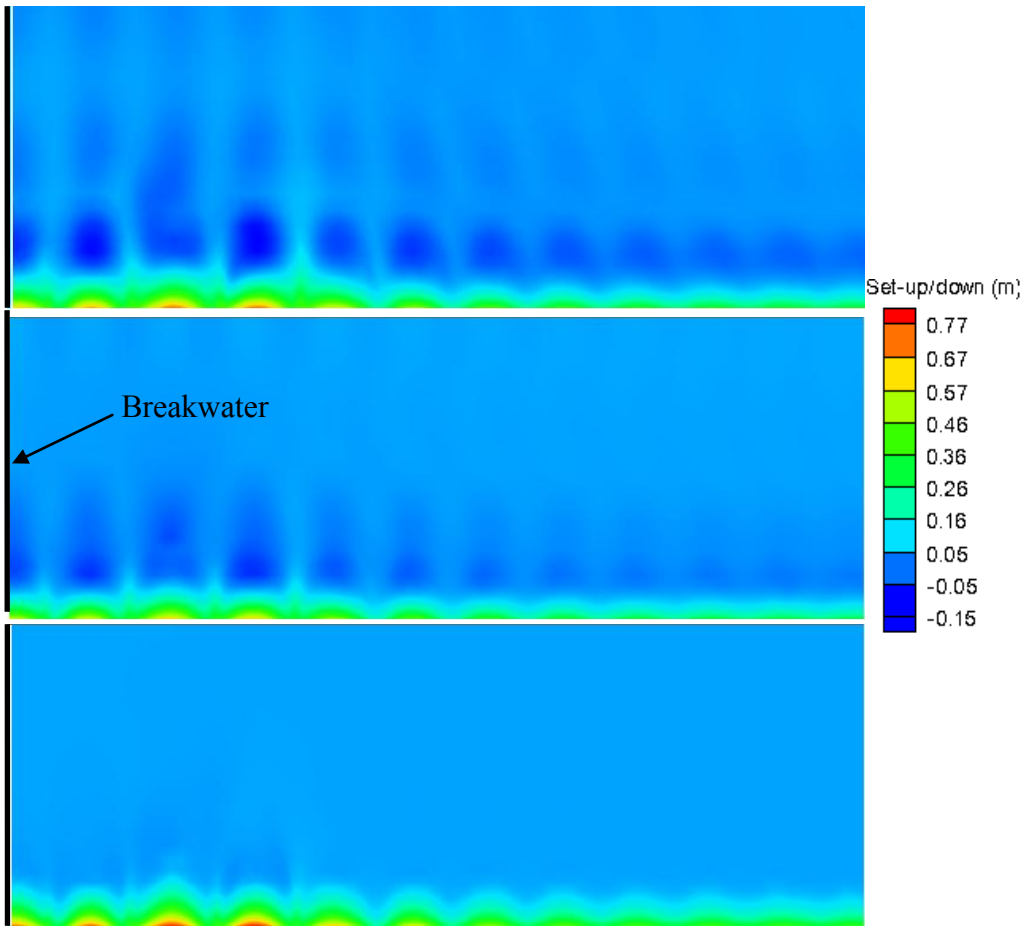


Fig. 5.9. Modeled wave set-up/down on the upwave side; the simplified approach (top), the generalized approach (center) and Dingemans' approach (bottom)

Fig. 5.9 and Fig. 5.10 depict the enlarged details (for Y<120 m only) of the modeled wave-induced set-up/down for the upwave side; the results are obtained with the three different approaches for wave forcing computation. Since the wave field is nearly progressive on the downwave side, all the three approaches are expected to produce almost similar results. Therefore, only the modeled current field and set-up/down corresponding to the generalized approach are shown (see Fig. 5.11).

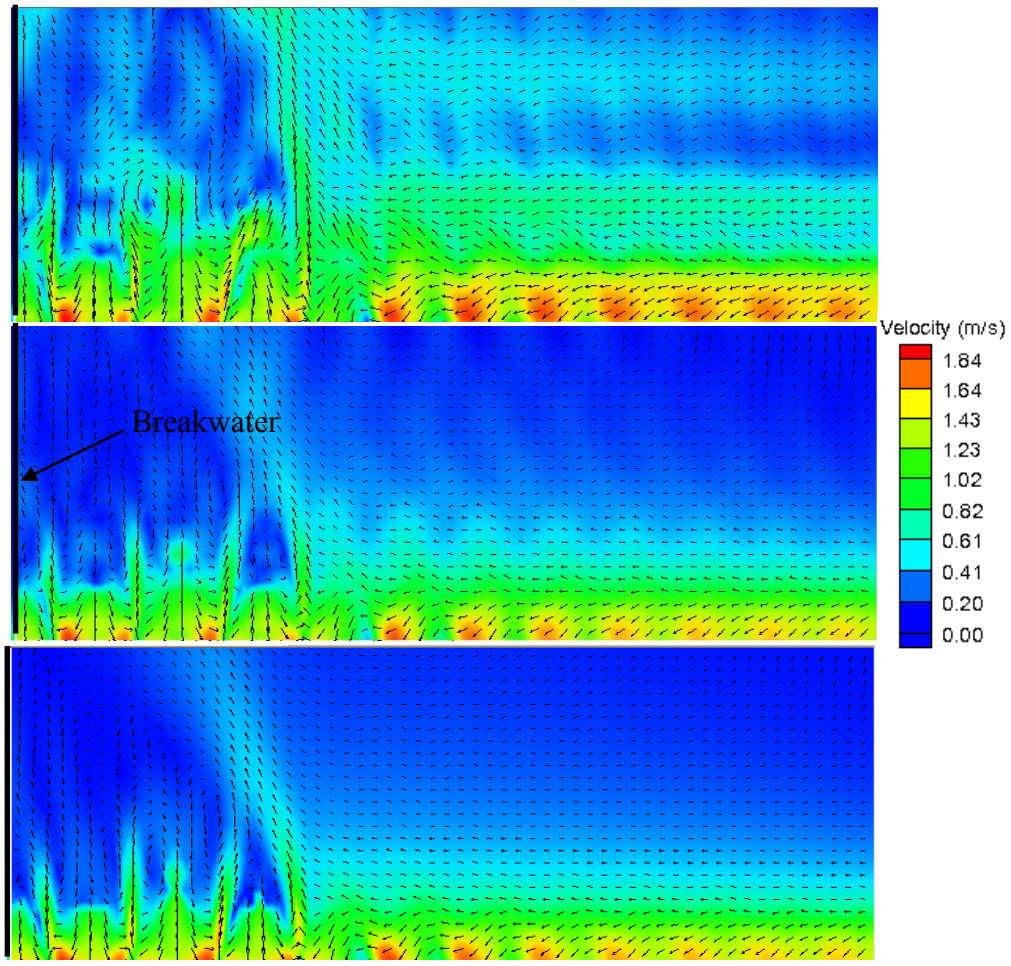


Fig. 5.10. Modeled current field on the upwave side; the simplified approach (top), the generalized approach (center) and Dingemans' approach (bottom)

To discuss the important features of the nearshore circulation, we first focus on the results obtained using the generalized approach (Figs. 5.9(center), Fig. 5.10(center) and Fig. 5.11). In the upwave neighborhood of the jetty, the presence of offshore-directed rip-currents at the nodal points is consistent with the published streamline plots (discussed later in this section) of current field by Liu and Mei (1976). The formation of rip-heads at the nodal points on the upwave side of the jetty was also confirmed by Dalrymple et al. (1975) in the laboratory experiments. In addition, in the region farther downstream, a longshore current (with some alterations due to wave reflection) generates as a result of wave striking the beach at an angle. On the downwave side, a similar feature of the longshore current directed away from the shadow region can be seen in Fig. 5.11. However, a counter-rotating cell near the boundary of the shadow zone in the published results of Liu and Mei (1967) (not shown here for the downwave side) is not seen in our modeled results (Fig. 5.11(top)). Like the previous case of the offshore breakwater where a cell system forms at the shadow boundary, here too, only the alongshore pressure gradients induced by the alongshore gradients of set-up/down can create a counter-rotating cell. However, in this case, probably the alongshore component of the wave forcing (due to obliqueness of the incident wave) directed away from the shadow region dominates the pressure gradients directed towards shadow zone. Apart from this, qualitative aspects of model results, such as the position of breaker line and the spatial variation in set-up/down, etc. match with the published results in Fig. 5.12. However, the published results in Fig. 5.12 are based on myriad hypotheses and approximations, precluding a quantitative comparison of the model results.

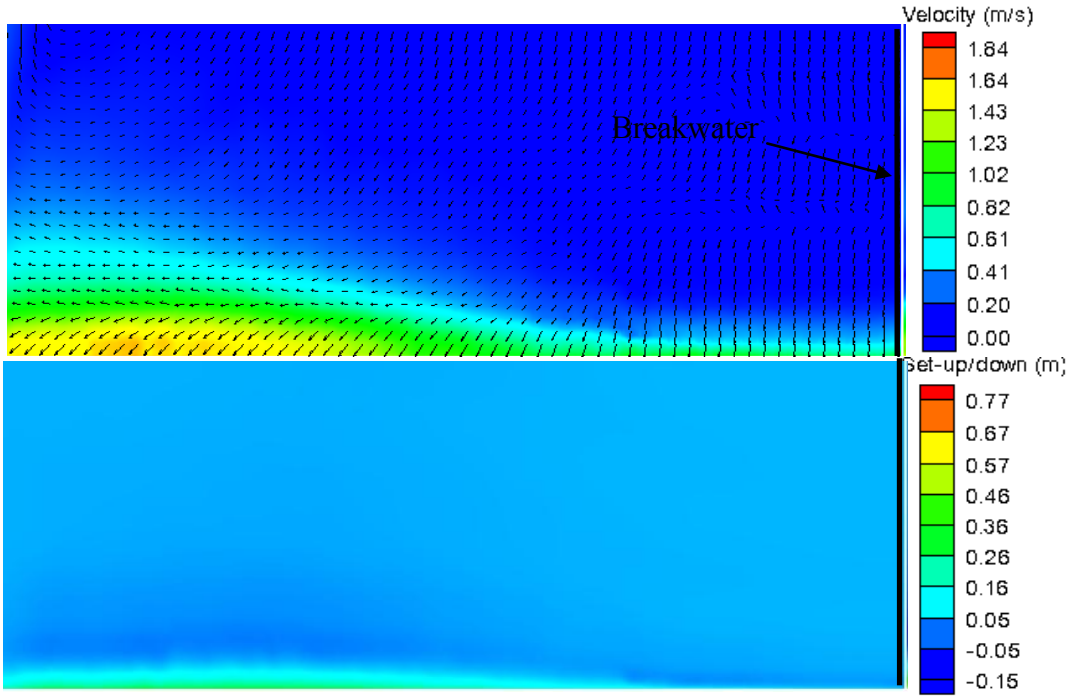


Fig. 5.11. Modeled current field (top) and set-up/down (bottom) on the downwave side; using the generalized approach

From Figs. 5.9-5.12, the differences in the modeled results with three different approaches are more distinct on the upwave side. It is again clear that the simplified approach produces erroneous results in the region where wave reflection is prominent and the correct information of wave propagation angle, which is used in the simplified formulation, is not available. Like the generalized approach and Dingemans' approach, the simplified approach is unable to properly model the assembly of rip currents on the upwave side. Some differences in the current field and set-up/down obtained between Dingemans' approach and the generalized approach may be attributed to the fact that the Dingemans' approach ignores the effect of wave reflection (as discussed in section 5.1.2). Notice that inside the surf-zone, Dingemans' approach is close to the generalized

approach because, as discussed earlier in this section, the wave-reflection affects the energy dissipation inside the surf-zone, and Dingemans' approach primarily simulates the effects of energy dissipation. Also, as expected, the set-down effect outside the surf-zone is ignored by Dingemans' approach. In addition, the results for current field over the entire domain presented in Fig. 5.13 show a jet-like feature in the results obtained with the simplified approach. However, the jet-like feature is not seen in the results obtained with other two approaches.

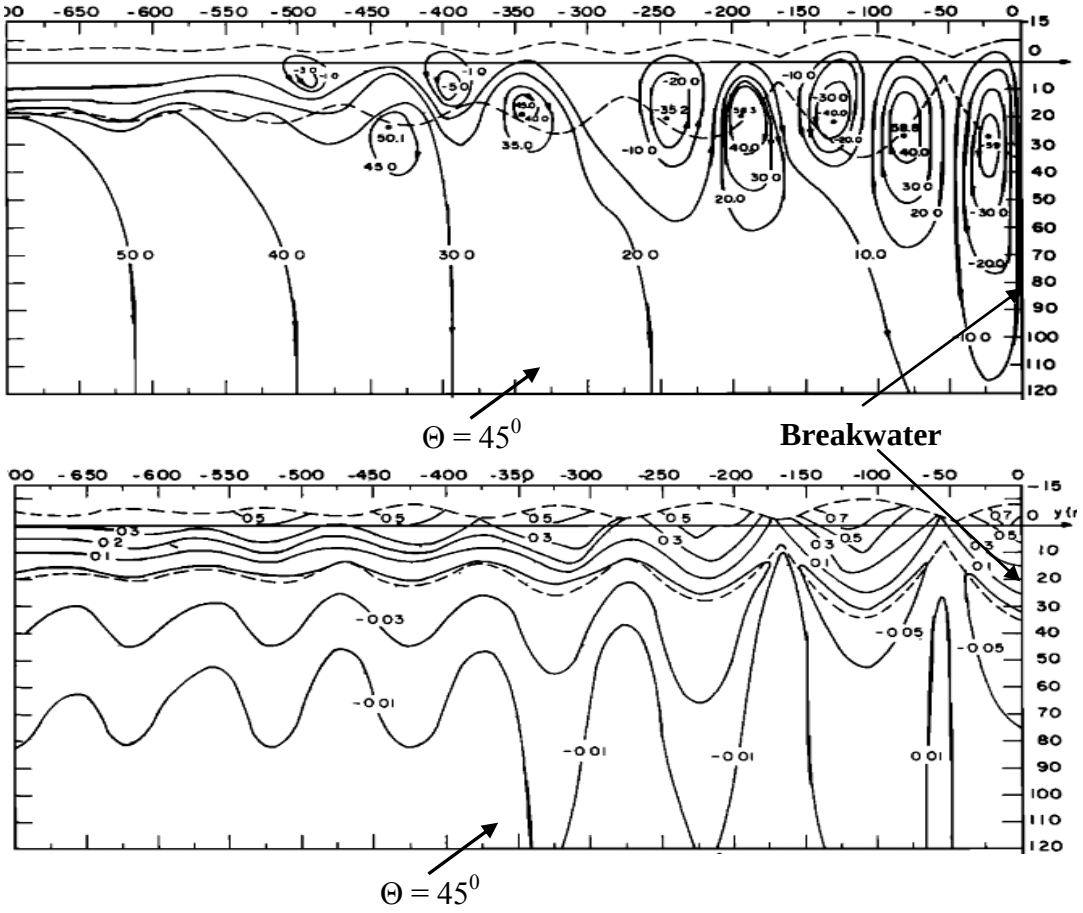


Fig. 5.12. Published results of Liu and Mei (1967); streamline of current field (top) and set-up/down (bottom) on the upwave side

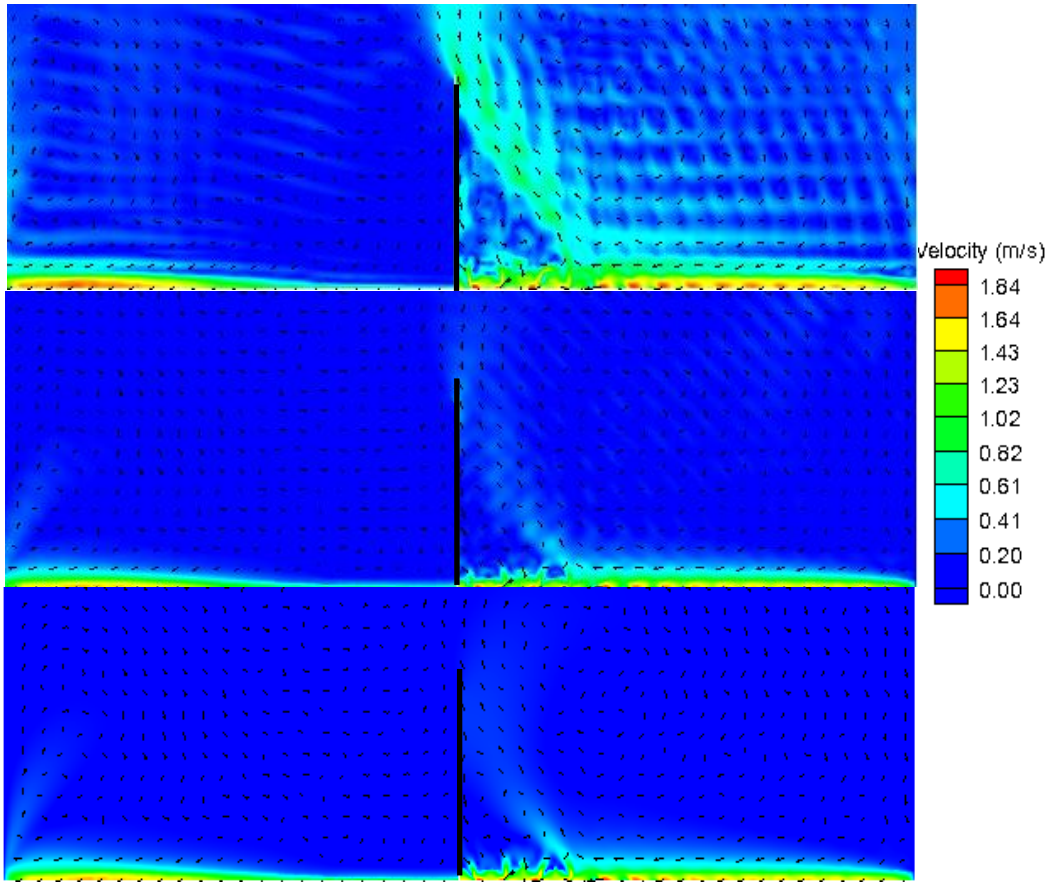


Fig. 5.13. Modeled current field over entire domain; the simplified approach (top), the generalized approach (center) and Dingemans' approach (bottom)

## 5.3 CERC shoal

### *5.3.1 Introduction*

In the previous numerical examples, we mainly dealt with the phenomena such as reflection and diffraction which can alter the progressive nature of the wave field. Apart from these phenomena, bathymetric irregularities in a coastal environment may cause the wave rays to cross and form a focusing region (caustic). One such example is the wave propagation over a submerged shoal where focusing zone may form behind the

shoal. In the next section, we study the wave-induced circulation over a submerged shoal (CERC Shoal). The model bathymetry (shown in Fig. 5.14) is obtained with the equations given by Vincent and Briggs (1989). In the following sections, we discuss the nature of wave-field and wave-induced circulation along with the differences in the results obtained with two different forms of the wave forcing.

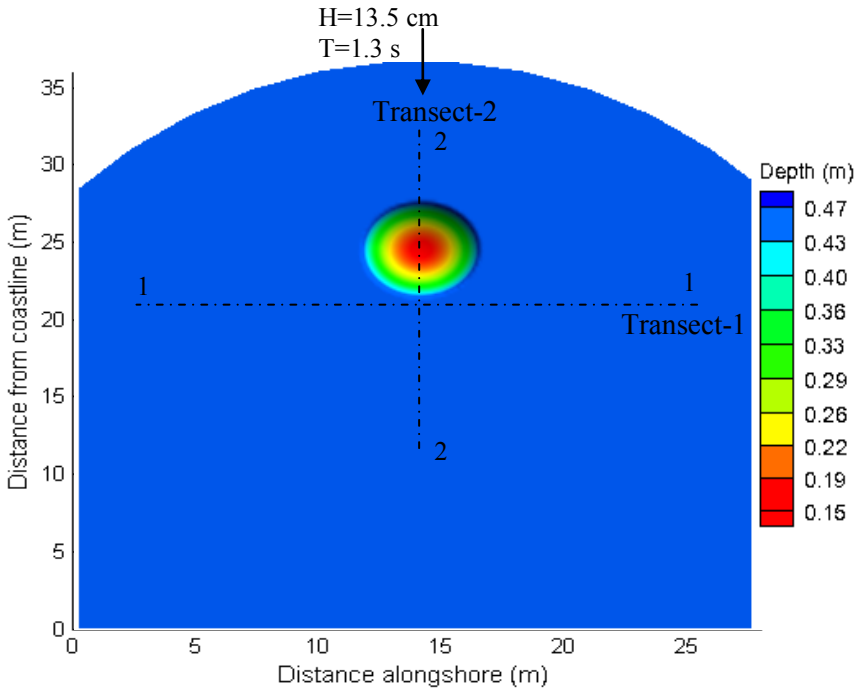


Fig. 5.14. Submerged laboratory shoal (Vincent and Briggs (1989)), model bathymetry

### *5.3.2 Numerical results and discussion*

For a monochromatic, normally-incident wave train of wave period, T=1.3 s and wave amplitude, A = 6.75 cm, the contour plots of modeled wave height and wave phase are shown in Fig. 5.15. Due to wave shoaling, the waves first increase in height over the

shoal and then break. Another important feature relevant to this study is the crossing of wave rays (see wave phase diagram in Fig. 5.15 (bottom)) behind the shoal.

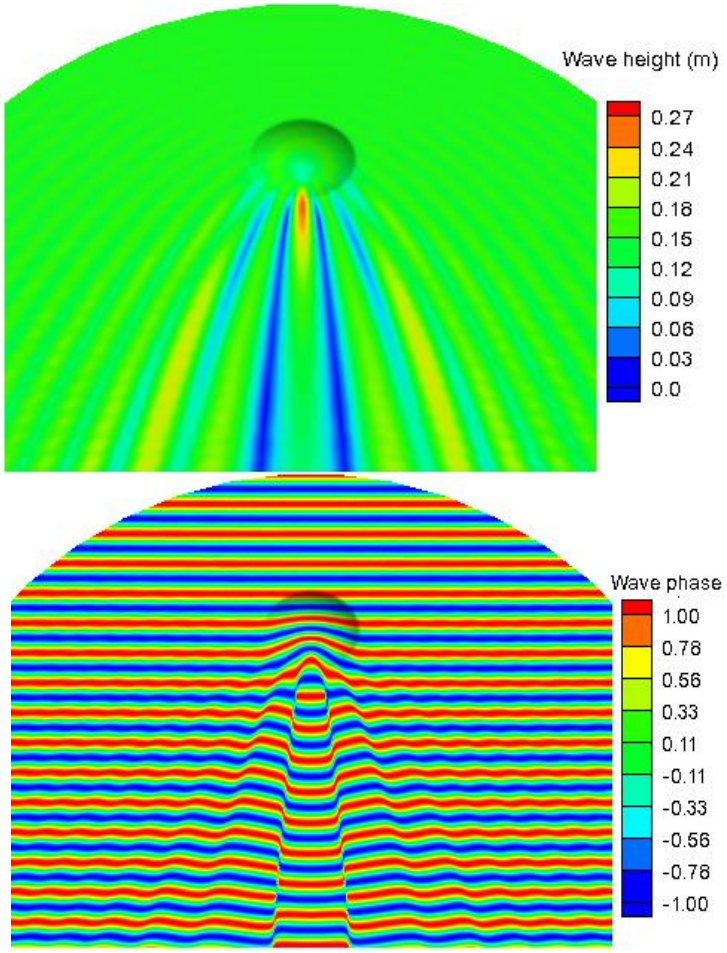


Fig. 5.15. Modeled wave height (top) and wave phase (bottom) diagram

For the wave field shown in Fig. 5.15 (top), the wave-induced forcing is evaluated using the generalized and the simplified approach. In the ADCIRC model, the open boundary and the coastline are considered as 'ocean' and 'mainland' (no-flow boundary) respectively. The variation in the surface elevation obtained with the ADCIRC model is shown in Fig. 5.16 (a) for the two approaches. The differences in the modeled results from two approaches are more pronounced in the region behind the

shoal. A comparison plot of modeled surface elevation along Transect-1 (see Fig. 5.14) is also presented (Fig. 5.16 (b)). It should be noted that this case of submerged shoal is a laboratory scale problem and the magnitude of the modeled surface elevation, which is comparable to the results published by Choi et al. (2009), is small. However, in real-life scenarios of bathymetric irregularities over a large area and comparatively stronger input wave conditions, larger sea surface elevations are expected.

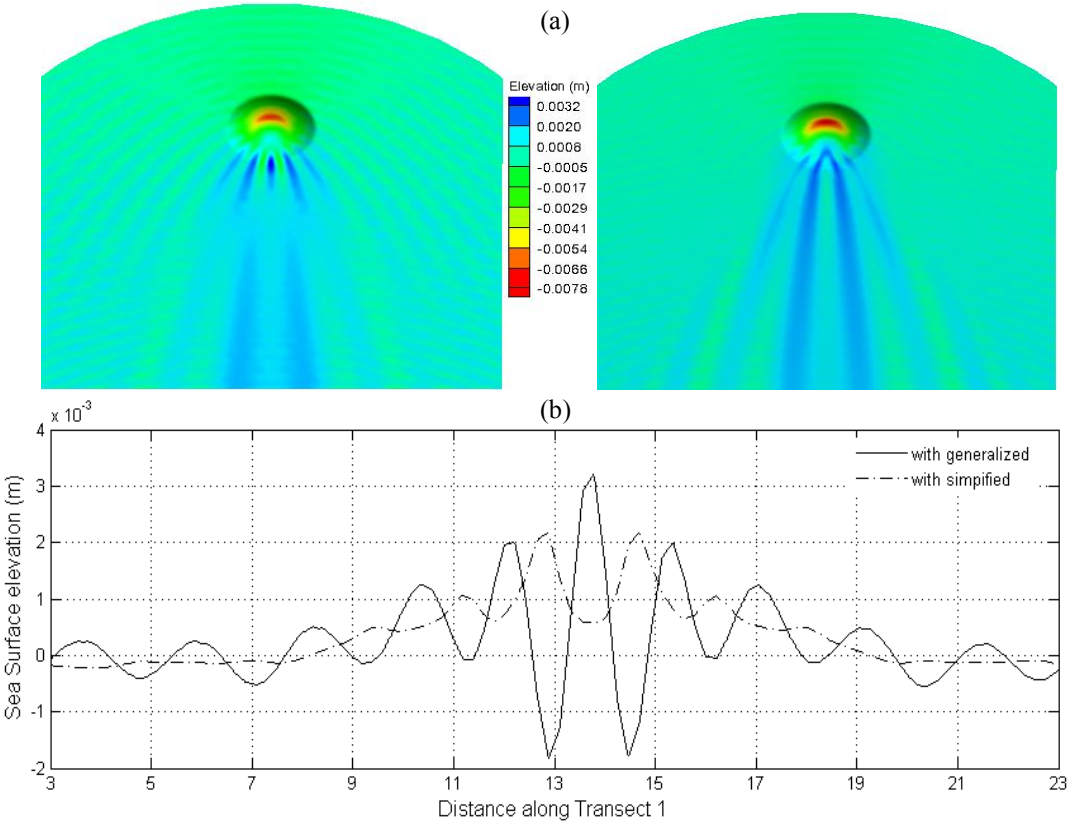


Fig. 5.16. (a) Modeled surface elevation; the simplified approach (left) and the generalized approach (right). (b) Comparison of modeled elevation along Transect-1

In addition, the results of wave-induced currents obtained with the two approaches are shown in Fig. 5.17(a). The circulation pattern is in agreement with the results of Choi et al (2009) obtained with the coupled SWAN-SHORECIRC system.

However, the results of Choi et al. (2009) are not considered for a qualitative comparison with the modeled results because their study also includes the wave-current

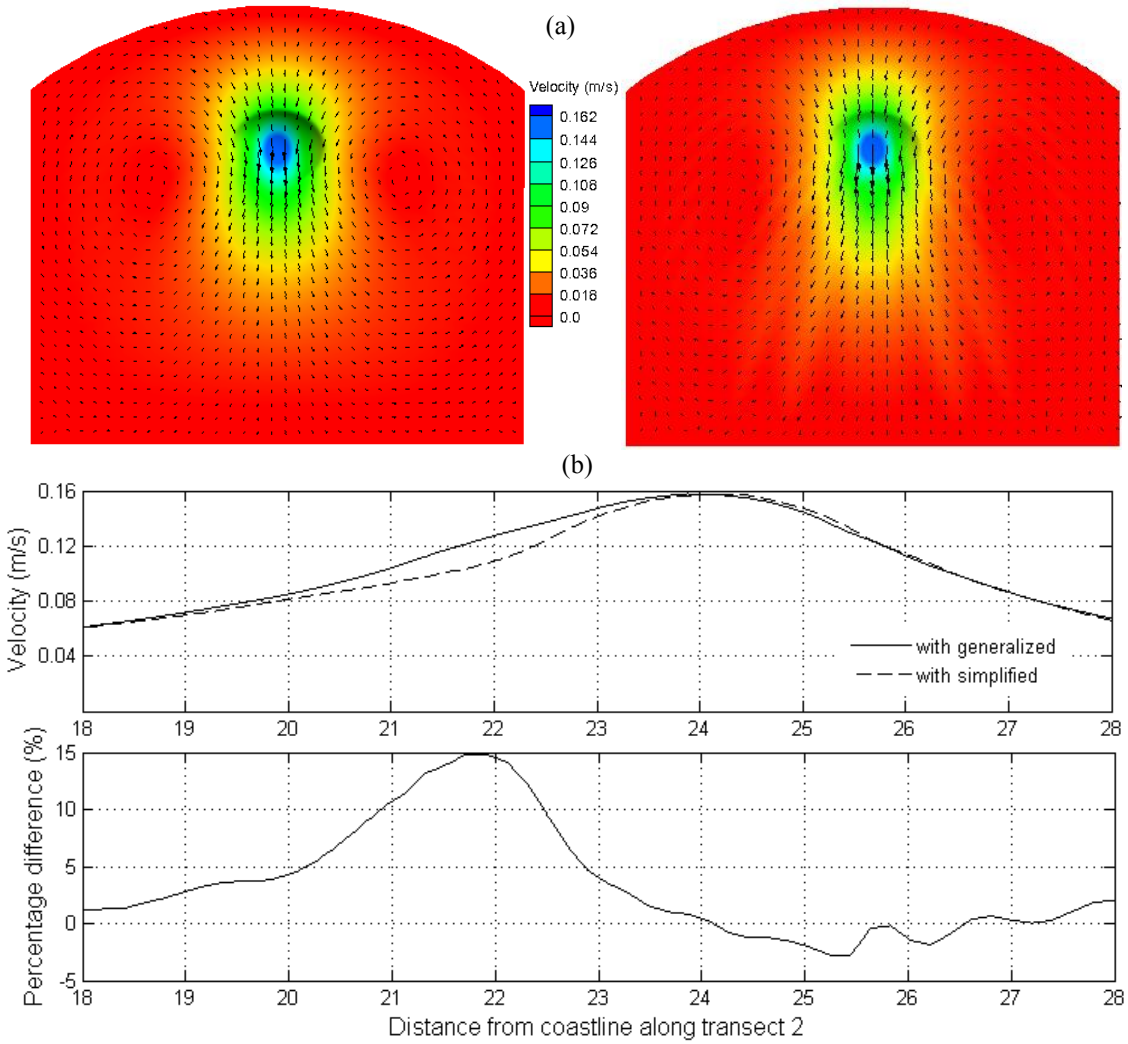


Fig. 5.17. (a) Modeled current field; the generalized approach (left) and the simplified approach (right). (b) Comparison of modeled elevation along Transect 2 (top) and the percentage difference (bottom)

interaction effects on the modeled circulation pattern. It was also pointed out (Choi et al. (2009)) that the use of simplified expression of radiation stress in a phase-resolving model may produce erroneous results of the current field as the information regarding the wave propagation angle is not available. A comparison plot with percentage differences in the current velocities obtained between the generalized approach and the simplified approach (along Transect-2 (see Fig. 5.14)) is shown in Fig. 5.17(b)). The differences up to 15%, observed in the region behind the shoal, are mainly due to the wave focusing effects.

## 5.4 Two adjacent submerged shoals

### *5.4.1 Introduction*

In Section 5.3, we studied the wave-induced circulation as a result of wave breaking over the submerged shoal. We also noticed that the simplified approach may produce erroneous results inside the focusing zone. However, the focusing zone was limited to a small area. We now consider a hypothetical case of two adjacent submerged elliptic shoals. The model bathymetry shown in Fig. 5.18 shows two adjacent elliptic shoals labeled as 'Shoal-1' and 'Shoal-2'. Shoal-1 and Shoal-2 have the centers located at (13.72, 6.10) and (13.72, 24.4). The length of the major and the minor axis for both the shoals are 23.76 m and 18.30 m respectively. The water depth over the shoals is given by the following equations:

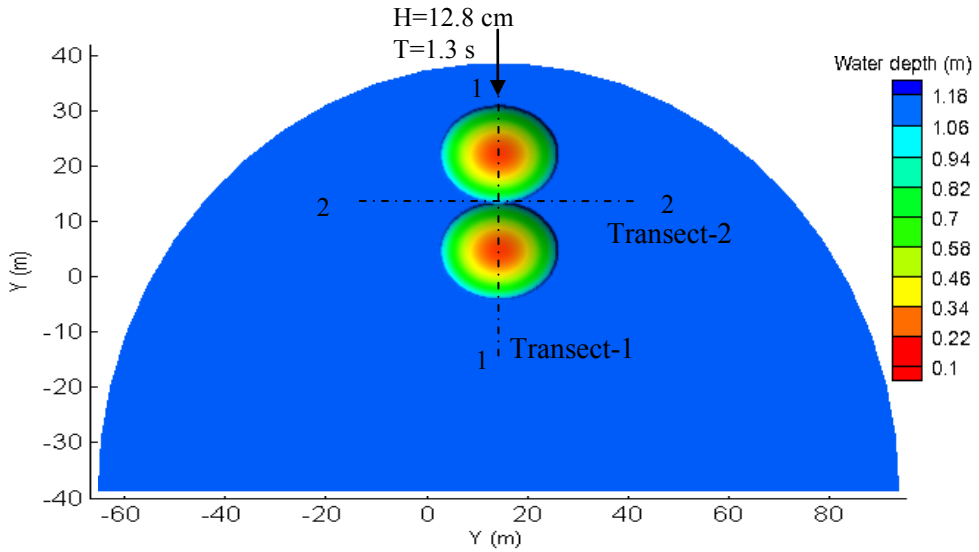


Fig. 5.18.Two adjacent submerged shoals, model bathymetry

$$h_1 = 2.27 - 2.0864\sqrt{-\left(\frac{X-13.72}{14.85}\right)^2 - \left(\frac{Y-6.1}{11.83}\right)^2 + 1} \tag{5.1}$$

$$h_2 = 2.27 - 2.0864\sqrt{-\left(\frac{X-13.72}{14.85}\right)^2 - \left(\frac{Y-24.4}{11.83}\right)^2 + 1} \tag{5.2}$$

where $h_1$ and $h_2$ are the water depths over Shoal-1 and Shoal-2 respectively and X and Y are the Cartesian coordinates. Elsewhere, the water depth has a uniform value of 1.15 m. The nature of wave field, wave-induced circulation, the performance of wave forcing formulations is discussed in the following sections.

### *5.4.2 Numerical results and discussion*

For a monochromatic incident wave train of wave period, T= 1.3 sec and wave height H=0.128 m, the results of modeled wave height and wave phase are shown in Fig. 5.19. The wave shoaling and breaking over the shoals can be observed in the contour

plot of wave height. In addition, wave phase diagram shows that the wave rays cross and generate a focusing zone over and behind Shoal 2. In comparison to the previous example, we get a larger number of points where wave rays are crossing.

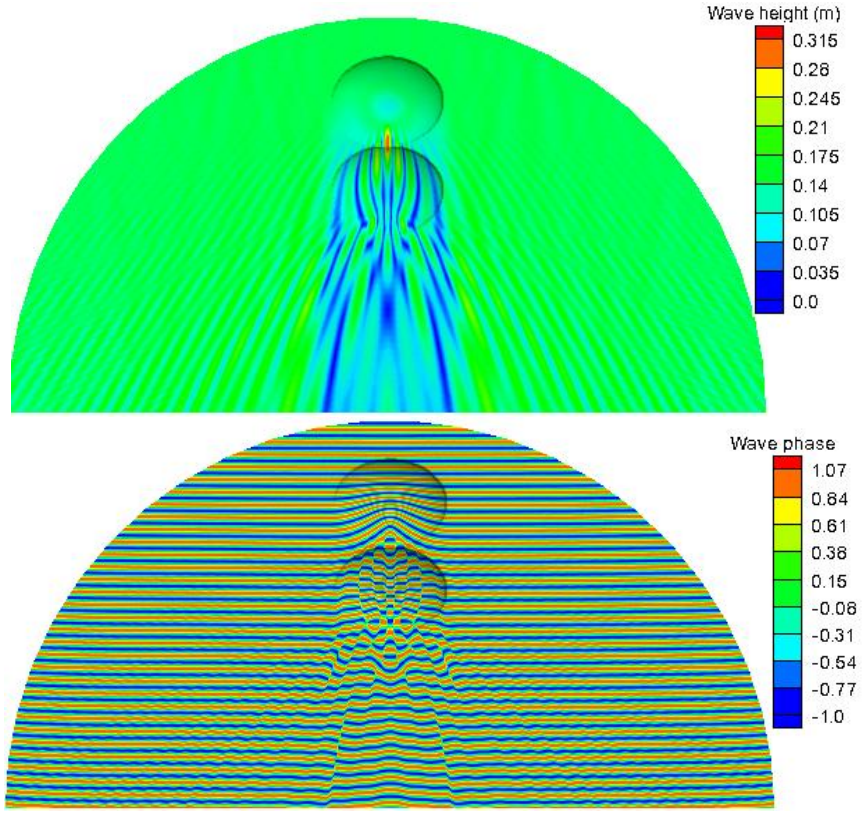


Fig. 5.19. Modeled wave-height and wave phase

To study the wave-induced circulation, we consider all three wave forcing formulations. The results of wave-induced set-up/down and current field are obtained

using the circulation model (ADCIRC) by imposing a no-flow boundary condition at all the boundaries.

In Fig. 5.20, the differences in the modeled results of set-up/down obtained between the simplified and the generalized approach are small and limited to the focusing zones: (1) between the two shoals and (2) over and behind Shoal-2. On the other hand, Dingemans' approach does not capture the variation in wave set-down appropriately (see Fig. 5.20(c)) in comparison to other two approaches. However, like the previous examples, results of current field (Fig. 5.21) obtained with Dingemans' approach are almost similar to the results obtained with the generalized approach. The simplified approach produces larger magnitude of velocities at some locations. These differences are most probably due to the effect of wave focusing and bottom slope. Note that the simplified approach is accurate only for a purely progressive wave field on a flat bottom.

For a better comparison of the modeled quantities, we consider results along transects (Transect-1 and Transect-2 in Fig. 5.18). Fig. 5.22(b) shows a comparison plot of current velocities along Transect-1 for the three approaches.

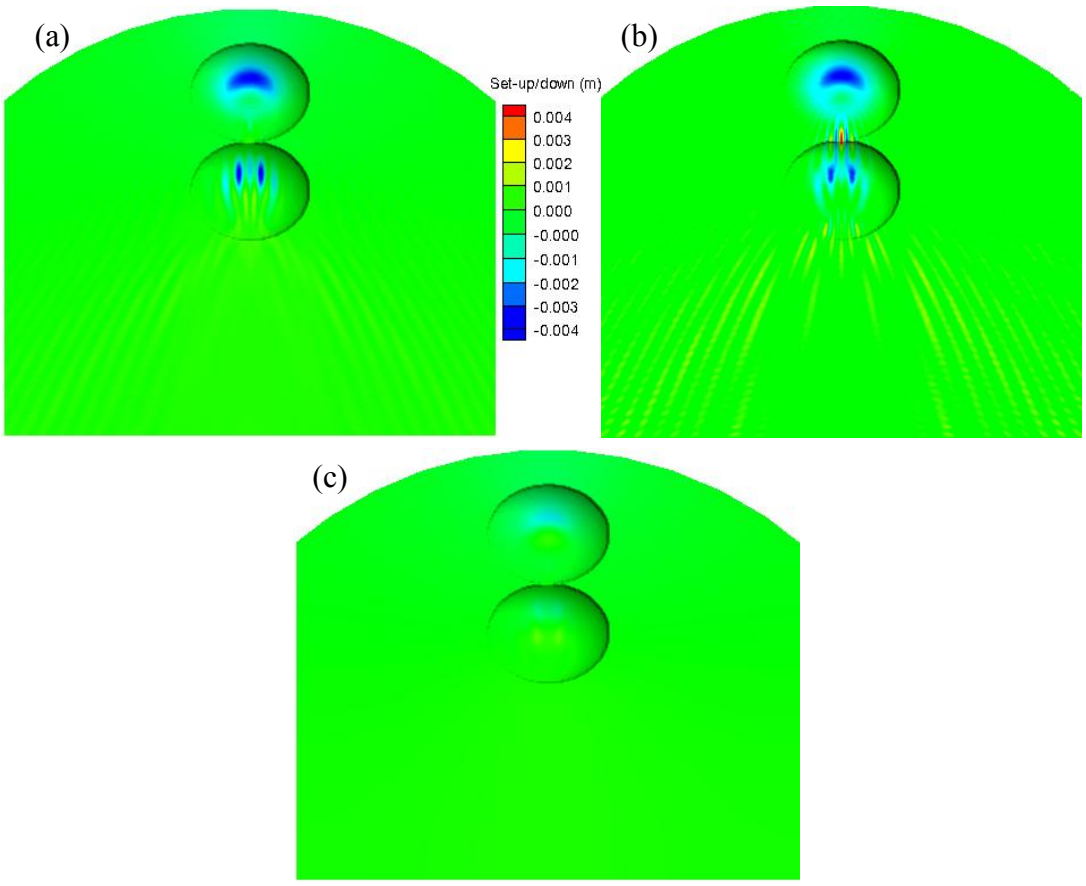


Fig. 5.20. Modeled wave set-up/down; (a) the simplified approach, (b) the generalized approach and (c) Dingemans' approach (bottom)

In addition, the percentage difference between the velocities obtained using the generalized formulation and the simplified formulation is shown in Fig. 5.22(a). It can be observed that with respect to the generalized approach, the simplified approach may produce errors up to 25% in the region above Shoal-1 where wave focusing is more pronounced. A comparison plot of wave set-up/down (along Transect-2) calculated with the simplified and the generalized approach is shown in Fig. 5.22(b).

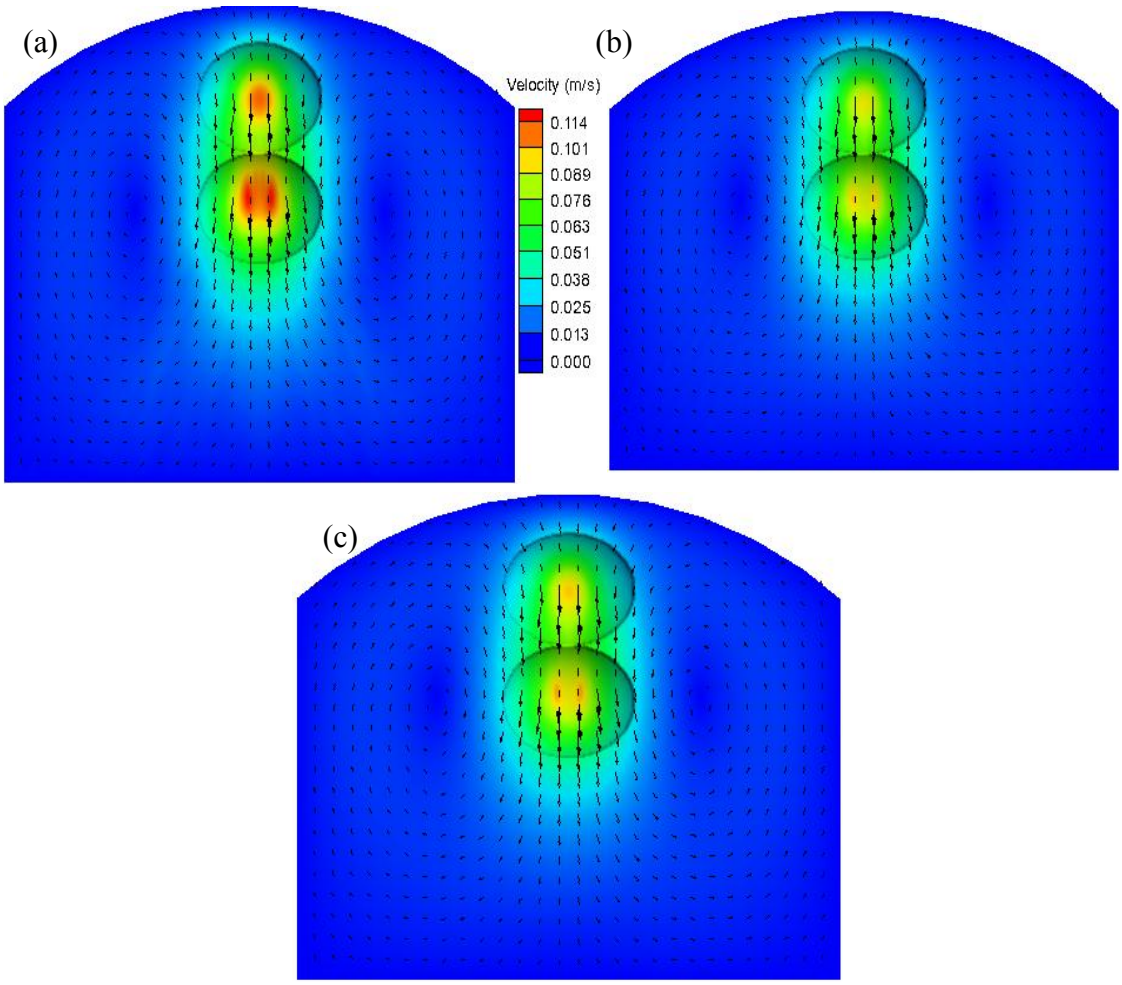


Fig. 5.21. Modeled current field; (a) the simplified approach, (b) the generalized approach and (c) Dingemans' approach (bottom)

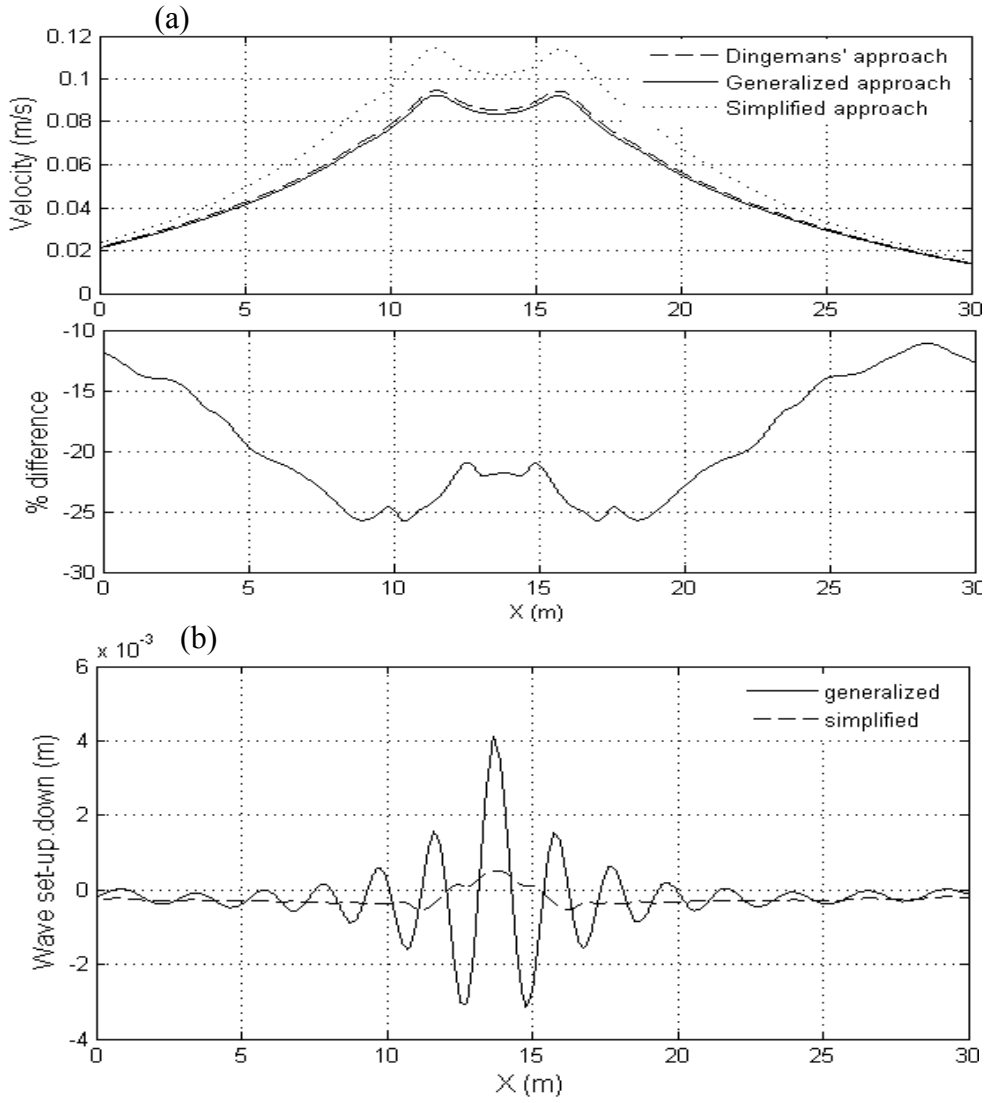


Fig.5.22 (a) Comparison of current velocity along Transect-1. (b) Comparison of set-up/down along Transect-2

In summary, we have considered some cases where phenomena like diffraction, reflection and focusing can alter the progressive nature of the wave field. The coupled system is now thoroughly validated and applied to some complex domains. Section 6 provides a brief summary and concluding remarks for this study.

# 6. SUMMARY AND CONCLUSIONS

In this study, we have simulated the wave-induced circulation in general coastal environments. Quantities of engineering interest, such as wave-induced current field and wave set-up/down are modeled for domains with structures (e. g. breakwater, jetty, etc.) and bathymetric irregularities (e. g. shoal, sandbar, etc.). Because of the known advantages of finite-element models to reproduce the correct shape of boundaries and geometric features by utilizing modern, highly-efficient grid generation tools, two finite-element based models: (1) an elliptic wave model and (2) a circulation model (ADICRC) are "one-way" coupled to obtain these quantities. The coupled system is able to model the general nearshore features, such as longshore current, rip-current, cell-circulation around structures, etc. In fact, the coupled system can now be applied to the domains with arbitrary shaped coastline and geometric features.

Some aspects of the wave-induced circulation, which has hitherto not been investigated in the literature, are considered in this study. For example, the effect of wave reflection and diffraction on the wave-induced circulation is explored by considering the standing wave case (Section 4) and by including the offshore region in the computational domain for the detached breakwater case in (Section 5).

The ability of the elliptic wave model to properly handle wave reflection, refraction and diffraction enables us to effectively simulate the wave field in this study. The modeling of energy dissipation due to wave breaking is crucial in such applications, and breaking criterion of Dally et al. (1985) was found to be satisfactory in most cases.

However, since the studies using the elliptic wave models to compute the wave forcing are limited in the literature, a detailed investigation of the performance of various wave forcing formulations with the elliptic wave model is carried out. Three wave forcing formulations: (1) the simplified wave forcing which is easy to implement in a wave model and is widely used in the literature, (2) the generalized expression which is relatively complex and has only been applied to limited studies and (3) Dingemans' approach whose performance in a general coastal environment is not known, are used to provide wave forcing for the ADCIRC model.

The following conclusions can be made regarding the performance of these wave-forcing formulations:

- The generalized wave forcing produces satisfactory results of wave-induced current field and set-up/down in most cases. However, an approximate grid resolution of L/10 or more (L=wavelength at a grid location) is preferred in the wave model to avoid the contamination of the modeled wave forcing owing to the calculation of higher-order derivatives.
- The simplified approach produces erroneous results in the region of wave reflection, diffraction and focusing, because the wave propagation angle in these situations is not defined. In some cases, it is observed that the simplified approach over-predicts the currents by 25%.
- Dingemans' approach produces smoother results in comparison to the generalized approach by ignoring the effects of wave diffraction and reflection. In fact,

Dingemans' approach primarily simulates the effect of energy dissipation, and the modeled results outside breaker-line (for example, wave set-down) are ignored.

- For large domains, where the desired grid resolution of L/10 or less is not achievable in the wave model, the generalized approach may produce erroneous results. In such cases, Dingemans' approach may be considered if reflection and diffraction related effects can be ignored.

Because of ADCIRC's capability to incorporate the wind forcing, tidal forcing and river or estuarine flow, the coupled system, in future, can be applied to more general applications. One such example is the numerical modeling of waves and circulation around coral reefs with a lagoon on the shoreward side. Steep slopes and shallow depths are usually encountered in the vicinity of coral reefs; the elliptic model can provide a reliable prediction of wave field and wave forcing.

In addition, an effort to include wave-current interaction will make this study more comprehensive. In future, the vertical variation in the generalized form of the wave forcing formulation will be considered; the formulations available in the literature, which account for the vertical variation, are valid only for the progressive wave field only.

# REFERENCES

Battjes, J.A. and Janssen, J. (1978). "Energy loss and set-up due to breaking of random waves." *Proc., 16th Int. Conf. Coastal Eng.* ASCE, New York, 569–587.

Berkhoff, J. C. W. (1976). "Mathematical Models for Simple Harmonic Linear Water Waves; Wave Refraction and Diffraction", Publ. No. 163, Delft Hydraulics Laboratory, Delft, The Netherlands.

Bettess, P. and Bettess, J. A. (1982). "A generalization of the radiation stress tensor". *Applied Mathematical Modeling,* 6(3), 146-150.

Blain, C.A. and Cobb, M. (2003a). "Application of a shelf-scale model to wave-induced circulation, Part I: Alongshore currents on plane and barred beaches." *NRL Formal Report, NRL/FR/7320-03-10,046,* Naval Research Laboratory, Department of the Navy.

Bondzie, C. and Panchang V. G. (1993). "Effects of bathymetric complexities and wind generation in a coastal wave propagation model." *Coastal Eng.* 21, 333-336.

Booij, N. (1981). "Gravity Waves on Water with Non-uniform Depth and Current." Doctoral thesis, Technical University of Delft, The Netherlands.

Booij, N., Ris, R.C. and Holthuijsen, L. H. (1999). "A third generation wave model for coastal regions 1. Model description and validation." *J. of Geophysical Res.* 104 (No. C4), 7649-7666.

Bowen, A.J., Inman, D.L. and Simmons, V.P. (1967). "Wave set-down and wave set-up." *J. Geophysics Res.* 73, 2569–2577.

Chamberlain, C. N. and Porter, D. (1995). "The modified mild-slope equation." *J. Fluid Mech.* 291, 393-407.

Chandrasekera, C. N. and Cheung, K.F. (1997). "Extended linear refraction-diffraction model." *J. Waterway, Port, Coastal Ocean Eng.* 123(5), 280-286.

Choi, J., Lim, C. H., Lee, J. I. and Yoon, S. B. (2009). "Evolution of waves and currents over a submerged laboratory shoal." *Coastal Eng.* 56, 297-312.

Cobb, M. and Blain, C. A. (2003b). "Application of a shelf-scale model to wave-induced circulation, Part 2: Rip currents." *NRL Formal Report, NRL/FR/7320-03-10,005,* Naval Research Laboratory, Department of the Navy.

Dally, W.R., Dean, R.G. and Dalrymple, R.A. (1985). "Wave height variation across beaches of arbitrary profile." *J. Geophys. Res.* 90(6), 11917–11927.

de Girolamo, P., Kostense, J.K. and Dingemans, M.W. (1988). "Inclusion of wave breaking in a mild-slope model." In: Schrefler, Zienkiewicz (Eds.), *Computer Modeling in Ocean Engineering.* Balkema, Rotterdam, 221–229.

Demirbilek Z. and Panchang V. (1998). "A coastal surface water wave model of the mild-slope equation. *Technical Report CHL-TR-98-26,"* US Army Corps of Engineers (USACE).

Dingemans, M.W., Radder, A. C. and Vriend, H. J. (1987). "Computations of the driving forces of wave-induced currents." *Coastal Eng.* 11 (5-6), 539-563.

Ebersole, B. A. (1985). "Refraction-diffraction model for linear water waves." *J. Waterway, Port, Coastal Ocean Eng.* 111(6), 939-953.

Edge, B. L. and Pandoe, W. W., (2003). "Effect of Baroclinic Circulation on Sediment Transport in an Idealized Ship Channel." *Proc. the International Conference on Coastal Sediments,* Clearwater Beach, FL

Herbich, J. B. (1991). "Chap. 18: Scour around pipelines, piles, and seawalls." *Handbook of Coastal and Ocean Engineering*, J. B. Herbich, ed., Gulf Pub., Houston, 867–958.

Irish, J. L., Resio, D. T., and Ratcliff, J. J. (2008). "The influence of storm size on hurricane surge," *J. Phys. Oceanogr.*, doi:10.1175/2008JPO3727.1, Vol. 38, No. 9, 2003-2013.

Jones D.F. (1975). "The Effect of Vertical Seawalls on Longshore Currents, unpublished PhD Thesis." Department of Coastal and Oceanographic Engineering, University of Florida, Gainsville, FL.

Jyothi, K., Mani, J. S. and Pranesh M. R. (2002). "Numerical modeling of flow around coastal structures and scour prediction." *Ocean Eng.* 29, 417-444.

Kirby, J. T. and Dalrymple, R. A. (1994). "Combined refraction/diffraction model REF/DIF 1." *Version 2.5, User Manual, Technical Report CACR-94-22.* University of Delaware.

Komar, P. D. (1979). “Beach slope dependance on longshore currents.” *J. of Waterwav, Port. Coastal Ocean Eng*. 105, 460-470.

Kostense, J.K., Dingemans, M.W. and P. Van den Bosch (1988). “Wave-current interaction in harbors.” In: Proc. *21st International Conference Coastal Engineering*, Malaga. 32-46.

Li, B. (1994). “A generalized conjugate gradient model for the mild-slope equation.” *Coastal Eng. 2*3, 215–225.

Liu, P. L. F. and Mei, C. C. (1976). “Water motion on a beach in the presence of breakwater 2. Mean Currents.” *J. of Geophysical Res.* 81 (18), 3085-3094.

Longuet-Higgins, M. S. and Stewart, R. W. (1964). “Radiation Stresses in Water Waves; a Physical Discussion with Applications.” *Deep Sea Res.* 11, 529-562.

Luettich, R.A., J.J. Westerink, and N.W. Scheffner. (1992). “ADCIRC: An Advanced Three-Dimensional Circulation Model for Shelves, Coasts, and Estuaries, Report 1: Theory and Methodology of ADCIRC-2DDI and ADCIRC-3DL.” *Technical Report DRP-92-6*, U.S. Army Corps of Engineers Waterways Experimental Station, Vicksburg, MS.

Luettich, Jr., R.A., J.L. Hench, C.W. Fulcher, F.E. Werner, B.O. Blanton and J.H. Churchill. (1999). “Barotropic tidal and wind driven larval transport in the vicinity of a barrier island inlet.” *Fisheries Oceanography*, 8 (Suppl. 2), 190-203.

Munk, W. H. (1949). “Surf beats.” *Transactions of the American Geophysical Union*, 30, 849-854.

Newell, C., Mullarkey, T. and Clyne, M. (2005). “Radiation stress due to ocean waves and the resulting currents and set-up/set-down*.” Ocean Dynamics,* 55, 499-514.

Panchang, V.G., Ge, W., Cushman-Roisin, B., Pearce, B.R. (1991). “Solution to the mild-slope wave problem by iteration.” *Appl. Ocean Res.* 13(4), 187–199.

Panchang, V., Chen, W., Xu, B., Schlenker, K., Demirbilek, Z. and Okihiro, M. (2000). “Exterior bathymetric effects in elliptic harbor wave model.” *J. Waterway, Port, Coastal & Ocean Eng.* 126(2), 71-78.

Pham, T. N. and Larson, M. (2009). “Model of Nearshore Waves and Wave-Induced Currents around a Detached Breakwater.” *J. Waterway, Port, Coastal & Ocean Eng.* 136(3), 156-176.

Putnam, J. A., Munk, W. H. and Traylor, M. A. (1949). "The Predictions of Longshore Currents." *Transactions of the American Geophysical Union,* 30, 338-345.

Rakha K.A., Kamphuis J.W. (1997). "Wave-induced currents in the vicinity of a seawall." *Coastal Eng.* 30(1-2), 23-52.

Ruggiero, P. and McDougal, W.G. (2001). "An analytic model for the prediction on wave set-up, longshore currents and sediment transport on beaches with seawalls**.**" *Coastal Eng.* 43(3-4), 161-182.

Silvester, R. and Hsu, J. R. C. (1997). *Coastal Stabilization,* World Scientific, Singapore.

Smith, J. M., Sherlock, A. R. and Resio, D. T. (2001). "STWAVE: Steady-state spectral wave model user's manual for STWAVE Version 3.0." *CE-ERDC/CHL SR-01-1,* U.S. Army Engineer Research and Development Center, Vicksburg, MS.

Sumer, B. M., and Fredsoe, J. (2000). "Experimental study of 2D scour and its protection at a rubble-mound breakwater." *Coastal Eng.* 40, 59–87.

Svendsen, I. A. (2006). *Introduction to Nearshore Hydrodynamics.* World Scientific, Singapore.

Vincent, C.L. and Briggs, M.J. (1989). "Refraction-diffraction of irregular waves over a mound." *J. Waterway, Port, Coastal Ocean Eng.* 115 (2): 269-284.

Watanabe, A. and Maruyama, K. (1986). "Numerical modeling of nearshore wave field under combined refraction, diffraction and breaking." *Coastal Eng. in Japan,* 29, 19-39, 1986.

Whitehouse, R. (1998). "Scour at Marine Structures." Thomas Telford Ltd., London.

Zhao, L., Panchang, V., Chen, W., Demirbilek, Z. and Chabbra, N. (2001). "Simulation of wave breaking effects in two-dimensional elliptic harbor wave models." *Coastal Eng.* 42, 359-373.

Zundel, A.K., Fugal, A.L., Jones, N.L., Demirbilek, Z. (1998). "Automatic definition of two-dimensional coastal finite element domains. In: Babovic, V., Larsen, L.C. (Eds.), Hydroinformatics98, *Proc. 3rd International Conerence of Hydroinformatics.* A.A. Balkema, Rotterdam, 693–700.

# VITA

Abhishek Sharma received his Bachelor of Technology degree in civil engineering, with honors, from the Institute of Technology, Banaras Hindu University (IT-BHU) in 2008. He entered the Ocean Engineering program at Texas A&M University in August 2008 and received his Master of Science in 2010.

His email is abhishek25.itbhu@gmail.com and he may be reached at the following address:

Address:

Department of Civil Engineering

c/o Dr. Vijay Panchang

Texas A&M University

College Station, TX 77843-3136